

DOCTORAL THESIS

Slotted-In Steel Plate Connections with Dowels in Cross-Laminated Timber Shear Walls

Eero Tuhkanen

TALLINN UNIVERSITY OF TECHNOLOGY
DOCTORAL THESIS
20/2021

Slotted-In Steel Plate Connections with Dowels in Cross-Laminated Timber Shear Walls

EERO TUHKANEN



TALLINN UNIVERSITY OF TECHNOLOGY

School of Engineering

Department of Civil Engineering and Architecture

This dissertation was accepted for the defence of the degree 24/03/2021

Supervisor:

Professor Alar Just
School of Engineering
Tallinn University of Technology
Tallinn, Estonia

Co-supervisors:

Professor Emeritus Karl Õiger, School of Engineering
Professor Targo Kalamees, School of Engineering
Tallinn University of Technology
Tallinn, Estonia

Opponents:

Professor Philipp Dietsch
Timber Engineering Section
University of Innsbruck
Innsbruck, Austria

Assist. Professor Robert Jockwer
Division of Structural Engineering
Department of Architecture and Civil Engineering
Chalmers University of Technology
Gothenburg, Sweden

Defence of the thesis: 05/05/2021, Tallinn

Declaration:

Hereby I declare that this doctoral thesis, my original research, and achievement, submitted for the doctoral degree at Tallinn University of Technology has not been submitted for doctoral or equivalent academic degree.

Eero Tuhkanen

signature



European Union
European Regional
Development Fund



Investing
in your future

Copyright: Eero Tuhkanen, 2021

ISSN 2585-6898 (publication)

ISBN 978-9949-83-686-4 (publication)

ISSN 2585-6901 (PDF)

ISBN 978-9949-83-687-1 (PDF)

Printed by Koopia Niini & Rauam

TALLINNA TEHNIKAÜLIKOO
DOKTORITÖÖ
20/2021

Sisefreesitud terasplaadiga naagelliited ristkihtliimpuidust jäikusseintes

EERO TUHKANEN



Contents

List of Publications	7
Author’s Contribution to the Publications	8
Abbreviations	9
Symbols	10
1 INTRODUCTION	12
1.1 Background	12
1.2 Aim and structure of the thesis.....	14
1.3 Research questions and objectives	15
1.4 Outline of the thesis.....	15
1.5 New knowledge and practical applications.....	15
2 CONNECTIONS IN PREFABRICATED MODULAR BUILDINGS	16
2.1 Framework	16
2.2 Optimised connections	16
2.3 Connection design criteria in prefabricated room modules	18
2.4 Cross-laminated timber for shear wall system	21
3 SLOTTED-IN STEEL PLATE CONNECTION WITH DOWELS.....	28
3.1 Framework	28
3.2 Previous studies on slotted-in steel plate connections.....	29
3.3 Design of slotted-in steel plate connection with two shear planes	30
3.4 Self-perforating dowels.....	31
3.5 Yield moment of the dowel.....	31
3.6 Embedment strength in solid timber	32
3.7 Embedment strength in cross-laminated timber	34
4 METHODS.....	37
4.1 General.....	37
4.2 Connection tests	37
4.2.1 Test methods and evaluation of the results	37
4.2.2 Description of the tested specimens.....	38
4.2.3 Methods for data validation and comparison.....	41
4.3 Embedment strength tests and databases	42
4.3.1 Test method and evaluation of the results	42
4.3.2 Description of the tested specimens.....	43
4.3.3 Methods for data comparison	50
4.3.4 Regression analysis for model prediction	51
4.4 Shear wall test.....	53
4.4.1 Test method and evaluation of the results.....	53
4.4.2 Description of the tested specimen	53
4.4.3 Selected models for test validation.....	54
5 RESULTS, ANALYSIS AND DISCUSSION	59
5.1 Embedment strength in cross-laminated timber	59
5.1.1 Results of database BU	59
5.1.2 Results of databases TO, TMS and 50 50	59
5.1.3 Influence of the moisture content	61
5.1.4 Influence of the density	61

5.1.5 Influence of the diameter	62
5.1.6 Influence of the loading angle.....	64
5.1.7 Influence of the layer thickness and layup.....	65
5.1.8 Remarks on influencing factors.....	69
5.1.9 Embedment strength model analysis and proposal.....	71
5.2 Connection test results	73
5.2.1 Yield moment of the dowel.....	73
5.2.2 The load-carrying capacity of the dowel and the rope effect	74
5.2.3 Comparison with EYM and the application of new embedment strength model .	77
5.3 Racking strength and stiffness of the wall	79
5.3.1 Test result.....	79
5.3.2 Comparison of the result with selected design models.....	79
6 CONCLUSION.....	83
References	85
Acknowledgements.....	93
Abstract.....	95
Lühikokkuvõte.....	96
Appendix	97
Curriculum vitae.....	98
Elulookirjeldus.....	99

List of Publications

The list of the author's publications where the main results of the thesis have been published:

- I Tuhkanen, E., Mölder, J., & Schickhofer, G. (2018). Influence of number of layers on embedment strength of dowel-type connections for glulam and cross-laminated timber. *Engineering Structures*, 176, 361–368. <https://doi.org/10.1016/j.engstruct.2018.09.005>
- II Tuhkanen, E., & Ojamaa, M. (2019). Early experimental investigations on slotted-in steel plate connections with self-perforating dowels in CLT. *Wood Material Science and Engineering*. <https://doi.org/10.1080/17480272.2019.1626482>
- III Tuhkanen, E., & Rauk, L. (2019). Potential of cross-laminated timber for independent shear wall systems. *Wood Material Science & Engineering*, 14(5), 355–365. <https://doi.org/10.1080/17480272.2019.1638450>
- IV Tuhkanen, E., & Hübner, U. (2021). Embedment strength of cross-laminated timber for dowels in slotted-in steel plate connections. (ACCEPTED for publication in *WCTE* 2021)

Author's Contribution to the Publications

The author of the thesis is the principal author in all of the publications.

In I, analysis of the measured data, writing of the manuscript and post-review editing was carried by the author.

In II, III and IV, the author performed the tests, analysed the measured data, wrote the manuscript and performed post-review editing.

Abbreviations

BIM	Building Information Modelling
CAD	Computer-Aided Design
CAM	Computer-Aided Manufacturing
CNC	Computer Numerical Control
CV	Coefficient of variation
DoP	Declaration of Performance
EYM	European Yield Model
FEA	Finite Element Analysis
HSS	High strength steel
LVDT	Linear variable differential transformer
LVL	Laminated veneer lumber
OSB	Oriented strand board
PoR	Point of rotation
RH	Relative humidity
SLS	Serviceability limit state
TRTL	Thickness ratio of a transverse layer in cross-laminated timber
ULS	Ultimate limit state
UHSS	Ultra-high-strength steel

Symbols

Latin capital letters

F	-	Load
$F_{ax,Rk}$	-	Characteristic withdrawal capacity of the fastener
$F_{C,x(z),m}$	-	Appearing load for connection according to the respective displacement of the connection
F_{max}	-	Maximum load
$F_{max,est}$	-	Estimated maximum load
F_{rg}	-	Load responsible for rocking
F_{sl}	-	Load responsible for sliding
F_u	-	Ultimate load
$F_{v,R}$	-	Load-carrying capacity of one shear plane
F_y	-	Yielding load
K_{ser}	-	Stiffness
$M_{y,R}$	-	Yield moment of the fastener
T	-	Tensile strength of the connection

Latin lower-case letters

d	-	Fastener diameter
d_{ref}	-	Reference diameter
f_c	-	Compressive strength of cross-laminated timber
f_h	-	Embedment strength
f_u	-	Tensile strength of the fastener
f_y	-	Yield strength of the fastener
h	-	Height of the wall
l	-	Length of the wall
m	-	Sample mass
Δm	-	Adhesive layer mass
n_{ef}	-	Effective number of fasteners
p	-	Share parameter
q	-	Uniformly distributed load
t_{CLT}	-	Total thickness of cross-laminated timber panel
t_{eff}	-	Width of the vertical lamellas of the panel
t_1	-	Timber thickness on one side of the steel plate, or the extent of the length of the dowel in the timber side
$t_{0,i}$	-	Thickness of the layers parallel to the grain direction of the outer layers in cross-laminated timber
$t_{90,i}$	-	Thickness of the layers perpendicular to the grain direction of the outer layers in cross-laminated timber
u	-	Moisture content
u_{ref}	-	Moisture content reference value
x	-	Compression zone length
x_m	-	Distance between PoR and connection m

Greek letters

α	-	Load-to-grain angle
ζ	-	Build-up factor of cross-laminated timber
v_{con}	-	Lateral displacement of the wall due to the connections
$v_{C,x,m}$	-	Lateral (horizontal) displacement of the connection m
$v_{C,z,m}$	-	Uplift (vertical) displacement of the connection m
v_{rg}	-	Lateral displacement of the wall due to the rocking
v_{sl}	-	Lateral displacement of the wall due to the sliding
v_u	-	Displacement at ultimate load
v_y	-	Displacement at yielding load
ρ	-	Density of wood

1 INTRODUCTION

1.1 Background

The timber construction sector today is increasingly moving towards prefabricated buildings using room modules (see Figure 1), especially in urban areas. The rapidly growing need for new and affordable living space is forcing producers to find responses to this demand. Systemisation, simplification and the associated reduction have (again) gained importance in today's construction (Schickhofer & Ganster, 2018). Use of repeated sections (modules) at the level of both building components (floors, walls) as well of three-dimensional room units creates premises for optimised structure, lean manufacturing, transportation, and on-site assembly.



Figure 1. Left: room module's manufacturing; right: on-site assembly. Photos by Harmet.

Off-site production shortens the entire building process and minimises the structure's exposure to rain, wind, and snow, which is the main disadvantage of on-site building. Thanks to BIM/CAD/CAM solutions and CNC machines, manufacturers' planning, preparation, production, and logistics are very advanced. In addition to the cutting of structural components, the assembly of modular parts (walls, floors) and complete modules is partially automated. Most finishing and service installations are done in a factory, meaning that the amount of on-site work is limited to the preparation of the ground, foundation and anchoring, and the closing of the interconnections between the modules. The use of timber in modules is also supported by its low weight and, consequently, by its more economical transport and assembly costs. One lift on the site equals an entire space unit, compared to one surface (wall, floor) or beam element for reinforced concrete.

Building construction and operations accounted for 36% of global end energy use and nearly 40% of energy-related carbon dioxide (CO₂) emissions in 2017 (International Energy Agency and the United Nations Environment Programme, 2018). This fact forces upon timber the responsibility to reduce CO₂ emissions in the construction sector. Trees bind carbon, which, through the use of wood, is removed from the carbon cycle for a long time. Moreover, local use of regionally available resources avoids long transport routes and strengthens rural areas, while also adding a positive sociological and political dimension. Consequently, the main reasons for the entry of prefabricated modular timber buildings into the urban construction market are the efficiency of the construction process and stricter environmental requirements.

Solid timber was previously used as a primary supporting structure that set the boundaries for the building. However, modern materials such as glued laminated timber

(glulam), cross-laminated timber, and various hybrid and composite structures are increasingly replacing or improving solid timber, creating new opportunities in building heights and free spans. Furthermore, cross-laminated timber enables us to use timber as a two-dimensional element with high in-plane strength and stiffness, allowing for greater architectural freedom.

Timber connections serve the purpose of connecting individual structural elements and building components effectively into one complete system. However, timber tends to fail brittle when loaded in tension, and connections are also needed to ensure a structure's plastic behaviour. Alongside load-carrying capacity, the connection's stiffness and ductility (plastic deformation capacity) must be considered in design (Gehri, 1993).

In prefabricated modular multi-storey buildings, the load-deformation behaviour of the connections affects the entire system, especially when calculating the lateral stiffness of a structure. Due to the complexity of a modular system, complicated design and ensuring structural integrity are the primary drawbacks and concerns in the modular building value chain (Sharafi et al., 2018). Therefore, a clear and easy-to-interpret stabilisation strategy would be an advantage. One possibility has been discussed in literature by Vessby & Olsson (2006) and Ringhofer & Schickhofer (2014), where continuous cross-laminated timber wall strips throughout the building's height were used. Such an approach ensures that horizontal loads are directly transmitted to the foundation, thus also enabling a simplified design (Ringhofer & Schickhofer, 2014). Expanding on this idea, an independent shear wall system for stabilisation can be obtained, avoiding the vertical load from the adjacent structure (see Figure 2). Independence is expressed both in the free placement of the wall and in the calculations, where horizontal load only is applied, separated from vertical actions. A crucial part of such a system is the shear wall connection to the foundation.

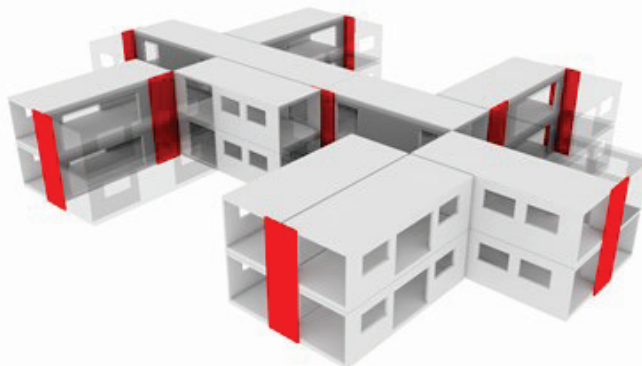


Figure 2. Independent shear wall system in modular building

Another important aspect of connection technique is related to the quick and accurate assembly of the modules. Conventional fasteners and connectors for on-site building may not be applicable for room modules, not only in terms of installation but also in terms of automated manufacturing. In the same context, it would also be relevant to introduce building recycling at the end of the lifecycle. An appropriate connection system must ensure the possibility of replacing or reusing individual load-bearing and non-load-bearing components or dismantling the entire structure to return the raw material to the natural cycle.

Prefabricated modules have great potential for highly standardised, automated, and flexible solutions, not only at the level of construction components but also in design. In essence, this must be strongly supported through the connection technique, considering the abovementioned areas.

Slotted-in steel plate connected with dowels is an appropriate solution to centre the connection, reduce local disturbances in the load transfer mechanism and increase the load-carrying capacity and stiffness. When using self-perforating dowels instead of smooth dowels, it is possible to overcome manufacturing-related issues of such a type of connection and automate the production. Furthermore, threaded parts of self-perforating dowels allow disassembling of the joint. For these reasons, a slotted-in steel plate connected with self-perforating dowels would be an essential supplement in the modular building value chain.

1.2 Aim and structure of the thesis

This thesis investigates the slotted-in steel plate connection with self-perforating dowels in cross-laminated timber shear wall. The focus lies on the input parameters of the connection design – embedment strength and properties of the dowel. The application of the work is dedicated to the efficient use of the connection in the shear wall. In the broadest sense, the subject is driven by bottlenecks in the construction and design of modular houses.

Figure 3 presents the overall framework and structure of the thesis. In the parameter study, embedment strength was researched in several unique laboratory experiments, and the design model validated and revised using an extensive database provided by Blass & Uibel (2007). The primary focus in this study was to find to what extent does the range of neighbouring crossed layers influence each other.

The tests performed with slotted-in steel plate connection had two purposes: to validate the results of embedment tests and to investigate the influence of the properties of self-perforating dowels to the load-bearing capacity of the connection. In addition to that, connections' load-deformation behaviour was studied for practical implementation. These results were used in the shear wall design.

To demonstrate the application and optimal use of slotted-in steel plate connection in cross-laminated timber shear wall, a full-scale test was performed. Test results were compared with the analytical method proposed by Flatscher (2017), to highlight the importance of the design model.

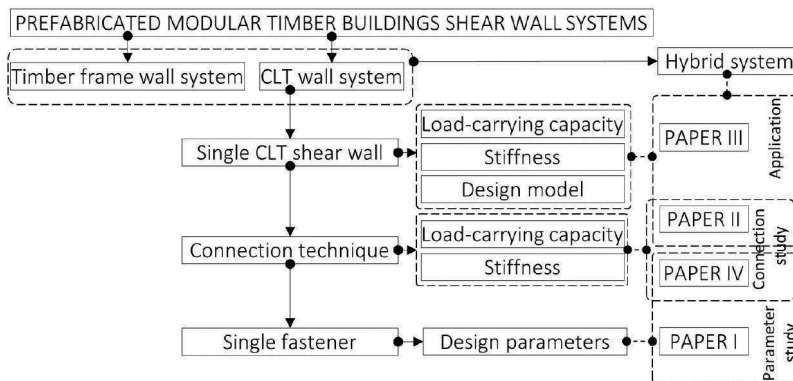


Figure 3. Structure of the thesis and appended papers

1.3 Research questions and objectives

The explicit objectives and research questions are as follows:

- How do the configuration and thickness of layers influence the embedment strength of cross-laminated timber?
- To what extent does the range of neighbouring crossed layers influence each other?
- How do the properties of a self-perforating dowel influence the connection's load-carrying capacity in cross-laminated timber?
- How to utilise the connection in the cross-laminated timber shear wall maximally?

1.4 Outline of the thesis

The thesis is divided into six chapters. The second chapter discusses the requirements of timber connections in prefabricated modular buildings and their shear-wall systems. The primary purpose is to provide broader insight into the topic. The third chapter focuses specifically on slotted-in steel plate connection with self-perforating dowels and input parameters for the design. This chapter defines the main research questions. The fourth chapter describes the methods to achieve the goals of the study. Important information about the test specimens and embedment strength database provided by Blass & Uibel (2007) is also summarised in chapter four. The fifth chapter presents the results of the tests, data analysis, and proposals made based on them. Chapter six concludes the outcome of the thesis.

1.5 New knowledge and practical applications

The thesis presents the following new knowledge:

- The factors affecting the embedment strength in cross-laminated timber for dowels were re-analysed, and influence of the layer thickness has been found.
- New embedment strength model for cross-laminated timber with layer thicknesses used in practice has been proposed.
- The influence of the drill tip and threaded part of the self-perforating dowel on the connection's load-carrying capacity has been found and explained.
- Application of slotted-in steel plate connection for the cross-laminated timber shear wall has been proposed, and the benefits of this type of connection were highlighted.

Stiffness K_{ser} is mainly related to the serviceability limit state (SLS) and is characterised by a linear part of the load-displacement curve of the connection. In a bolted connection, additional play due to the borehole must be considered – expressed by the additional axis in Figure 4. The consideration of stiffness is due to the need to limit the total vertical displacement of long-span structures with multiple joints such as trusses, or horizontal displacement (storey displacement) in shear wall systems. In ultimate limit state (ULS), connections with high stiffness have the advantage in bracing systems, such as improving structural performance. For more sophisticated non-linear analysis of statically indeterminate structures, prediction of the complete load-slip curve instead of stiffness may be required (Thelandersson & Larsen, 2003).

In design, a balance between load-carrying capacity, ductility, and stiffness must be achieved, resulting in an optimised connection. When looking for similarities with steel structures, a bilinear load-deformation relationship of low carbon steel would be desirable for timber connections. High stiffness in the linear elastic part and pronounced plastic behaviour are qualitative measures for optimal connection – see Figure 4. For example, using a glued lap joint in a tension member, high stiffness and capacity without any ductility can be reached. When replacing the lap joint with a glued-in rod connection, ductile behaviour is possible but must be targeted at the steel rod to avoid possible brittle failure modes (Tlustochowicz, 2011; Tlustochowicz et al., 2011). Commonly used connections with dowel-type fasteners loaded perpendicular to their axis can show very high plastic deformation capacity, but with low stiffness and degree of utilisation of the cross-section. For efficient use of the member loaded in tension, the load path in the connection must be as undisturbed as possible. Holes in the connected members and complicated load path through contact surface between dowel and timber will reduce the load-carrying capacity by up to 50% compared to the member without connection (Schickhofer, 2009). Furthermore, in the case of a connection with one shear plane, additional stresses due to the high eccentricity must be considered (Rug & Mönck, 2015) – see Figure 5 (left).

A slotted-in steel plate could be an appropriate solution to reduce local disturbances in the load transfer mechanism and increase the stiffness – see Figure 5 (right). According to EN 1995-1-1 (CEN, 2009a), the stiffness of the steel-to-timber connection is multiplied by 2.0 compared to the timber-to-timber connection. When using smooth dowels instead of bolts, the borehole play presented in Figure 4 can be ignored.

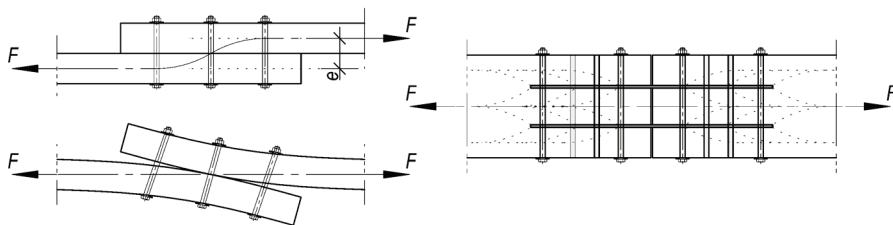


Figure 5. Left: eccentric connection; right: centred connection with slotted-in steel plate

2.3 Connection design criteria in prefabricated room modules

Three criteria (load-carrying capacity, stiffness of the connection and ductility) discussed in Chapter 2.2 are crucial for timber trusses and frames, where brittle failure in tensile members is somewhat likely, or stiffness of the connection plays a key role in structural performance. The load-bearing components of a prefabricated room module – walls and floors – are usually timber frame structures or cross-laminated timber plates. For transportation, the reasonable dimensions of the modules are 5.3×14.5 m, with a height of up to 4.5 m. In such constructions, the connections between the structural components are generally accomplished through contact surfaces (beam-column; plate-wall), and fasteners are used for fixing purposes. The typical timber frame and cross-laminated timber room modules are presented in Figure 6, and relevant examples of connections between components in Figure 7.



Figure 6. Left: timber frame module; right: cross-laminated timber module (Huß et al., 2018)

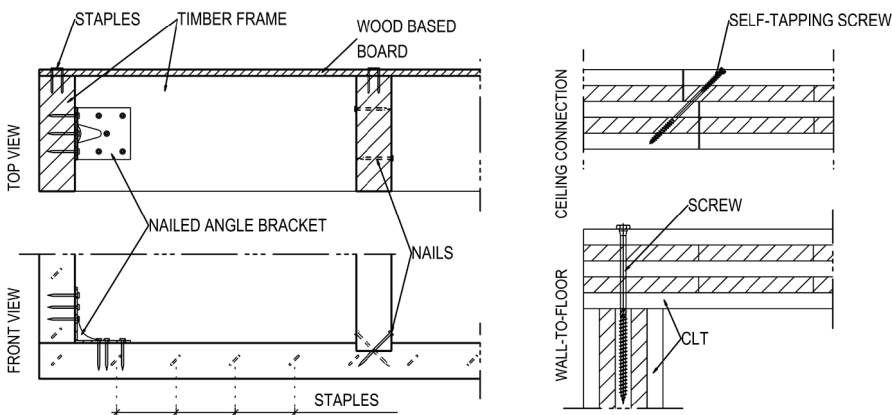


Figure 7. Left: connections in timber frame wall element; right: cross-laminated timber room module connections

In these connections, the requirements are more related to production speed and automation. Trimming of timber frame parts or cross-laminated timber panel processing in a computer numerical controlled (CNC) milling station is already part of the process for many medium-sized companies. Automated framing stations and robot portals are the next level of the assembly process – see Figure 8. Connections between module components affect this in terms of process speed and cost-effectiveness. Fasteners that

do not require pre-drilling or are quick to install – small nails, screws, and self-perforating dowels – would be an advantage.

Completed modules are transported to the building site and assembled. At this stage of construction, the requirements for joints between modules and connections to the foundation are related to site erection speed, feasibility, and accessibility.

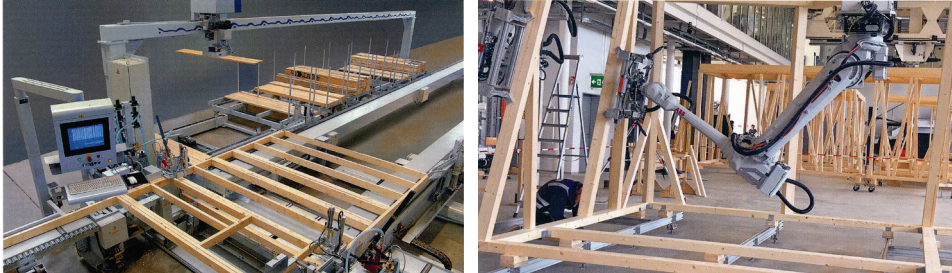


Figure 8. Left: production of a stud frame at a framing station (Kaufmann et al., 2018); right: robotically controlled room module assembly (Huß et al., 2018)

Finally, the complete building must be able to withstand the loads assigned to it, highlighting the need for optimally designed connections, which affects the behaviour of the entire system. From an engineering perspective, this primarily concerns ensuring the lateral stiffness and integrity of a structure. A modular system with its deceptive simplicity – installation of room cells on top of each other – conceals several complications, paradoxically related explicitly to modularity. These are explained in the paragraphs below.

The stabilising strategy of traditional buildings follows the principle where the floor level forms a rigid diaphragm to transfer horizontal loads, i.e. wind and seismic loads, to the shear walls. Adequate racking resistance at each floor level, down to the foundation, must be provided to stabilise the building, schematically shown in Figure 9. The diaphragm consists of the ceilings of adjacent modules, which are connected with a wood-based board, such as OSB, plywood or LVL. See the principle of the room module system and interconnections in Figure 10.

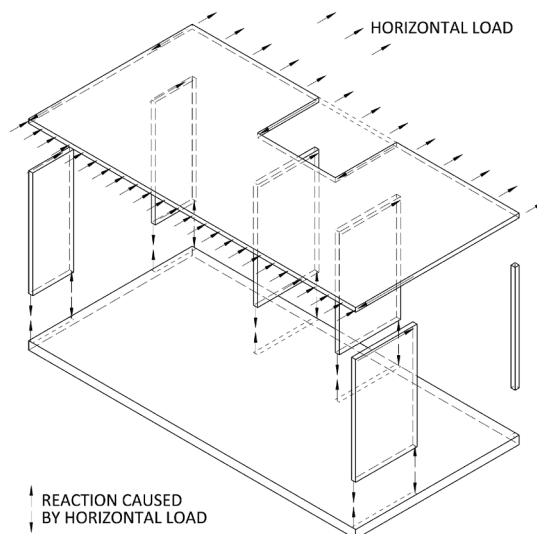


Figure 9. Building stabilisation principle (in one direction): floor diaphragm and shear walls

The connection between diaphragm and shear wall depends on the shear wall type. Determined by the height of the building and fire regulations, the use of reinforced concrete staircase or elevator shaft is a relatively common strategy in use to ensure the horizontal stiffness of the building. The main disadvantage of this system is the difference in work character and tolerances, adding further operations to the construction and the entire project. Concrete work is done on-site, while modules are produced in a factory in a controlled environment with high precision. These tolerances must be considered when detailing the connection between module and concrete structure. There is also a difference in the long-term behaviour of the modules and the concrete wall. In practice, long-term vertical displacement of around 5 mm per floor is taken into account when designing the transition of a timber frame module to a more rigid structure. In cross-laminated timber buildings, this issue is also investigated by Serrano et al. (2010, 2014).

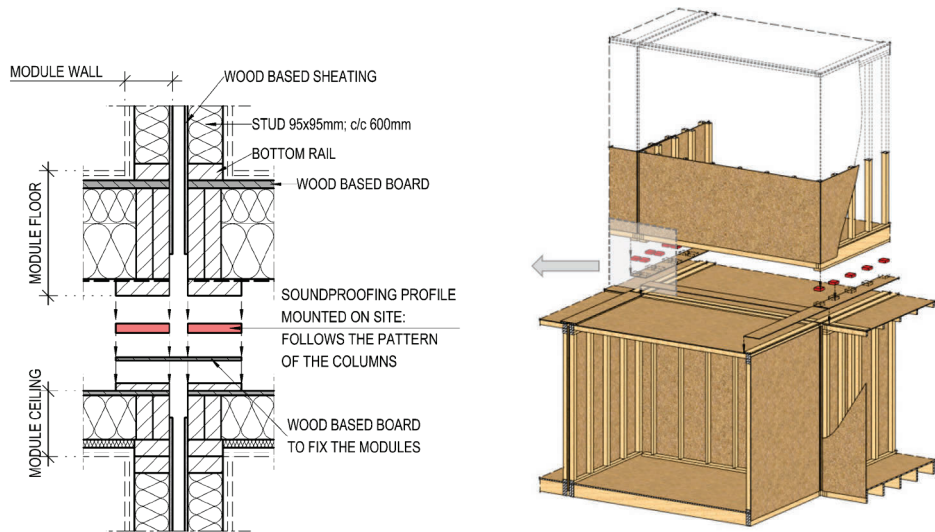


Figure 10. Principle of the interconnection between modules

Another way to stabilise the complete building is by using natural module walls. It requires engaging the engineer in the early stages of process planning. Modules must have a sufficient number of walls in two transverse directions placed on top of each other throughout the building height, which sets the boundaries for architecture and restricts the freedom in floor plans. However, the functionality of such a shear wall is questionable for the following reason.

In the final stage, when the building is completed, inner floors and walls are doubled, and there is free space between the room units. Modules within one storey are connected using a wood-based board at the ceiling level, and vertical joints are found only on the outer perimeter of the building, rather than in the modules' intersections. For connections between the room units on different storeys, the outer border is bound with a wood-based board. In other places, the modules remain on one another, with a resilient soundproofing profile between them, having no continuity in a vertical direction against uplift – see Figure 10.

Missing structural integrity in the vertical direction against uplift sets limits for the design of the shear wall for horizontal loads. The standard for timber structures,

EN 1995-1-1 (CEN, 2009a) differentiates between two simplified methods for racking resistance verification:

- Method A is most commonly used in Europe in domestic house calculations, and it assumes the leading stud of the wall is anchored to avoid overturning.
- According to Method B, the destabilising effect is prevented by the length of the wall base fixing (Porteous & Kermani, 2007). In the context of a multi-storey building, no further information is given.

Källsner & Girhammar (2009) developed a plastic model based on Method B, considering the real situation in common timber frame building practice. It also applies to multi-storey buildings, presuming that walls at the floor level are continuously anchored, and also that transverse walls can be considered. Since sufficiently large ductility of the joints between sheathing and frame is assumed in this model, special attention must be paid to this. The recommendations for detailing these connections are given in (Girhammar & Källsner, 2016).

An extended model, which considers the effect of the connections to the foundation and between floors, when they are accomplished in a point-fixing manner (by using angle brackets or hold-downs), was developed by Casagrande et al. (2016). The method is also suitable for CLT shear walls. However, taking into account the principle of the modular system in Figure 10, anchoring the leading studs or continuous sheathing in the internal wall intersections may be complicated or infeasible. Furthermore, the anchors will affect the reduction of flanking transmission provided by the rubber layer (Morandi et al., 2018).

One way to solve this is to avoid uplift forces in the shear wall corners by balancing it with the module's self-weight, which might lead to a very complex calculation. Using finite element software, a compression-only connection between modules in floor level requires a non-linear model. Especially complicated and time-consuming is the modelling of timber frame with wood-based board sheathing because the shear wall is an assemblage of one- or two-dimensional elements in the sense of finite elements. Lateral stiffness of the wall is mainly affected by the sheathing to framing connection (Colling, 2017). Depending on the level of detail, describing these relations in the software will increase the file size of the model, which requires high-performance hardware.

2.4 Cross-laminated timber for shear wall system

An alternative stabilisation strategy, which uses a continuous cross-laminated timber wall strip through the building's height, can be found in the literature by authors such as Vessby & Olsson (2006) and Ringhofer & Schickhofer (2014). This type of approach to stabilisation ensures that horizontal loads (wind and earthquake) are directly transmitted to the foundation, also enabling a simplified design (Ringhofer & Schickhofer, 2014).

Cross-laminated timber is increasingly used as the main structure in conventional multi-storey buildings, as well in three-dimensional modules (Huß et al., 2018; Kaufmann et al., 2018). Its production is almost entirely automated, and building components are prefabricated. Therefore, this product fits perfectly into the paradigm of modular construction.

In the context of a prefabricated modular system, a continuous cross-laminated timber shear wall could be implemented in different ways. The modules are naturally placed as a pattern of boxes with some space between them, which allows the placement of the shear wall without changing the main structure significantly. Avoiding any direct

vertical load on the shear wall will make the system independent – the stabilising wall is placed freely in a relevant position on the plan as required, also reducing architectural planning restrictions. Moreover, the manufacturer can develop a system with repetitive components and modules forming the main structure, and this will be combined with the independent stabilising system. The only connection is the floor-to-wall joint to transfer the horizontal load from the ceiling diaphragm to the shear wall. It may not be necessary on every floor, and the connection may be omitted. Such an arrangement also minimises the flanking transmission along with the structure. See the independent shear wall system principle in Figure 11.

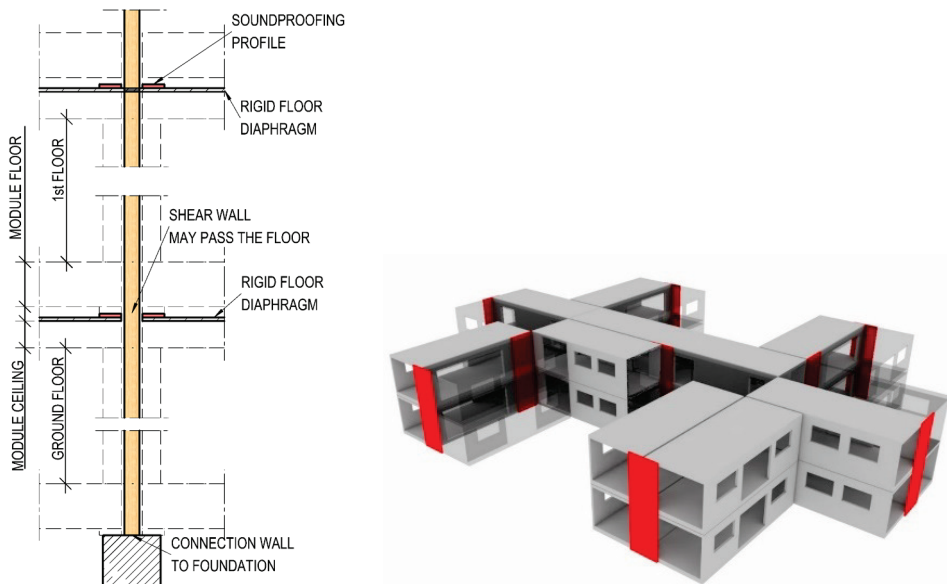


Figure 11. Principle of independent shear wall system in modular building

One of the possible ideal outputs for such an approach is the $n \times [M]$ raster-based standardisation and prefabrication system discussed by Schickhofer & Ganster (2018). Raster not only simplifies the production of repetitive elements, but is also a prerequisite for parametric design and simplified, or even tabulated calculation. It seems to be useful to keep the module's structure as simple as possible, preferably as a post-slab type. Doing so makes it easier to separate non-load-bearing parts – internal walls and even façades – from the load-bearing structure. Floors and columns of three-dimensional room units care for the entire vertical load, while the additional part from the wind is transferred to separate shear walls. As an example, System 369, Tallinn Pattern Building (Project AURP, 2019) is presented in Figure 12.

The shear wall configuration may be merely a robust cross-laminated timber plate connected to the foundation through the lower edge (see Figure 12 left) or combined with steel columns at the side edges, presented in Figure 13. In the latter case, the cross-laminated timber plate is loaded only in shear since the steel columns are anchored to the foundation and will take the compression and tension caused by the horizontal load. An additional benefit of such a system is that the shear wall may be part of the three-dimensional room module and not separated from the main structure.

The use of cross-laminated timber in shear walls depends significantly on the connections (Brandner et al., 2016). In order to improve the structural performance of the system, optimised connections, as discussed in Chapter 2.2, are crucial for exploiting the full potential of cross-laminated timber. Studies concerning cross-laminated timber shear walls are mostly related to the seismic behaviour of the building, and research and developments of the connections focus on ductility and energy dissipation, while cross-laminated timber plates are almost considered to be rigid bodies (Ceccotti et al., 2013; Hristovski et al., 2013, 2018). Examples of commonly used angle brackets, nailing plates and hold-downs presented in Figure 14 are investigated by Gavric et al. (2015), Latour & Rizzano (2015); Pozza et al. (2018), for example. The majority of innovative developments in improving energy dissipation are based on friction and steel plasticisation in the connection. Hashemi et al. (2017) investigated Resilient Slip Friction (RSF) joints, Polastri et al. (2017) X-rad system. A dissipative X-bracket concept was studied and tested by Scotta et al. (2016) and Trutalli et al. (2019).

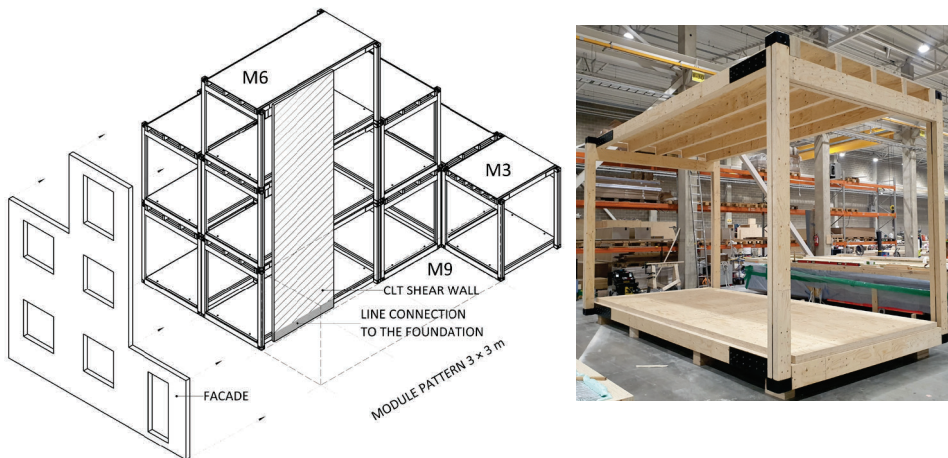


Figure 12. Left: the principle of the System 3-6-9, Tallinn Pattern Building (Project AURP, 2019); right: prototype of module M6 (photo taken by Egle Vogt)

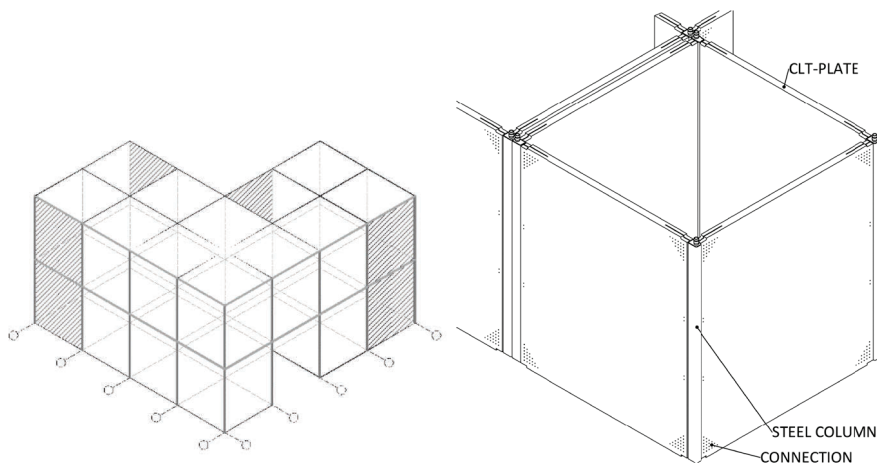


Figure 13. Left: the principle of the raster-based box system – shear walls are hatched; right: an example of one module with steel columns

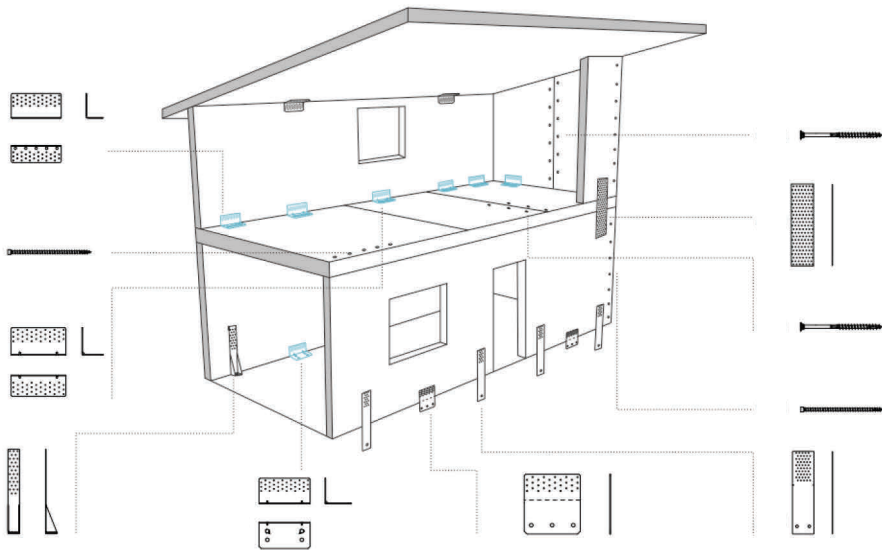


Figure 14. Connection technique for timber building (Rothoblaas, 2019)

The main concern in non-seismic areas is wind load, and in calculations, the decisive factor is wall stiffness rather than load-bearing capacity. Although EN 1995-1-1 (CEN, 2009a) sets no limits for horizontal displacement, a maximum permitted storey drift of $h/500$ can be found in some countries on a national level, such as in the Finnish Handbook (RIL205-1, 2017) and the German national standard DIN (DIN, 1994). h indicates the height of the floor or building. When applying a horizontal force to the top of the cross-laminated timber wall, four possible deflection types will occur – (a) sliding, (b) rocking of the rigid body, (c) shear deflection of the wall, and (d) bending (see Figure 15). In ordinary cases, deformation types (c) and (d) are neglected while the contribution of the connections is determinative, except for walls with large height-to-length ratios, see, e.g. (Casagrande et al., 2016). The most crucial part is the connection to the foundations, as this determines the efficiency of the entire system.

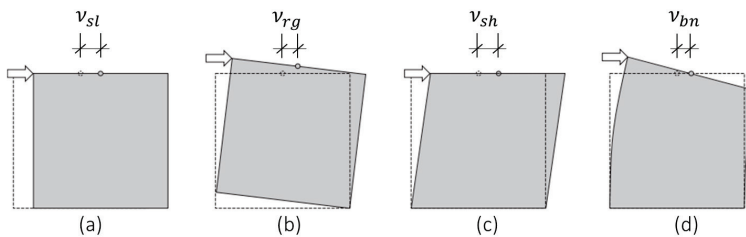


Figure 15. Deflection types of the cross-laminated timber shear wall

The angle brackets and hold-downs in Figure 14 are located outside the panel, and the load transfer to the substructure is eccentric to the wall axis. Connections with high eccentricity cause greater deformations and reduce the load-carrying capacity (Tomasi & Smith, 2015). Furthermore, laboratory tests are the only reliable means for determining design capacities for certain types of angle bracket connections. For floor-to-wall connections, improved angle brackets for shear and tensile loads combined with screws have been developed by (D'Arenzo et al., 2019) – see Figure 16 (left).

However, the eccentricity at half of the wall thickness remains, and such a solution is not suitable for connection to the foundation. Furthermore, angle brackets may be infeasible in a modular system.

The connection should be applied to the wall centre to exploit cross-laminated timber's potential as much as possible. One example of a centred wall connection is X-RAD (Polastri et al., 2017). The prefabricated system is designed to connect the cross-laminated timber plates at corners using bolts on the building site. The corner piece is a complex combination of steel and hardwood, screwed into the panel – see Figure 16 (right). Due to the accuracy and diverse range of joint configurations, it is a suitable solution for building systems made entirely of planar cross-laminated timber elements. While it is mainly intended for use in seismic areas, the failure of the connection is targeted to the steel part to have sufficient ductility in the corner. On the other hand, a high load concentration in the panel corner will increase the risk of unexpected brittle failure modes. Polastri et al. (2018) registered six failure types due to the sophisticated design of X-RAD.



Figure 16. Left: angle bracket Titan V; right: X-RAD fastening system (Rothoblaas, 2019)

Nakashima, Kitamori, Komatsu, et al. (2014) tested a cantilever cross-laminated timber shear wall connected at the lower corners with a slotted-in steel plate using conventional smooth dowels with a diameter of 16 mm. During the test, rolling shear, group shear, and split failure in the corner joint with multiple dowels were observed. In the pure tensile test with the same lamination configuration and dowel diameter of 12 mm in multiple rows, split failure on the sides prevailed (Nakashima et al., 2016). No bolts were used in the connection to prevent splitting. New types of failures in cross-laminated timber connections due to the crossed layers are also noted by Zarnani & Quenneville (2015), Blass & Uibel (2007) and Ottenhaus et al. (2016).

Another aspect of using smooth dowels is manufacturing effort. Slotted-in steel plate connection needs precise drilling separate for steel plate as well as for cross-laminated timber plate. Installation of the dowels is entirely feasible under factory conditions, although, in the case of multiple steel plates, it is particularly problematic (Mischler, 2001). For on-site assembly, somewhat greater tolerances are foreseen, which reduces the load-carrying capacity and stiffness of the connection.

A different concept and case studies were provided by Bernasconi (2016a, 2016b). The connections between the foundation and the shear wall, as well as between the floors, were realised as continuous lines, not a punctual manner. T-shape steel and self-perforating dowels were part of the connection, presented in Figure 17. According to the author's claims, this configuration would be the only way to avoid the concentration of the forces in the wall panel, assure regular force flow, and maximise the potential of cross-laminated timber.

The second reason for avoiding commonly used angle brackets in those projects was their low stiffness, and load resistance (also discussed previously). In addition to that, a self-perforating dowel was considered to be the simplest solution due to the building tolerances. Based on experience, it could be argued that installation of the self-perforating dowel needs a considerable amount of pressure by drilling, which can be challenging to achieve from a horizontal position on the building site. Therefore, a prefabricated solution or semi-automatic pre-installation on the building site would be more appropriate.

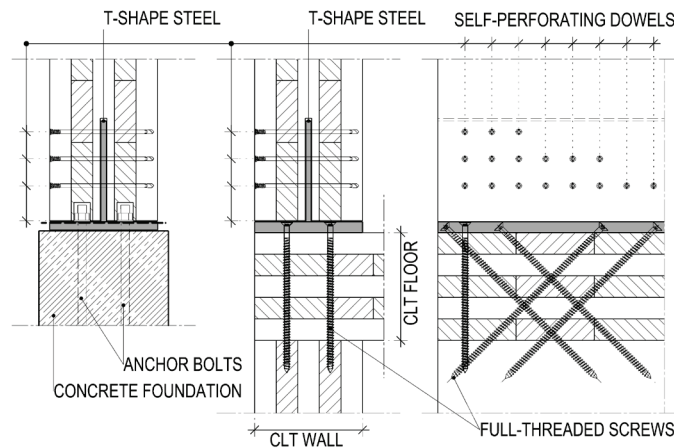


Figure 17. Shear wall connection with a T-shape steel. Left: Connection to the foundation; right: connection in the floor level. Drawing is reproduced from (Bernasconi, 2016a, 2016b)

In addition to choosing the proper connection type for shear wall, an appropriate calculation model can help to maximise the result obtained. Design of cross-laminated timber shear wall includes an assessment of load-carrying capacity and stiffness. Considering the deflection types presented in Figure 15, wall geometry and connection properties are the input data for the equilibrium equation to resist external loading. A comprehensive overview of the available strength assessment methods is given in (Lukacs et al., 2019). Most of the available approaches treat connections resisting sliding and rocking (overturning) separately, i.e., vertical and horizontal forces in the connections do not interact and are taken by hold-downs and angle brackets accordingly. A more sophisticated iterative method is proposed by Gavric & Popovski (2014) where both shear and tension are considered in angle brackets, but not in hold-downs. In this case, the corresponding properties of the connections must be defined, and as stated in (Tomasi & Smith, 2015), laboratory tests may be the only reliable means.

In a complete building, when assuming the floor diaphragm to be rigid or semi-rigid, the distribution of the horizontal load between the walls depends on the stiffness of the walls (Chen et al., 2014). Five available stiffness assessment methods are also summarised in (Lukacs et al., 2019). Four of these analytical approaches allow the calculation of different type of deflections presented in Figure 15 when the maximum load is acting on the shear wall. Stiffness is calculated based on total wall displacement, which is the sum of all contributions (a)-(d).

A fundamentally different, displacement-based method proposed by Flatscher (2017) predicts the load-displacement behaviour of the cross-laminated timber shear wall. The most important difference for force-based models is that the outcome of the

iterative calculation process is the maximum permissible lateral load. The model takes into account the non-linear behaviour of the connection, and in advance, permits the consideration of the post-maximum softening branch, if it exists. As sliding and overturning behaviour are not analysed separately, the percentage of use of the connection as well as contributing connections under the wall can be maximised. Elastic deformation from panel shear and bending are added separately.

The most critical input of this calculation model is the displacement-based function to describe the behaviour of the connection in two directions: rocking and shear. It may be any linear, multi-linear or polynomial function; some analytical methods are discussed and proposed by Flatscher (2017). Therefore, the connection's precise, and clearly predictable load-displacement behaviour is preferable. Here, slotted-in steel plate connection with dowels may have the advantage due to its simplicity over the conventional angle brackets and hold-downs. Steps required to implement the method by Flatscher (2017) are described in Chapter 4.

3 SLOTTED-IN STEEL PLATE CONNECTION WITH DOWELS

3.1 Framework

A slotted-in steel plate connection is advantageous in the load transfer mechanism, as highlighted in the previous chapter. Therefore, this type of solution is also favoured in building component extension joints (Gehri, 2000; Schickhofer, 2009). As they are usually visible, smooth dowels with a round cross-section are often preferred to bolts for their visual appearance (Blass & Sandhaas, 2017), allowing for a concealed connection. Furthermore, in a concealed connection, exposure of steel parts to fire is diminished. Steel elements heat up quickly under fire conditions, and the cross-sectional temperature increase reduces the fire resistance of the connection (Erchinger, 2009).

Self-perforating dowels have been developed to overcome the issues in manufacturing, especially in the case of multiple steel plates (Mischler, 2001). Inevitable fabrication tolerances may reduce the load-carrying capacity due to the uneven load distribution in the connection (Rossi et al., 2016). A special drill-tip allows for accurate semi- or fully automated installation without pre-boring holes in timber and steel – see the example in Figure 18 (left). The shaft of the dowel fits perfectly in the timber as well as in the steel plate. The connection will activate without initial slip as soon as the load is applied (cf. Figure 4), also providing a stiffer joint.

Due to the dowel's geometry, it is naturally concealed on one side, and the cylindrical head is easy to hide and cover with caps, see Figure 18 (right). For these reasons, a self-perforating dowel would be an essential supplement in the modular building value chain.

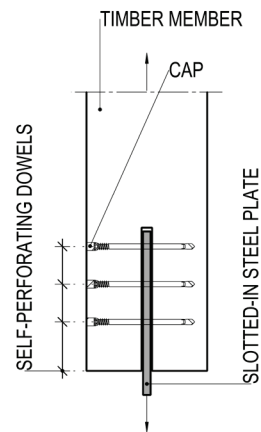


Figure 18. Left: Semi-automated installation of self-perforating dowel (SFS-Intec, 2019); right: concealed self-perforating dowel in the connection

This chapter briefly summarises the studies performed with slotted-in steel plate connections and introduces design rules. Then, two types of self-perforating dowels are presented to highlight their geometric characteristics compared to smooth dowels. The most relevant aspects of embedment strength as one of the main input parameters for design are outlined and then discussed from a cross-laminated timber perspective, which raises the main research questions of this thesis.

3.2 Previous studies on slotted-in steel plate connections

Slotted-in steel plate connections with smooth dowels are prevalingly used in trusses and frames; therefore, the primary research is related to solid timber and glulam. Mischler (1998) has investigated the significance of the ductility in steel-to timber connections. Sawata et al. (2006) has estimated the shear strength of the dowel type connection with multiple slotted-in steel plates according to the European Yield Theory, focusing on the spacing and numbers of the steel plates, and the timber thickness. Dorn et al. (2013) studied the load-carrying behaviour of the slotted-in steel plate connection in detail, changing the wood density and thickness. All loading stages from the initial contact between dowel and wood up to the ultimate load and failure were included. Additionally, the effects of lateral reinforcement and dowel roughness were assessed. A parametric study aimed at preventing a brittle failure in connections with multiple steel plates was conducted by Rossi et al. (2016).

Brittle failure modes in steel-to-timber connections loaded parallel to the grain are reviewed and assessed by Cabrero & Yurrita (2018); some approaches for the load direction perpendicular to the grain are discussed in (Jockwer & Dietsch, 2018). In her thesis, Sandhaas (2012) developed a three-dimensional material model for timber to consider anisotropy, different failure modes and the combination of brittle and ductile behaviour within one single model. In the tests made for validation purposes, dowels made of high strength (HSS) and ultra-high-strength steel (UHSS) steel were used (Sandhaas, 2012).

When considering the use of slotted-in connections in planar building components, such as a shear wall, cross-laminated timber seems to be a predominant choice as a base material. An example by Nakashima, Kitamori, Komatsu, et al. (2014) has already been mentioned. Kanazawa et al. (2018) used this connection type in cross-laminated timber plate corners infilled in steel frames. Application in cross-laminated timber frame extension joints was studied and demonstrated by Kitamori et al. (2014). More detailed, connection-specific investigations with cross-laminated timber made of Japanese cedar (*Cryptomeria japonica*) have been conducted by the same authors (Nakashima et al., 2012, 2016). A study about the effects of an arrangement of multiple steel plates in the cross-laminated timber connection can be found in (Sawata et al., 2016). Ottenhaus et al. (2016) and Ottenhaus et al. (2018) investigated structural performance, ductility and overstrength of large-scale dowelled cross-laminated timber connections under monotonic and cyclic loading. However, there is also an example of the use of slotted-in steel plate connection in the timber frame shear wall made of mechanically joined light-weight I-beams, I-studs and plyboard (Daerga et al., 2012).

There is very little research on self-perforating dowels, especially in cross-laminated timber. Mischler (2001) performed tests in glulam and concluded that, thanks to the slender dowels and not oversized holes in a steel plate, a ductile connection with high load-carrying capacity and stiffness could be attained. Schreyer et al. (2004) compared slender dowel-type fasteners, including self-perforating dowels under monotonic and cyclic loading in solid timber. They concluded that the advantages of a self-perforating dowel lie in the easier manufacturing process as well as slightly improved monotonic stiffness and strength.

The use of slotted-in steel plate connected with self-perforating dowels in cross-laminated timber was presented and discussed at both the conceptual and practical (case study) levels by Bernasconi (2016a, 2016b).

3.3 Design of slotted-in steel plate connection with two shear planes

In a slotted-in steel plate connection, the fastener is subjected to shear. The European Yield Model (EYM) first proposed by Johansen (1949) is based on the limit state approach and assumes that timber under embedding stress and the dowel under bending action behave as a rigid plastic material (Thelandersson & Larsen, 2003). The load-carrying capacity $F_{v,R}$ for one shear plane is derived from the equilibrium condition of forces and dowel bending moments in the connection, and is expressed as the minimum of Eq. (1).

$$F_{v,R} = \min \begin{cases} f_h \cdot t_1 \cdot d & \text{(f)} \\ f_h \cdot t_1 \cdot d \cdot \left[\sqrt{2 + \frac{4 \cdot M_{y,R}}{f_h \cdot d \cdot t_1^2}} - 1 \right] & \text{(g)} \\ \sqrt{4 \cdot M_{y,R} \cdot f_h \cdot d} & \text{(h)} \end{cases} \quad (1)$$

, where the designations in formulas and failure mode markings (f), (g) and (h) correspond to those given in EN 1995-1-1 (CEN, 2009a): t_1 - timber thickness on one side of the steel plate, or the extent of the length of the dowel in the side timber [mm]; f_h [N/mm²] - embedment strength of the timber; $M_{y,R}$ [Nmm] - yield moment of the fastener; d [mm] - fastener diameter. Three corresponding failure modes are presented in Figure 19.

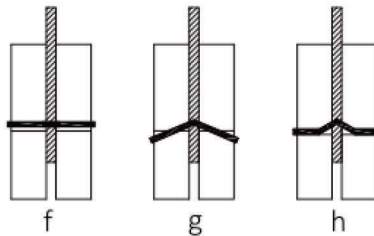


Figure 19. Failure modes of a slotted-in steel plate connection

Besides the joint and dowel geometry, the strength properties of the wood or wood-based material and the fastener must be dealt with independently. It must be noted that in EN 1995-1-1 (CEN, 2009a), the strength values in Eq. (1) are calculated for the characteristic instead of the mean. Therefore, additional partial safety coefficients are used in mode (h) for steel and timber (Blass & Sandhaas, 2017).

As shown in Figure 19, in failure mechanisms (g) and (h), the fastener is inclined over half of the length. The resulting tensile force in the inclined section pulls the fastener out of the timber. In the event of sufficient withdrawal resistance, an increase of the load-carrying capacity by a component parallel to the joint line may apply. The component perpendicular to the joint line may cause friction between the steel and the timber, which further increases connection capacity (Thelandersson & Larsen, 2003). This phenomenon, the rope effect, is expressed in EN 1995-1-1 (CEN, 2009a) by an additional member $\frac{1}{4} \cdot F_{ax,Rk}$ in formulas (g) and (h), where $F_{ax,Rk}$ is the characteristic withdrawal capacity of the fastener. The rope effect does not apply to smooth shank fasteners such as dowels, which can withstand very low pull-out forces (Blass & Sandhaas, 2017).

3.4 Self-perforating dowels

The most common types of self-perforating dowels in Europe are WS provided by SFS Intec (2013) and SBD by Rothoblaas (2017) – see Figure 20 (left). According to the Declaration of Performance (DoP) of the dowels (Rothoblaas, 2017; SFS Intec, 2013), EN 1995-1-1 (CEN, 2009a) will apply in the design. The only exception is the yield moment of the fastener ($M_{y,R}$), which is declared in DoP.

WS is a smooth dowel 7 mm in diameter with a separate welded drill-tip and underhead thread, which makes for quick and precise closure with the possibility to remove the dowel. SBD's nominal diameter is slightly larger – 7.5 mm – and it is made of hardened steel with a drill-tip. It also has a second thread against the tip, which facilitates screwing. Therefore, one can assume the activation of the rope effect due to the threads, which is excluded from smooth dowels.

The concealed cylindrical head of both dowels ensures optimal appearance and fire protection, but also determines the symmetry of the connection. Type WS has a thin, sharp drill-tip that cannot be incorporated into the calculations. For the unconcealed dowel, the extent of the bearing length t_1 is not equal in connection with two shear planes.

The drill-tip of the SBD is part of the same alloy (see Figure 20 (right)), and there are no indications in the product documents that this part should not be taken into account. However, due to the complicated half-flat shape, its full contribution is questionable. Depending on the position of the flat side of the tip in relation to the load direction in the joint, in the most unfavourable case, 40% of the area may need to be considered in calculations. The simplified re-calculation gives a 10mm equivalent length to be used instead of the full extent of the tip. For example, the length of 85 mm applies for dowel SBD-7.5x95 instead of the actual length of 95 mm.

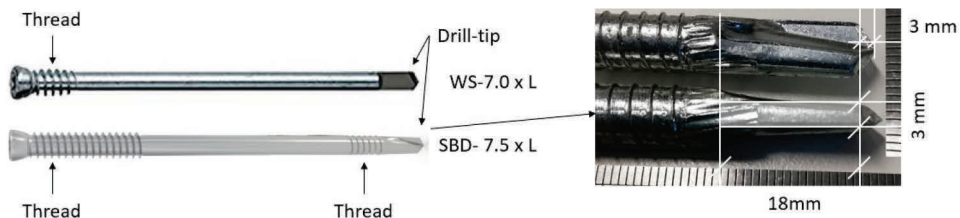


Figure 20. Left: dowels WS (SFS-Intec, 2013) and SBD (Rothoblaas, 2019); right: SBD tip dimensions

3.5 Yield moment of the dowel

EN 1995-1-1 (CEN, 2009a) specifies the analytical expression for the characteristic yield moment $M_{y,Rk}$:

$$M_{y,R} = 0,3 \cdot f_{u,k} \cdot d^{2,6} \quad (2)$$

, where d [mm] - fastener diameter; $f_{u,k}$ [N/mm²] - characteristic tensile strength of the fastener.

Eq. (2) was derived by (Blaß et al., 2001) with the assumption that dowels with a large diameter do not reach the full plastic hinge because of the low bending angle when the connection is tested up to 15 mm deformation, as stated in EN 26891 (CEN, 1999).

In general, the bending angle increases as the fastener diameter decreases, in which case it might be reasonable to use an equation from mechanics theory (Meyer, 1957):

$$M_{y,R} = \frac{1}{6} \cdot f_y \cdot d^3 \quad (3)$$

In doing so, the yield strength $f_y = 0.8 \cdot f_u$ needs to be used to consider strain hardening at large bending angles (Thelandersson & Larsen, 2003). As such, steel grades with a yield-to-ultimate strength ratio of about 0.65 are considered (Blaß et al., 2001). However, this is not the case for dowels made of HSS and UHSS as found in (Sandhaas & van de Kuilen, 2017): the yield-to-ultimate strength ratio was 0.94 for both HSS and UHSS dowels. As mentioned previously, $M_{y,R}$ for self-perforating dowels is declared in DoP. Corresponding values are $M_{y,R,k} = 31.93$ Nm for WS, and $M_{y,R,k} = 42.0$ Nm for SBD.

3.6 Embedment strength in solid timber

In EN 383 (CEN, 2007), embedment strength is defined as the average compressive stress at ultimate load in a piece of timber under the action of a stiff linear fastener. By testing, the axis of the fastener must be perpendicular to the timber surface and the fastener loaded perpendicular to its axis. Embedment strength is a system's property, characterising the interaction between fastener and wood (Blass & Sandhaas, 2017; Ehlbeck & Werner, 1992). Therefore, the testing method and conditions have a great influence on the results.

Three available testing standards are the European EN 383 (CEN, 2007), American ASTM D5764-97a (ASTM International, 2018) and the international ISO 10984-2 (ISO, 2009). Detailed information about these documents is provided in (Franke et al., 2018), but the fundamental choice stands for the full-hole or half-hole testing method. The first one presents the conditions around the fastener more accurately, similar to the real connection. However, the result may be affected by dowel bending in the case of slender dowels – it is possible that the full plastic capacity of the timber will not develop before failure occurs (Pope & Hilson, 1995). If the fastener bends, the stress distribution is not uniform, which may trigger the splitting (Mischler, 1998). The slenderness λ – the ratio of specimen thickness to fastener diameter – is limited to four in EN 383 (CEN, 2007).

In order to achieve comparable results, the specimens must be conditioned at ambient conditions (20°C/65% RH) to constant moisture content before testing. It is known that increasing moisture content will decrease the embedment strength (Koponen, 1991; Rammer & Winistorfer, 2001). Gehri (1982) claims, based on tensile tests with bolts in slotted-in steel plate connection, that a 3% change in load-carrying capacity for every percentage point difference in moisture content will apply. The same relation, but for compression strength parallel to the grain, is given in EN 384 (CEN, 2016). In the case of hardwood, Hübner (2013) found that the embedment strength changed 3% when loaded perpendicular to the grain; the corresponding value for parallel to the grain was 4%.

The surface of the dowel will also have a considerable influence. Schmid (2002) found that a rough surface may increase the embedment strength of up to 13.8%. In the case of very smooth dowels, the value decreased by 8.2% compared to the reference series. FEA and tests measured with contact-free measurement system conducted by Sjödin et al. (2008) will confirm this. They also show the effect of friction between the timber and dowel on the failure mode and result variability. However, the exact roughness is

usually not declared by the scientists, only the steel grade and description of the coating (smooth/galvanised dowel; strength class S235, e.g.).

In general, the circumstances that the designer cannot influence are not declared or mentioned but may be relevant to the interpretation of the test results. For example, the annual ring orientation does not directly affect embedment strength value (Hübner, 2013). Still, it may help to avoid splitting in a direction parallel to the grain when they are oriented about 45 degrees to the dowel's axis (Sandhaas et al., 2010). The poor quality of the drill hole with torn fibres may reduce the embedment strength compared to the precisely made holes (Spörk, 2007). In contrast, an oversized hole up to 2mm does not show a significant influence on the embedment strength (Koponen, 1991).

The much more significant impact has the evaluation method, which may lead to incompatibility in results between studies. Franke & Magnière (2014) found a difference of embedment strength up to 76% and stiffness up to 200% by taking the load value corresponding to an absolute displacement of 5 mm as recommended by EN 383 (CEN, 2007) and by offsetting the elastic-linear part of 5% of the fastener's diameter as suggested in American ASTM D5764-97a (ASTM International, 2018). This topic is still under discussion (Franke & Magnière, 2014).

In EN 1995-1-1 (CEN, 2009a), embedment strength for dowels loaded parallel to the grain is expressed by the empirical Eq. (4), which is based on an extensive number of tests by (Ehlbeck & Werner, 1992; Whale et al., 1987) and was proposed for design code in (Ehlbeck & Werner, 1992):

$$f_{h,0} = 0.082(1 - 0.01d)\rho \quad (4)$$

where $f_{h,0}$ [N/mm²] - embedment strength parallel to the grain; d [mm] - diameter of dowel-type fastener; ρ [kg/m³] - density of wood. There is an assumption that the same relationship will apply for characteristic values (Whale, Smith, & Larsen, 1987), as it is presented in EN 1995-1-1 (CEN, 2009a).

It turns out, from the designers perspective, dowel diameter and wood density are the only properties to determine for the Eq. (4). It has been agreed on the embedment strength increases linearly with density (Thelandersson & Larsen, 2003). However, Hübner (2013) proposed the model for embedment strength in hardwood where the influence is exponential, namely $\rho^{1.57}$ for characteristic value. The same applies to dowel diameter – Hübner (2013) showed that embedment strength does not increase linearly with decreasing diameter, as it turns out from the Eq. (4). It is instead punishing for small dowel diameters, and in the proposed model, the exponent $d^{-0.2}$ was used. Traetta & Schickhofer (2007) tested pine (*Pinus sylvestris*) and spruce (*Picea abies*), and found the ratio to the diameter $d^{-0.15}$.

According to (Hankinson, 1921), the crushing strength value in solid timber is highly dependent on the load-to-grain angle. In EN 1995-1-1 (CEN, 2009a) the reduction of embedment strength value for fasteners with pre-drilled holes by increasing load-to-grain angle α [°] is expressed by Hankinson's function and factor k_{90} :

$$f_{h,\alpha} = \frac{f_{h,0}}{k_{90} \sin^2 \alpha + \cos^2 \alpha} \quad (5)$$

Depending on the type of timber and dowel diameter, embedment strength for dowels loaded perpendicular to the grain is approximately 30-45% lower than parallel to the grain.

3.7 Embedment strength in cross-laminated timber

Dowels inserted on the plane side of cross-laminated timber are in a unique situation – the fastener penetrates the panel layers, which are perpendicular to one another. Load-to-grain angle changes within the timber and dowel contact area, and the embedment strength is differentiated along the dowel. The formulas in Eq. (1) are derived with an assumption that embedment value is constant within the bearing length t_1 .

Blass & Uibel (2007) showed that applying EYM for cross-laminated timber leads to very complex equations even in the simplest case – they derived equations for steel to three-layer cross-laminated timber connection with one shear plane. (Pirnbacher et al., 2006) expanded Johansen's theory in cross-laminated timber and performed a parameter study for three-layer timber-to-timber connection with one shear plane. Both studies conclude that in order to solve all possible failure modes, the use of electronic data processing software would be appropriate. Sawata et al. (2016) tested connections with five-layer cross-laminated timber and two slotted-in steel plates and compared the results with the theoretical calculation. The application of Johansen's theory ended up with a thirty-nine yield mode, which is far from a practical solution. An alternative design approach is proposed by Nakashima, Kitamori, Mori, et al. (2014), but this applies only for a particular layer configuration.

Blass & Uibel (2007) proposed using a homogenised embedment strength in EYM instead of differentiated value. They showed that depending on the load direction relative to the outer layers of cross-laminated timber, load-carrying capacity might differ from the exact solution by to 4-6%. Therefore, it is appropriate to maintain the original form of the design model and treat the embedment strength as a constant value within the connection, similar to solid timber.

Current standards do not provide an analytical formula for embedment strength in cross-laminated timber. Blass & Uibel (2007) proposed two models based on extensive testing according to EN 383 (CEN, 2007), although the standard is intended for a homogenous embedment characteristic of solid timber. However, it is suitable for laminated products such as glulam and cross-laminated timber when assuming similar, uniform embedment behaviour. Model 1 considers the build-up ratio of the panel, whereas Model 2 does not. These are expressed as follows:

$$f_{h,pred,1} = 0.032(1 - 0.015d)\rho^{1.20} \left[\frac{\sum_{i=1}^n t_{0,i}}{t_{CLT}(1.6\sin^2\alpha + \cos^2\alpha)} + \frac{\sum_{i=1}^n t_{90,j}}{t_{CLT}(1.6\cos^2\alpha + \sin^2\alpha)} \right] \quad (6)$$

$$f_{h,pred,2} = \frac{0.035(1 - 0.015d)\rho^{1.16}}{1.1\sin^2\alpha + \cos^2\alpha} \quad (7)$$

where d [mm] - diameter of dowel-type fastener; ρ [kg/m³] - density of wood; $t_{0,i}$ [mm] - thickness of the layers parallel to the grain direction of the outer layers; $t_{90,j}$ [mm] - thickness of the layers perpendicular to the grain direction of the outer layers; t_{CLT} [mm] - thickness of cross-laminated timber panel; α [°] - loading angle to the outer layers. Both models are applicable in the build-up range $\zeta = \frac{\sum t_{0,i}}{\sum t_{90,j}} = 0.95 \dots 2.1$.

The correlation coefficients of Eq. (6) and Eq. (7) are $r = 0.77$ and $r = 0.75$, respectively.

Kennedy et al. (2014) developed a design equation for embedment strength in cross-laminated timber for threaded fasteners – lag screws and self-tapping screws. There, tests on unthreaded portions of the lag screw were included. A new model is independent of the panel layout and the fastener diameter and considers density and the loading angle as the only variables.

Dong et al. (2020) investigated the influence of the four factors on embedment strength in cross-laminated timber – density, loading angle, fastener’s diameter, and thickness ratio of a transverse layer (TRTL) to the total thickness – tests were based only on the three-layer specimen. Contrary to the findings of Kennedy et al. (2014), diameter as influencing parameter is represented in the model. Since the formula also includes TRTL value, according to the author’s conclusion, it can be used for glulam as well. In the case of TRTL = 0, all layers are parallel to the load direction, while where TRTL = 1, layers are perpendicular.

It must be emphasised that the last two approaches were derived according to the half-hole test and 5% evaluation, while the full hole test and 5mm evaluation was the base of Eq. (6) and Eq. (7). Therefore, as mentioned previously, the comparison of models on different bases may be questionable. However, laterally loaded fasteners inserted via side face of cross-laminated timber behave in a mostly ductile manner. Thanks to the orthogonal layout, where transverse layers act as a natural reinforcement, early failures in tension perpendicular to the grain are prevented (Ringhofer et al., 2018). It is clear that adjacent layers are affected by each other – having a locking effect – and this fact should give an advantage to the full-hole test, which describes the situation in the connection more realistically.

Eq. (6) and (7) were developed based on experiments with three- and five-layer specimens (Blass & Uibel, 2007). It seems reasonable given the conditions in the real connection. Although there are seven- or even nine- and eleven-layer cross-laminated timber panels in the market, it is unlikely that more than five layers will be affected if EYM is applied in the connection design.

The complete overview of specimen configurations tested by Blass & Uibel (2007) is presented in Chapter 4, but highlighting here the specificities of the database, mostly thin layers from 3.5 to 17 mm have been used to produce specimens. It was probably grounded due to the dowel slenderness limit set in EN 383 (CEN, 2007). For example, maximum specimen thickness 64 mm for dowel diameter 16 mm does not leave much room to configure the five-layer panel with thicker layers. For a 12 mm dowel, the corresponding value is 48 mm. The most common panel thicknesses in the market start from 90 mm and layer thicknesses from 20 mm. This is the drawback of the full-hole test – the possibility to test common configurations in practice is limited.

The applicable build-up range $\zeta = 0.95 \dots 2.1$ in Blass & Uibel model means that 33 to 51 % of layers in the panel are transverse – TRTL as mentioned above. Dong et al. (2020) tested specimens with TRTL values of 0, 0.2, 0.33, 0.4, 0.5, 0.6, and 1.0. They concluded there were significant differences between embedment strength of these groups. However, two extreme values at each end are not relevant in practice, two of which are glulam. It is also important to notice that the conclusion was based on absolute strength values; the effect of the density was not considered.

Although TRTL may seem appropriate from a testing point of view, it could be irrelevant in the connection. Figure 21 (left) presents a cross-laminated timber connection with one shear plane. Both connected members have the same TRTL value, but obviously, the adjacent layers in both panels will interact differently. A middle layer

in a 60 mm member is more likely to be affected than the middle layer in the 120 mm panel, which raises the question of the importance of the thickness of the layers. In other words, to what extent does the range of neighbouring crossed layers influence each other?

This query is also relevant for a slotted-in steel plate connection, especially with self-perforating dowels. In Figure 21 (middle and right), a slotted-in steel plate connection in cross-laminated timber is presented. In both cases, the load is applied parallel to the grain direction of the outer layers. In the middle figure, the load-bearing conditions for the smooth dowel on both sides of the steel plate are equal. Furthermore, due to the relative thick middle layer compared to the thickness of a steel plate, a parallel layer is likely next to the shear plane.

In contrast, in the right figure, the middle layer is almost entirely missing due to the slot. Taking into account even the slightest manufacturing tolerance or misplaced slot, embedment conditions on either side of the steel plate may be completely different. Moreover, as already described in Chapter 3.1, self-perforating dowels are naturally concealed on one side, and this will lead to a situation where not every layer is penetrated. In the particular case in Figure 21 (right), the locking effect on the left side of the steel plate is more likely; the worst scenario is on the right: the crossed layer is the only bearing layer.

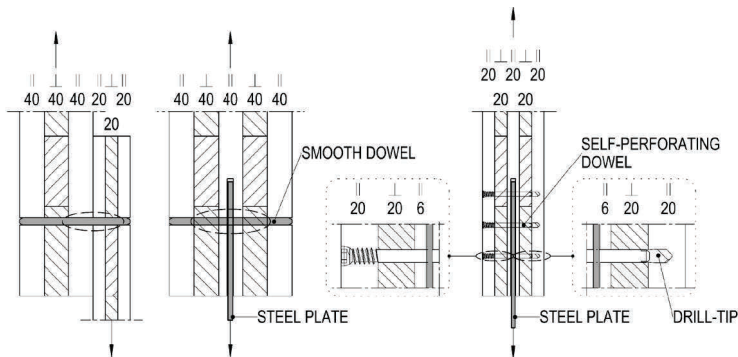


Figure 21. Left: cross-laminated timber connection with one shear plane; middle: symmetrical connection with slotted-in steel plate and smooth dowel; right: unsymmetrical connection with slotted-in steel plate and self-perforating dowel

The previous discussion was motivated mainly by the geometrical nature of the cross-laminated timber connection. However, when estimating the embedment strength in cross-laminated timber with a model proposed by (Blass & Uibel, 2007), both studies – (Kennedy et al., 2014) and (Dong et al., 2020) – found that the mean value is overestimated. But once again, it must be emphasised that these experiments were carried out on different bases.

This thesis investigates the embedment strength in cross-laminated timber based on the database provided by Blass & Uibel (2007) and several unique experiments. The primary focus is on the effect of the thickness of adjacent layers.

The tests performed with slotted-in steel plate connection had two purposes: to validate the results of embedment tests and to investigate the influence of the properties of self-perforating dowels (especially geometrical) to the load-bearing capacity of the connection. Full-scale cross-laminated timber shear wall tests were done to highlight the benefits of this type of connection.

4 METHODS

4.1 General

The following experiments were performed to achieve the objectives of this thesis:

- Connection tests
- Embedment strength tests
- Full-size shear wall test

The corresponding sub-chapters first describe the test methods and evaluation of the results. Then, the detailed description of test specimens is given. Lastly, the basis of the data processing, description of selected validation models and methods to develop the model (if relevant) is presented.

It is essential to note that the same type of wood – European spruce (*Picea abies*) – has been used in all of these experiments.

As the primary input parameter in connection design, the embedment strength was studied together with the existing database compiled by Blass & Uibel (2007). A summary of relevant information on these tests and specimens is also provided here.

4.2 Connection tests

4.2.1 Test methods and evaluation of the results

The standard for the determination of connection strength and deformation characteristics is EN 26891 (CEN, 1999). All specimens were loaded on a Zwick/Roell Z250 testing machine, while displacements were measured with LVDTs and recorded with an HBM Quantum MX840B universal amplifier and Catman DAQ Software (HMB, 2019). Loading followed the protocol set out in the test standard and was continued up to the failure point – see Figure 22. The standard states that loading must be adjusted so that the maximum load is reached within (480 ± 150) s after the preloading phase – point No. 21 in Figure 22. The estimated maximum load was found in preliminary experiments. The machine was controlled by force for up to 70 % of the estimated load. The displacement-controlled regime was applied starting from that point (No. 27). Connection strength is defined as the maximum load before deformation of 15 mm. For specimens loaded over this limit, the load-carrying capacity was taken at 15 mm.

After completing the tests, clear wood samples were taken to determine moisture content by performing an oven-dry method and the density by measuring the specimen dimensions. If the moisture content differed from the reference value $u_{ref} = 12\%$, density was corrected according to EN 384 (CEN, 2016) by the following:

$$\rho_{corr} = \rho [1 - 0,005(u - u_{ref})] \quad (8)$$

, where ρ [kg/m³] - measured density of the specimen; u [%] - moisture content at testing; u_{ref} [%] - reference moisture content.

Apart from connection tests, the yield moment of fastener M_y , and tensile strength f_u were determined experimentally based on standards (EN 409, 2009) and (EN 1383, 2016) accordingly. Bending tests were carried out at the Karlsruhe Institute of Technology.

4.2.2 Description of the tested specimens

The connection under study was the 6 mm slotted-in steel plate (S235), connected in a 100 mm cross-laminated timber with self-perforating dowels SBD-7.5x95 (Rothoblaas, 2017) – see Figure 23 (left). The test specimen had five layers of 20 mm each. Due to the 7 mm slot in the middle, in the ideal case, the lamella configuration on one side of the steel plate (one shear plane) was $6.5+20+20 = 46.5$ mm.

Additional tests with longer dowels SBD-7.5x195 and the same specimen thickness were carried out to identify the influence of the drill tip and possible rope effect. Also, dowel types WS-7x95 and WS-7x153 or WS-7x233 (SFS-Intec, 2013) were used to see the impact of the yield moment of the fastener. The positioning of all tested dowels with respect to the specimen thickness is presented in Figure 24.

All connections were loaded in tension and therefore anchored to the base plate with threaded bars and bolts. Loading angles were varied parallel, perpendicular and at an angle of 45 degrees to the grain of the outer layers. Fixing of the specimen, measuring points and an example of a 45-degree sample is presented in Figure 23 (middle and right, respectively). In order to reduce the risk of splitting, the area around the connection was held together with full threaded screws or clamping crews. However, this measure was only necessary for specimens with long dowels (without threaded part inside the timber).

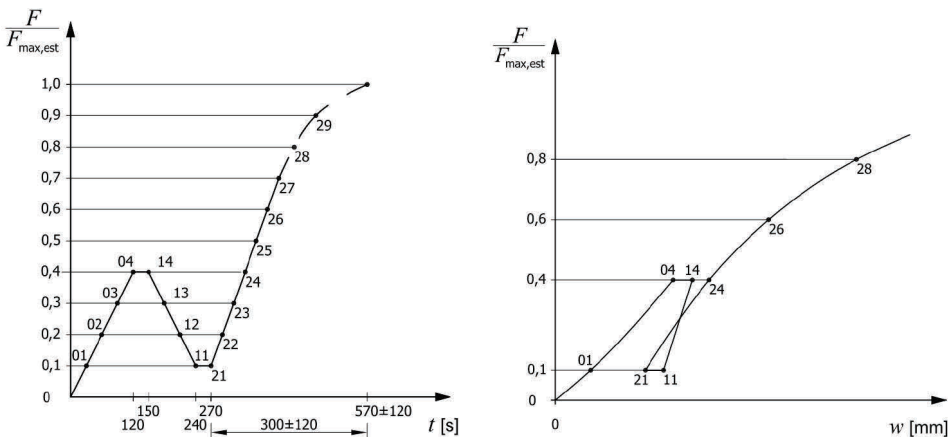


Figure 22. Left: loading procedure, according to EN 26891 (CEN, 1999) and EN 383 (CEN, 2007). Note: time axis represents a condition for EN 383, the corresponding value after preloading phase in EN 26891 is 480 ± 150 [s]; right: idealised load-deformation curve and measurement

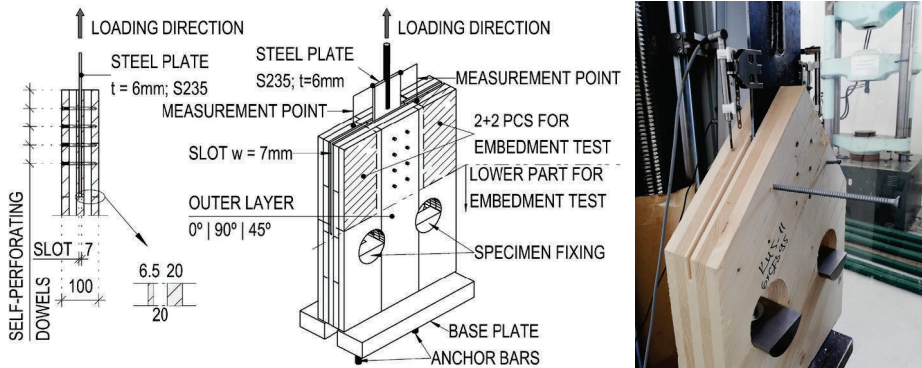


Figure 23. Left: tested connection type; middle: the principle of the specimen; right: an example of 45-degree specimen (reinforced)



SBD 7.5x95

SBD 7.5x195

WS 7x153 or WS 7x233

Figure 24. Positioning of longer dowels to avoid possible rope effect

Different setups with one, four and five dowels in one row (together with two rows) were tested for specimens 0 and 90 degrees. For 45-degree samples, dowel placement followed the shape of the corner in some cases. In addition to the initial test, pieces around the connections and anchorage area were cut out for embedment tests. These are specified in Chapter 4.3.2.1.

Figure 25 presents the steps for loading and cutting the specimens. Table 1 summarises all connection tests, including the number of samples, loading angles and densities. It must be noted that density values were calculated as mean values based on all samples cut from the upper part of the specimen, including the density of embedment test samples next to the connection.

Table 1. Configurations and densities of connection test specimens. α is loading angle to the grain direction of the outer layers

α	Dowel type	All dowels in one row	Number of tests	Density $\rho \left[\frac{kg}{m^3} \right]$			CV $[\rho_{12}]%$
				Group's mean, $u=12%$	All mean, $u=12%$	All 0.05, $u=12%$	
0°	SBD 7.5×95	2 1	4	467	465	444	2.8
		8 4	3				
		10 5	1				
0°	SBD 7.5×195	2 1	4	460	465	444	2.8
		8 4	1				
	WS 7×153	8 4	2	460			
45°	SBD 7.5×95	10 placed according to Figure 25	2	460	465	444	2.8
		4 placed according to Figure 25	1				
	WS 7×233	3 placed according to Figure 25	4	455			
		6 3	2	458			
	WS 7×95	6 3	2	469			
	90°	SBD 7.5×95	2 1	4			
8 4			4				
10 5			1				
SBD 7.5×195		2 1	3	470			
		8 4	1				
WS 7×153		8 4	1	483			

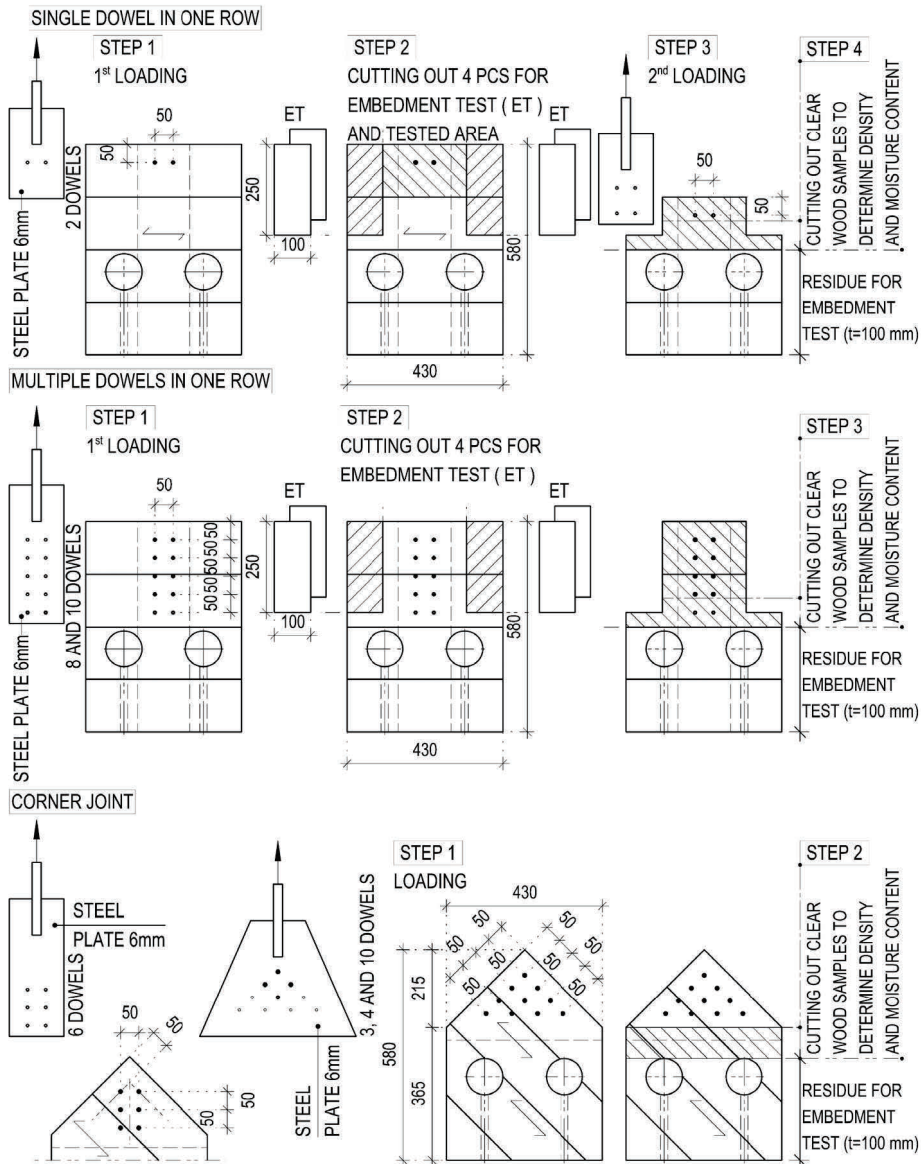


Figure 25. Steps taken for loading and cutting of specimens

4.2.3 Methods for data validation and comparison

EYM, expressed by Eq. (1) presented in Chapter 3.3, was used to validate the test results. The corresponding input parameters are given in the results chapter. For comparison of the results of different groups, test values were referenced to mean density by following:

$$\bar{F} = F \cdot \left(\frac{\rho_{mean}}{\rho} \right)^c \quad (9)$$

, where F [N] - test value; ρ [kg/m³] - measured density of the specimen; ρ_{mean} [kg/m³] - mean density of specimen groups; c - exponent found by experiments.

4.3 Embedment strength tests and databases

4.3.1 Test method and evaluation of the results

All the unique embedment test series were done on a Zwick/Roell Z250 testing machine, according to EN 383 (CEN, 2007) (full-hole test, loaded in compression). Displacements were measured with LVDTs and recorded with an HBM Quantum MX840B universal amplifier and Catman DAQ Software (HMB, 2019). The steel apparatus for specimens of different thickness is presented in Figure 26. Thick side blocks were used to avoid elastic deformations and keep the dowel as straight as possible.

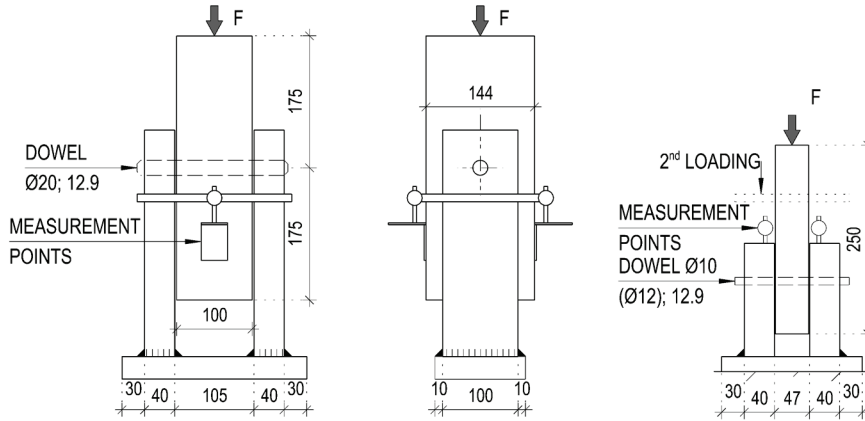


Figure 26. Steel apparatus for tested specimens. Left and middle: for up to 100 mm specimen; right: for up to 45 mm specimen

The standard states that loading must be adjusted to ensure the maximum load is reached within (300 ± 120) s after the preloading phase – point No. 21 in Figure 22. For up to 70 % of the estimated load, the machine was controlled by force. The displacement-controlled regime was applied starting from that point (No. 27).

The parametric study TMS (described in Chapter 4.3.2.2) had to be approached somewhat differently, as there were tests on both glulam and cross-laminated timber for comparison reasons. Due to the different maximum load level that defines the estimated load $F_{max,est}$, displacement-controlled loading of 0.8 mm/min was applied directly after the preloading phase. Therefore, glulam always achieved maximum load slightly before, and cross-laminated timber after the timeframe set in the standard.

The embedment strength was calculated according to Eq. (10):

$$f_h = \frac{F_{max}}{d \cdot t} \quad (10)$$

where d [mm] - diameter of the dowel; t [mm] - thickness of the test specimen. Maximum load F_{max} [N] is defined as the highest value achieved at a deformation of 5 mm, load at 7 and 9 mm was also recorded.

After completing the tests, clear wood samples were taken to determine moisture content by performing an oven-dry method and the density by measuring the specimen dimensions. Unlike the connection tests, the density was strictly determined next to the embedment area only. The test results, which were influenced by knots, were excluded from the database. If the moisture content differed from the reference value $u_{ref} = 12\%$, density was corrected according to Eq. (8).

As noted earlier, embedment strength value depends on the moisture content, and therefore, all results were normalised before data processing and analysis. This was done according to EN 384 (CEN, 2016), which states, “test values for compression parallel to the grain of specimens not tested at the reference moisture content shall be adjusted by the following”:

$$f_{c,0,corr} = f_{c,0} + f_{c,0} \cdot [0.03(u - u_{ref})] \quad (11)$$

, where $f_{c,0}$ [N/mm²] - measured compression strength parallel to the grain of the specimen; u [%] - moisture content at testing; u_{ref} [%] - reference moisture content. Note: here, measured embedment strength f_h instead of $f_{c,0}$ was used.

4.3.2 Description of the tested specimens

Embedment strength in cross-laminated timber has been studied using the test specimen groups listed below, from now on referred to as “databases”. The abbreviations of the databases are explained in the corresponding sub-sections.

1. Database TO: samples cut from connection test specimens.
2. Database TMS: a parameter study.
3. Database 50/50: specimens with build-up factor $\zeta = 1$
4. Database BU: the existing database provided by Blass & Uibel (2007).

4.3.2.1 Database TO: samples cut from connection test specimens

Since part of the results are published in (Tuhkanen & Ojamaa, 2019), the abbreviation TO is used hereafter. The cutting of the samples was already presented in Figure 25. The final dimensions are shown in Figure 27, which satisfy the minimum requirements set out in EN 383 (CEN, 2007). Test pieces cut next to the joint had a total maximum thickness of 45 mm instead of the original 46 mm. The thin layer thickness was around 6.5 mm, depending on the accuracy of the slot in the connection test specimen. The outer layer was planed slightly to fit better in the steel apparatus; therefore, the thickness was somewhat thinner than 20 mm. The test piece from residue had five layers of 20 mm, for a total thickness of 100 mm – see Figure 27 (right).

For the 45 mm-thick specimens, dowel diameters 10 and 12 mm were used, while 100 mm specimens were loaded with a dowel of diameter 20 mm. According to EN 383 (CEN, 2007), the recommended thickness should not be greater than four times the diameter, which does not meet the requirements set by the standard. However, to prevent plastic deformations in the dowel, all diameters with a strength class 12.9 according to ISO 898-1:2013 (ISO, 2013) were used. Additionally, side blocks of steel apparatus (see Figure 26) were made 40 mm thick to clamp the dowel ends and reduce elastic bending. The measured tensile and yield strengths of 20 mm dowel according to EN ISO 6892-1 (CEN, 2009b) were 1347 MPa and 1293 MPa, accordingly. A simple FEA showed maximum elastic deformation of the 20 mm dowel in the middle of the span should not exceed 0.3 mm. Being sufficient for the purposes, only one dowel of each diameter was used for all tests and no residual deformation was measured. The surface of the dowels was not measured but can be described as slick.

Table 2 summarises all tests in the database TO, including loading angle α , diameters, build-up factors ζ and the number of samples.

Table 2. Test and specimen parameters of Database TO. α is loading angle to the grain direction of the outer layers

α	Dowel \varnothing [mm]	Specimen thickness [mm]	Build-up ratio $\zeta = \frac{\sum t_{0,i}}{\sum t_{90,j}}$	Number of tests	$\rho \left[\frac{kg}{m^3} \right]$		CV $[\rho_{12}] \%$
					mean, $u=12\%$	0.05, $u=12\%$	
0°	10	45	~ 1.25	48	466	427	4.7
	12	45		28	469	423	5.3
	20	100		10	470	447	3.8
45°	20	100	1.5	12	459	432	4.1
90°	10	45	~ 1.25	53	476	435	6.2
	12	45		28	475	434	4.8
	20	100		11	471	453	2.5
ALL SPECIMENS				190	471	429	5.2

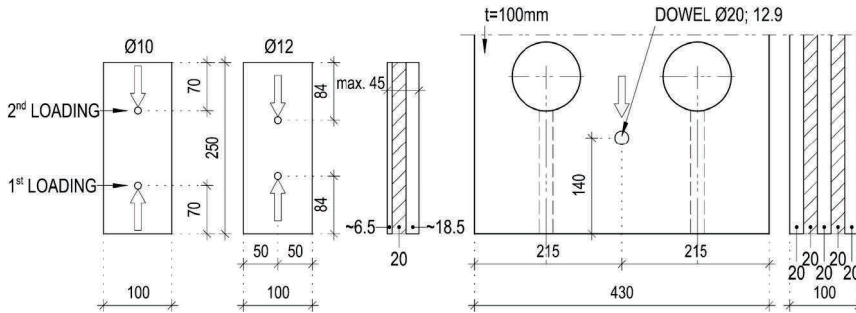


Figure 27. Embedment strength specimen dimensions in the database TO

4.3.2.2 Database TMS: a parameter study

The aim of parameter study TMS (abbreviated from the names of the authors), published in (Tuhkanen et al., 2018), was to analyse the failure pattern and embedment strength and stiffness values of cross-laminated timber by increasing the number of layers and decreasing layer thickness.

The full thickness of the specimen was 100 mm, and the build-up ratio ζ kept constant, namely $\zeta = 1.5$. The number of layers varied between 3, 5 and 9 layers, with 20 repetitions for each type, for a total of 60 specimens. The base material, boards with a cross-section of 50×100 mm, was distributed in 20 groups to obtain as equal density for each group as possible. For this purpose, each board was measured, weighted and the moisture content was found with electromagnetic moisture detector. Then, the density of the board was calculated and referenced to the moisture content of $u_{ref} = 12\%$. After that, the boards were ranked by corrected density and distributed to the groups. As a result, the mean density of each group did not differ by more than 5%.

Every group contained five boards, and from each group, three cross-laminated timber and three glulam specimens were produced. Every board in one group was divided into four and flitched to the required thickness. Then, every individual fourth was halved – one for cross-laminated and one for glulam specimen. The purpose of the corresponding glulam specimens was to find the influence of the adhesive surface

strength. A 160 g/m² Purbond adhesive film and the hydraulic press was used to glue the pieces. Samples were conditioned (20 °C, 65% RH) until mass constancy was reached. The cutting schema of the boards in one group and distribution between series by the example of a 5-layer sample is presented in Figure 28, the configuration of all glulam and cross-laminated timber specimens in Figure 29 and Table 3.

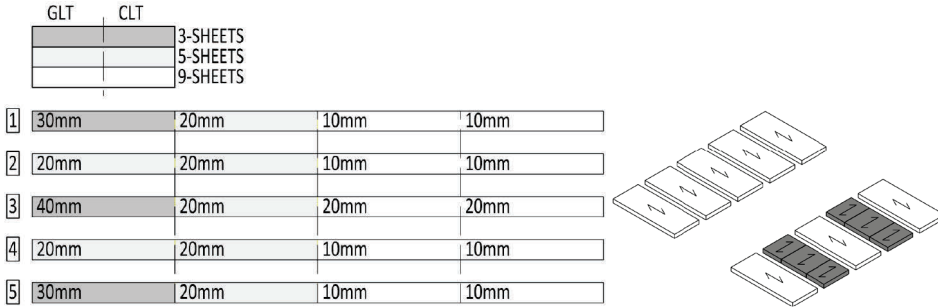


Figure 28. Cutting schema for boards and distribution between series by example of five-layer specimen (Tuhkanen et al., 2018)

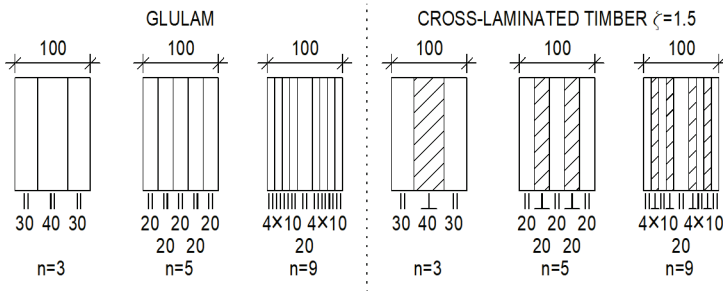


Figure 29. Configuration of the specimens in the parameter study TMS

Table 3. Specimen parameters of the database TMS

Group	Series	Number of layers	Build-up ratio ζ	Build-up: thickness of lamellas	Number of tests	Dowel \emptyset
Glulam	GLT 3	3	-	30-40-30	20	20
	GLT 5	5	-	20-20-20-20-20	20	
	GLT 9	9	-	10-10-10-10-20-10-10-10-10	20	
Cross-laminated timber	CLT 3	3	1.5	30-40-30	20	
	CLT 5	5		20-20-20-20-20	20	
	CLT 9	9		10-10-10-10-20-10-10-10-10	20	

An additional means of keeping the conditions for test pieces as equal as possible and thereby minimizing influence parameters was by noting the knots. Segments of the boards in Figure 28 were selected visually to obtain a knot-free testing zone for all specimens – see Figure 30. All measurements of samples will satisfy the requirements in EN 383 (CEN, 2007), except the thickness. However, the same high-strength dowel diameter 20 mm described in Chapter 4.3.2.1 was used.



Figure 30. Left: measurements of specimens and knot-free zone; right: visual selection of layers for 5-layer cross-laminated timber specimen

In Table 4, mean values, the 5 %-quantiles, and the CV of the density of tested specimens are presented in consideration of layer number.

Table 4. Density values of the database TMS

n	ρ_{mean} u=12% [kg/m ³]		ρ_{05} u =12% [kg/m ³]		CV [%]	
	GLT	CLT	GLT	CLT	GLT	CLT
3	457	451	439	434	3,0	2,5
5	456	452	438	438	2,2	2,4
9	465	464	453	456	1,9	1,6
ALL	459	456	439	438	2,6	2,5

One can recognize the remarkable increase of density in 5%-quantiles by 9-layer samples, which is due to homogenisation, also known as the system effect. This phenomenon has been well described by Brandner (2012) and Ringhofer et al. (2015), e.g. However, the difference in mean value should not be so significant. Therefore, the mass of the adhesive has been removed from the density calculation by the following formula:

$$m_{corr} = m - \Delta m_{(n-1)} \quad (12)$$

where m_{corr} [g] - corrected sample mass; m [g] - original sample mass; $\Delta m_{(n-1)}$ [g] - mass of all adhesive layers in the sample. Film mass was expected to be 160g/m² (Purbond, 2018).

A similar procedure for pull-out tests with self-tapping screws was applied by Ringhofer et al. (2015).

The corrected density related to the 3-layer specimen and series comparison in the meaning of the boxplots are presented in Figure 31 and Figure 32, respectively. Since the difference in the mean density value is up to 1.5 %, it can be concluded that it does not differ between series. The somewhat higher difference is in 5 %-quantile, up to 3 %.

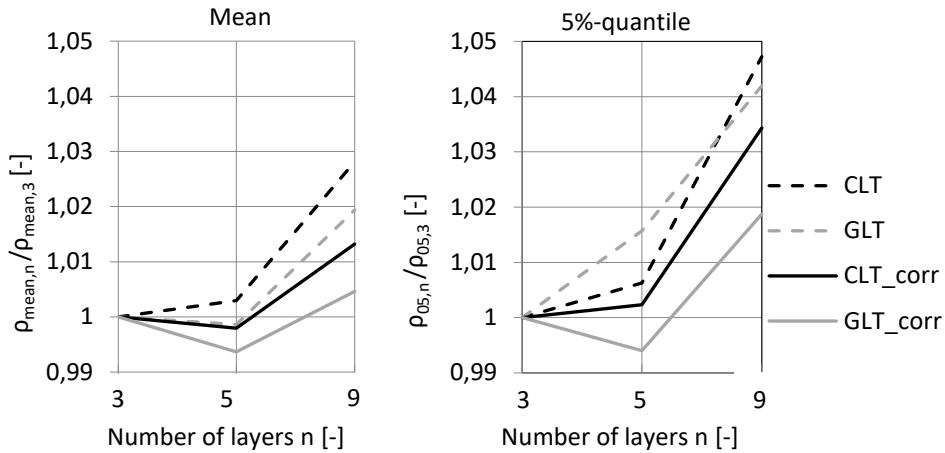


Figure 31. Adhesive mass-corrected density values related to 3-layer specimen. GLT = glulam; CLT = cross-laminated timber

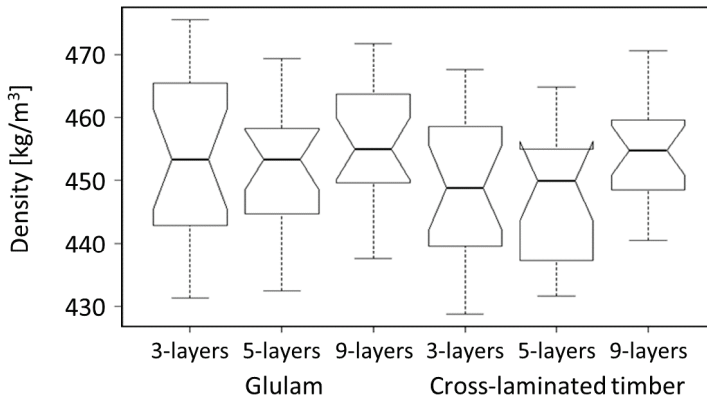
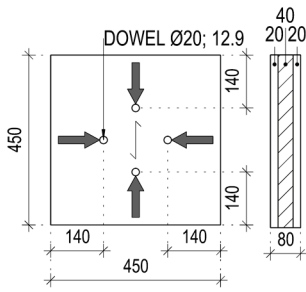


Figure 32. Comparison of mass-corrected densities of glulam and cross-laminated timber

4.3.2.3 Database 50/50: specimens with build-up factor $\zeta = 1$

A particular campaign was conducted with test specimens with a build-up factor $\zeta = 1$, meaning that by 3-layer specimens, the outer layers have the same thickness as the inner layer, namely 20+20 mm and 40 mm, for a total of 80 mm. The aim was to find the influence of the loading direction in a seemingly similar situation. A total of nine specimens were prepared, and each test piece was loaded four times, one on each side. The configuration of the samples is presented in Figure 33, and density data in Table 5. Test results that were influenced by knots were excluded from the database. Samples were tested on the same steel apparatus as 100 mm thick specimens.

Table 5. Density values of the database 50/50



α	Number of tests	$\rho \left[\frac{kg}{m^3} \right]$		CV ρ_{12} [%]
		mean, $u=12\%$	0.05, $u=12\%$	
0°	11	431	401	4.9
90°	16	419	385	7.1
ALL	27	424	387	6.2

Figure 33. Test specimen of Database 50/50

4.3.2.4 Database BU (Blass & Uibel, 2007)

By far the most extensive full-hole test series to date has been conducted by Blass & Uibel (2007). In this thesis, the abbreviation BU is used to refer to the database. It aimed to develop, through multiple regression analysis, the design model for embedment strength in cross-laminated timber. Although this study covers the embedment strength of dowels, screws, and nails, positioned in the plane side and edges of the cross-laminated timber plate, only the values for smooth dowels in the plane side were used in this thesis.

In total, 438 tests with seven different layup configurations, three loading angles, and five dowel diameters were conducted. Additionally, the position of the fastener related to the areas with or without gaps was considered. Figure 34 presents a schematic sketch of the load directions and dowel positions. In Figure 35, the distribution of the samples by configuration and dowel diameter, and in Figure 36 by loading angles are shown.

Tests followed the EN 383 standard (CEN, 2007). In all cases, specimen thickness met the requirements set by the standard. The dowels were not clamped at the ends to reduce bending but were made of heat-treated or hardened steel. No specific information regarding the dowel surface was given. In order to prevent block shear in the samples loaded at an angle of 45 degrees, the size of the test pieces was increased.

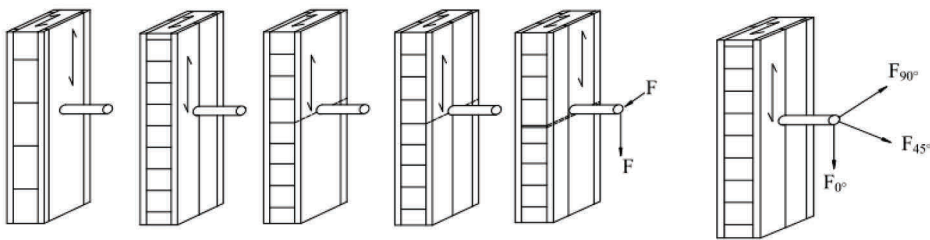


Figure 34. Positions of fasteners and load direction in embedment tests—schematic sketch from (Blass & Uibel, 2007)

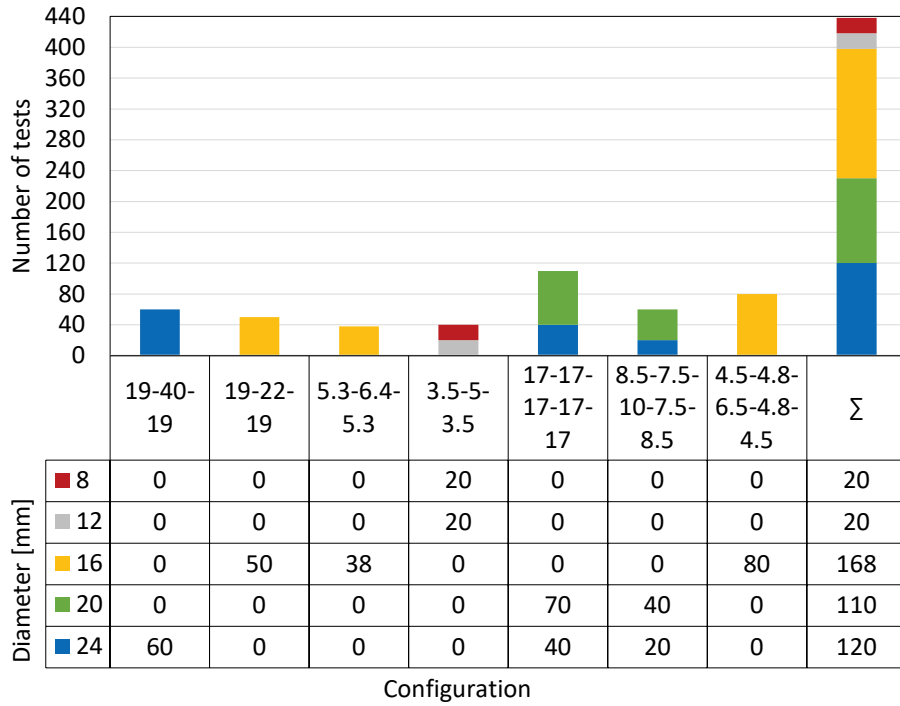


Figure 35. Specimens distribution by configuration and diameter

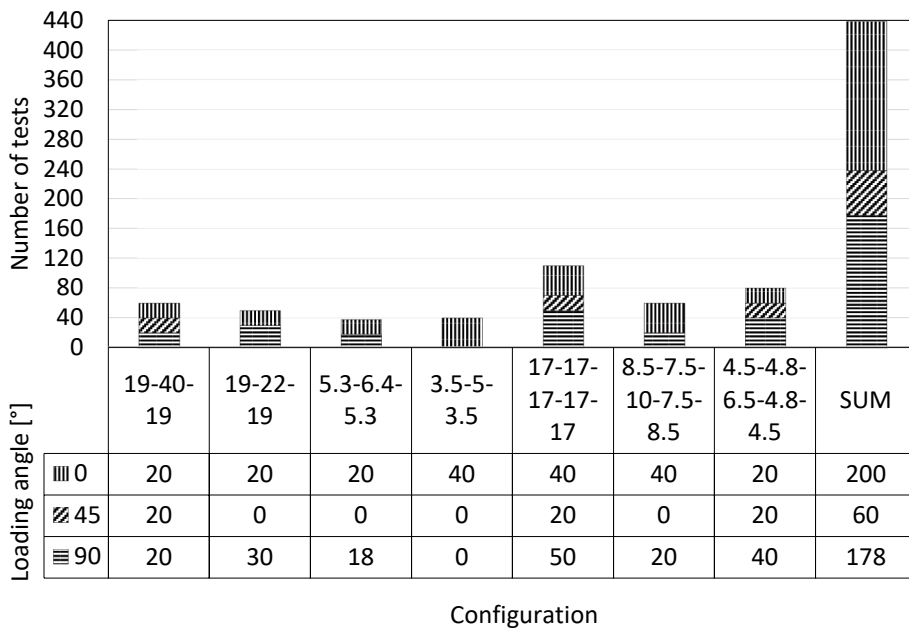


Figure 36. Specimens distribution by configuration and loading angles

In the test report (Blass & Uibel, 2007), the density values were represented at ambient conditions (20°C/65% RH). However, in order to assess the results equal to the original tests described in previous chapters, both density and embedment strength were corrected before data analysis, according to Eq. (8) and Eq. (11) respectively. Specimen data with updated density values are presented in Table 6.

Table 6. Specimen data, dowel diameters and moisture corrected densities in BU database

Configu- ration	Specimen thickness [mm]	$\zeta = \frac{\sum t_{0,i}}{\sum t_{90,j}}$	Dowel \emptyset [mm]	α	No. of tests	$\rho \left[\frac{kg}{m^3} \right]$		CV [ρ_{12}] %
						mean, $u=12\%$	0.05, $u=12\%$	
17-17- 17-17-17	85	1.5	24	0°	20	470	433	4.3
				90°	20	467		
			20	0°	20	467		
				90°	30	474		
				45°	20	491		
19-40-19	78	0.95	24	0°	20	458	408	7.9
				90°	20	453		
			45°	20	462			
8.5-7.5- 10-7.5- 8.5	42	1.8	24	0°	20	465	431	4.1
				90°	20	464		
			20	90°	20	467		
19-22-19	60	1.72	16	0°	20	431	389	5.9
				90°	30	432		
5.3-6.4- 5.3	17	1.66	16	0°	20	455	417	5.2
				90°	18	464		
4.5-4.8- 6.5-4.8- 4.5	25	1.6	16	0°	20	468	429	5.6
				90°	40	456		
				45°	20	468		
3.5-5-3.5	12	1.4	12	0°	20	481	448	5.4
3.5-5-3.5	12	1.4	8	0°	20	473	424	6.7
ALL SPECIMENS					438	462	416	6.5

4.3.3 Methods for data comparison

The cross-laminated timber is not covered by the current standard EN 1995-1-1 (CEN, 2009a). Therefore, in Europe, analytical models for embedment strength provided by Blass & Uibel (2007) are often referred to in European Technical Assessment (ETA) documents. Since the Model 2 expressed by Eq. (7) has a more practicable form, and the difference in results compared to Model 1 is not significant, it has been taken as the basis of this thesis. The test data was first validated using Model 2.

The analysis of the influencing factors of the embedment strength included a comparison between different specimen groups. Therefore, the effect of density was excluded or referenced to the specific density by the following equations:

$$\bar{f}_h = \frac{f_h}{\rho^c} \quad (13)$$

$$\bar{f}_h = f_h \cdot \left(\frac{\rho_{ref}}{\rho} \right)^c \quad (14)$$

, where f_h [N/mm²] - embedment strength test value; ρ [kg/m³] - density of the specimen; ρ_{ref} [kg/m³] - reference density, c - exponent, found by experiments.

The influence of the diameter was excluded by referencing the test value to the specific diameter d_{ref} by the following:

$$\bar{f}_h = \frac{f_h}{(d/d_{ref})^c} \quad (15)$$

, where f_h [N/mm²] - embedment strength test value; d [mm] - dowel diameter; d_{ref} [mm] - reference diameter of dowel ; c - exponent, found by experiments.

4.3.4 Regression analysis for model prediction

The new model for embedment strength in cross-laminated timber is proposed in such a format, to consider the effect of the diameter exponentially:

$$f_h = A\rho^B d^C \quad (16)$$

where f_h [N/mm²] - embedment strength; ρ [kg/m³] - density of timber; d - dowel diameter; A , B and C are model parameters.

The analysis is based on n simultaneous observation of embedment strength as the dependent material property, and the density and the diameter of the dowel as indicative properties. A linear relationship between the logarithms of the variables is assumed to perform multiple linear regression:

$$\log(f_h) = \log(A) + \log(\rho) \cdot B + \log(d) \cdot C \quad (17)$$

Multiple linear regression was performed using MATLAB (The MathWorks Inc., 2019).

Ordinary least square regression and percentile value – referred (Köhler, 2020)

The prediction of relevant variables based on information on other related variables is based on a linear regression model. An ordinary least square regression model describes the relation between realisations of a response variable y_i , and the realisations of the l explanatory variables $x_{i,j}$ as:

$$y_i = \sum_{j=0}^{l-1} x_{i,j} \cdot \beta_j + \epsilon_i \quad (18)$$

, where $\beta_0, \beta_1, \dots, \beta_{l-1}$ are the regression parameters and ϵ_i are the realisations of the so-called error term. This relation can be written in matrix notation as:

$$y = X\beta + \epsilon \quad (19)$$

With, for n realisations:

$$y = \begin{bmatrix} y_1 \\ y_2 \\ \vdots \\ y_n \end{bmatrix} X = \begin{bmatrix} x_{1,0} & x_{1,1} & \cdots & x_{1,l-1} \\ x_{2,0} & x_{2,1} & \cdots & x_{2,l-1} \\ \vdots & \vdots & \cdots & \vdots \\ x_{n,0} & x_{n,1} & \cdots & x_{n,l-1} \end{bmatrix} \epsilon = \begin{bmatrix} \epsilon_1 \\ \epsilon_2 \\ \vdots \\ \epsilon_n \end{bmatrix} \quad (20)$$

$$\beta = [\beta_0 \ \beta_1 \ \cdots \ \beta_{l-1}]^T$$

The variable $x_{i,0}$ is fixed at one, so that $\beta_0 x_{i,0} = \beta_0$ is constant for all i . For ordinary linear regression, the conditional variances $Var[y_i|\beta, X] = \sigma^2$ are assumed to be equal for all i , and the realisations y_i are conditionally independent given β, σ, X .

If n simultaneous observation on \hat{y} and \hat{X} are made, the corresponding best estimate of the l model parameters β can be obtained by minimisation of the sum of the squared residuals, i.e., $\sum_{i=1}^n \hat{\epsilon}_i^2 = \hat{\epsilon}^T \hat{\epsilon}$:

$$\hat{\beta} = \arg \min_{\beta} [(\hat{y} - \hat{X}\beta)^T (\hat{y} - \hat{X}\beta)] \quad (21)$$

The estimated parameters $\hat{\beta}$ correspond to expected values, i.e., $\hat{\beta} = E[\beta]$ and are obtained by the solution of Eq. (22):

$$\hat{X}^T (\hat{y} - \hat{X}\beta)^T = 0 \quad (22)$$

Hence, $\hat{\beta}$ results in:

$$\hat{\beta} = (\hat{X}^T \hat{X})^{-1} \hat{X}^T \hat{y} \quad (23)$$

The estimates of β are uncertain a given σ and y they follow a normal distribution, i.e. $\beta|\sigma, y \sim N(\hat{\beta}, V_{\beta}\sigma^2)$, with:

$$V_{\beta} = (\hat{X}^T \hat{X})^{-1} \quad (24)$$

σ^2 is following an inverse- χ^2 distribution with $n - l$ degrees of freedom, i.e. $x^2|y \sim \text{Inv} - \chi^2(n - l, s^2)$.

The sample standard error of the model, s^2 is assessed from the residuals between the model and the data:

$$s^2 = \frac{(\hat{y} - \hat{X}\hat{\beta})^T (\hat{y} - \hat{X}\hat{\beta})}{n - l} \quad (25)$$

The distribution of future (unobserved) observations \tilde{y} has an expectation of

$$E[\tilde{y}|\tilde{X}, \hat{\beta}] = \tilde{X}\hat{\beta} \quad (26)$$

The corresponding variance is derived as:

$$\text{var}[\tilde{y}|\tilde{X}] = (I + \tilde{X}V_{\beta}\tilde{X}^T)\sigma^2 \quad (27)$$

i.e. conditional on σ^2 the variance has two terms, $\sigma^2 I$ representing the sampling variation, and $\tilde{X}V_{\beta}\tilde{X}^T\sigma^2$ due to the uncertainty in the regression parameters β . The uncertainty in σ^2 can be integrated our considering the inverse- χ^2 distribution.

The percentile value indicates the non-exceedance probability of a realisation of a random variable. If $x_{p=0.05}$ corresponds to the 5th percentile value of the random variable X , a random realisation of X , x , has a non-exceedance probability of 0.05.

Percentile value is to be estimated based on a regression model (based on information on X), and Monte Carlo Simulation is to be utilized. Thousand random values based on mean values and covariation of parameters A , B and C will be generated, resulting in 3×1000 matrix. Normal distributed random values for ϵ_i will be generated based on the mean value of one.

The range of variables was selected as follows: $d_i = 1,2,3 \dots 24$ (vector d); $\rho_i = 100,101, \dots 800$ (vector ρ). Thousand values for every d_i and ρ_i will be calculated using the following equation:

$$f_i = \exp(A_i)\rho_i^{B_i}d_i^{C_i\exp(\epsilon_i)} \quad (28)$$

, where A_i, B_i, C_i and ϵ_i are (generated) random values. A three-dimensional matrix will be generated according to the results and variable pairs d_i and ρ_i . For every pair, 5th percentile is to be found, resulting in vector length $27 \times 701 = 16824$. Multiple linear regression will be performed with input values of d, ρ and $f_{0.05}$.

4.4 Shear wall test

4.4.1 Test method and evaluation of the results

The standard EN 594 (CEN, 2011) specifies the test method to be used in determining the racking strength and stiffness of timber frame wall panels. Therefore, for cross-laminated timber shear wall, the standard was applied with some modifications.

The specimen was loaded horizontally with a manually operated Enerpac RC506 hydraulic cylinder (Enerpac, 2019). A constantly increasing load was applied to the wall and racking strength F_{rg} was reached when the panel collapsed, or the panel achieved global lateral displacement of 100mm, whichever occurred first. The rate of loading should ensure that 90% of the racking load is reached within (300 ± 120) s. Loading was done stepwise to monitor the residual deformations. The given time limit was applied to the final loading up to the failure. The load was measured using a separate Zemic BM24R - C3-28t-15G load cell (Zemic Europe B.V, 2019). The racking stiffness R of the wall was calculated based on the deformations as $0.2 \cdot F_{rg}$ and $0.4 \cdot F_{rg}$. LVDTs were used to measure displacements, and the values were recorded with an HBM Quantum MX840B universal amplifier and Catman DAQ Software (HMB, 2019).

4.4.2 Description of the tested specimen

Two types of shear walls were tested and analysed within the study – cross-laminated timber plate with steel columns and a cantilever wall with a line connection. Only one of the latter type – Setup L-I – is presented in this thesis; the results of others are published in (Tuhkanen & Rauk, 2019). Such a choice was made to show the importance of the calculation model for the effective implementation of the connection.

A cantilever wall with dimensions 1.45×3.2 m was cut from a 100 mm thick cross-laminated timber plate (5 layers of 20 mm, European spruce *Picea abies*). The wall was connected continuously to the steel beam on the floor with a slotted-in steel plate using self-perforating dowels SBD 7.5×95 mm. The connection included 14 dowels in two rows (altogether 28 dowels) in increments of 100mm. Between the cross-laminated timber plate and steel beam, 10mm-thick oiled film-faced plywood was used to minimise friction. Global lateral top displacement, vertical displacement on both walls' bottom ends, and the sliding was measured during the test. The measuring points are marked with the letter M in the drawing. The test setup is presented in Figure 37.

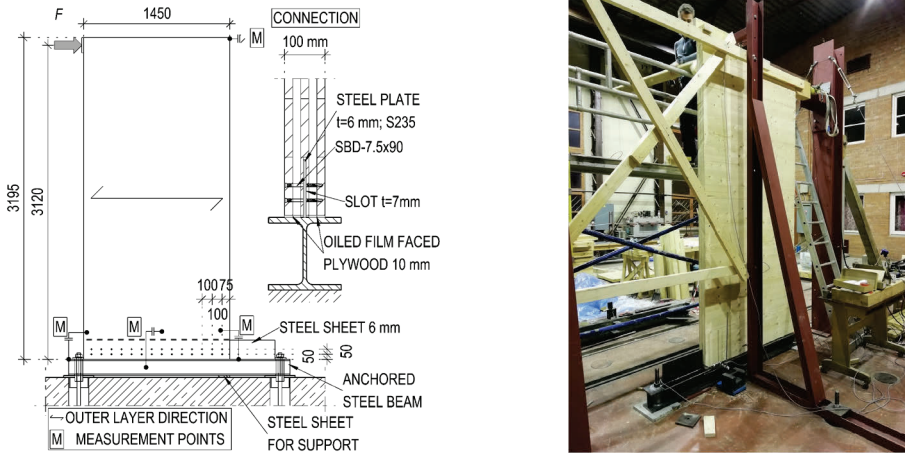


Figure 37. Line-connected cantilever shear wall

4.4.3 Selected models for test validation

4.4.3.1 General

Shear wall test results were compared with models proposed by Reynolds et al. (2017) and Flatscher (2017). The first one is a linear method where the load-carrying capacity of the connection unit (two dowels) is directly applied to the calculation, without considering the stiffness. The second one is a displacement-based method, where the racking strength is found through an iterative process and thereby maximises the potential of the connection. The comparison of these two expresses the importance of the design model in accomplishing the potential of the shear wall and connection.

4.4.3.2 Model by Reynolds et al. (2017)

The model proposed by Reynolds et al. (2017) considers cross-laminated timber as a rigid body. The tensile capacity of the connections under the wall is distributed triangularly, and compression zone at the wall end is also considered – see Figure 38.

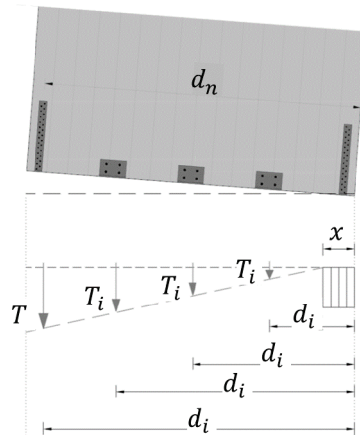


Figure 38. Triangular distribution of tensile capacity and compression zone. Drawing is reproduced from (Lukacs et al., 2019)

Following steps are required to determine the lateral resistance of the shear wall F_{rg} (referred to (Lukacs et al., 2019)):

1. Determine the tensile strength (T) of the connector furthest from the point of rotation
2. Calculate the tensile capacity (T_i) of remaining connectors based on a triangular distribution

$$T_i = T \cdot \frac{d_i}{d_n} \quad (29)$$

, where d_n [m] - distance from the panel edge to the furthest connector. T_i should not exceed the maximum capacity of the actual connector.

3. Calculate the compression zone (x) of the wall

$$x = \frac{q \cdot l + \Sigma T_i}{f_c \cdot t_{eff}} \quad (30)$$

, where q [kN/m] - uniformly distributed load (if it exists); l [mm] - length of the wall; f_c [N/mm²] - compressive strength of cross-laminated timber; t_{eff} [mm] - width of the vertical lamellas of the panel.

Note: in this thesis, compression zone length was measured from the point of rotation (PoR), not calculated.

4. Determine the lateral resistance (F_{rg})

$$F_{rg} = \frac{1}{h} \cdot \left[\sum_{i=1}^n T_i \cdot \left(d_i - \frac{x}{2} \right) + \frac{q \cdot l^2}{2} - (q \cdot l) \cdot \frac{x}{2} \right] \quad (31)$$

, where h [m] - height of the wall.

4.4.3.3 Model by Flatscher (2017)

The model proposed by Flatscher (2017) predicts the total load-displacement behaviour of cross-laminated timber shear wall based on connection behaviour. The influence of the connections is calculated on the assumption that the wall plate acts as a rigid body. In order to find a total top displacement of the wall, elastic deformation from panel shear and bending must be added separately. In this thesis, the focus is on the connection, and wall deformations were not considered. Figure 39 presents the elements and notations of the model (referred to (Flatscher, 2017)).

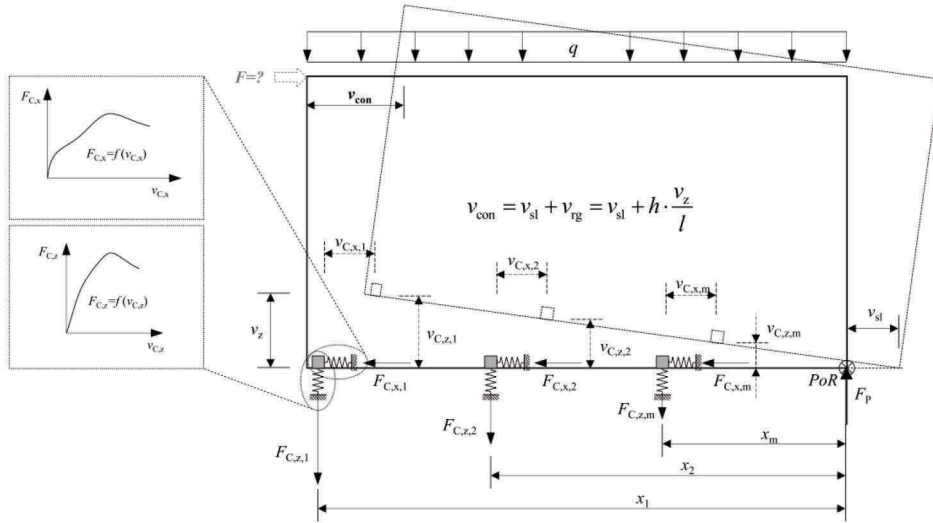


Figure 39. Elements and notations of the displacement-based model (Flatscher, 2017)

Since the rocking and sliding of the wall cannot be analysed separately, the calculation process is iterative and divided into the following six steps:

1. Estimation of sliding and rocking contribution to the applied (connection-based) lateral displacement (v_{con}) through the share parameter $0 \leq p \leq 1$:

$$v_{sl} = p \cdot v_{con} \quad (32)$$

$$v_{rg} = (1 - p) \cdot v_{con} \quad (33)$$

2. Computation of lateral and vertical displacement for every connection considered in the wall:

$$v_{C,x,m} = v_{sl} = p \cdot v_{con} \quad (34)$$

$$v_{C,z,m} = x_m \cdot \frac{v_{rg}}{h} = x_m \cdot \frac{(1 - p) \cdot v_{con}}{h} \quad (35)$$

, where $v_{C,x,m}$ [mm] - lateral (horizontal) displacement of the connection; $v_{C,z,m}$ [mm]- uplift (vertical) displacement of the connection; x_m [mm] - distance between PoR and connection m.

3. Calculation of appearing load for each connection according to the respective displacement. Any linear elastic, multilinear or other methods may apply for this purpose:

$$F_{C,x,m} = f(v_{C,x,m}) \quad (36)$$

$$F_{C,z,m} = f(v_{C,z,m}) \quad (37)$$

Note: Flatscher (2017) proposed in his thesis a displacement-based analytical method, where the resulting graph is forced to go through three points, A, M and B (see Figure 40), which also considers the post maximum softening of the connection.

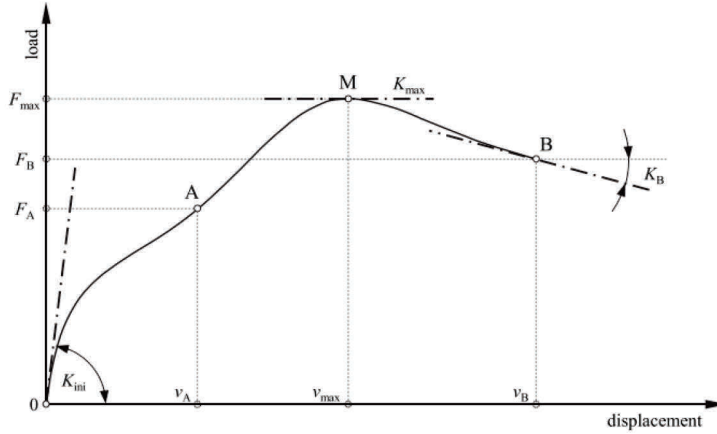


Figure 40. Proposed analytical model and corresponding parameters (Flatscher, 2017)

The simplified equation and its first derivation are expressed by the following:

$$F(v) = \frac{v + C_1 * v^2 + C_2 * v^3}{C_3 + C_4 * v + C_5 * v^2 + C_6 * v^3} \quad (38)$$

$$K_T(v) = \frac{dF}{dv} = \frac{1 + 2 * C_1 * v + 3 * C_2 * v^2}{C_3 + C_4 * v + C_5 * v^2 + C_6 * v^3} - \quad (39)$$

$$- \frac{(C_4 + 2 * C_5 * v + 3 * C_6 * v^2) * (v + C_1 * v^2 + C_2 * v^3)}{(C_3 + C_4 * v + C_5 * v^2 + C_6 * v^3)^2}$$

, where C_1 - C_6 - coefficients to be determined by boundary conditions (see Appendix).

Another simplification stands for defining the positions of points A and B in Figure 40 through maximum load:

$$F\left(v = \frac{v_{max}}{2}\right) = F_A \quad (40)$$

$$F(v = v_B) = \frac{4}{5} * F_{max} \quad (41)$$

4. Calculation of the lateral load to the CLT wall based on the connection displacements in the vertical and horizontal direction:

$$F_{sl} = \sum_{i=1}^n F_{C,x,m} + \left(\sum_{i=1}^n F_{C,z,m} + q \cdot l \right) \cdot \mu_f \quad (42)$$

$$F_{rg} = \frac{1}{h} \cdot \left[\sum_{i=1}^n (F_{C,z,m} \cdot x_m) + \frac{q \cdot l^2}{2} \right] \quad (43)$$

, where F_{sl} [kN] - load responsible for sliding, F_{rg} [kN] - load responsible for rocking. The second part of the Eq. (42) is to consider friction between wall and foundation.

- Since only one lateral load F can act at the same time, the constraint in Eq. (44) shall have complied. If the estimation in step 1 is not satisfied, steps 1 to 4 must be repeated, until the maximum lateral load to the wall is derived.

$$F = F_{sl} = F_{rg} \quad (44)$$

- According to the maximum load found in step 5, the calculation of the final elastic deformation of CLT wall (not handled in this thesis).

Note: the original formula for rocking load Eq. (43) does not consider the actual compression zone. As suggested by Flatscher (2017), the reduction of rocking capacity was taken into account assuming the compression (bearing) load to act on one third of the compression zone (originally marked as l_p) – see Figure 41. In this thesis, compression zone length was measured from the point of rotation (PoR), not calculated.

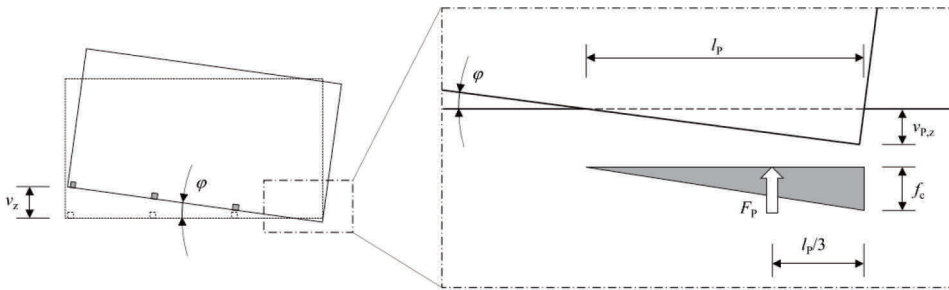


Figure 41. Consideration of compressional stress and indentations (Flatscher, 2017)

5 RESULTS, ANALYSIS AND DISCUSSION

5.1 Embedment strength in cross-laminated timber

5.1.1 Results of database BU

The complete set of tables of the results of database BU are provided in (Blass & Uibel, 2007). Model 1 and Model 2 expressed by Eq. (6) and (7), respectively, were developed based on this database. Figure 42 compares the original data of database BU with predicted values, according to Eq. (7), which was selected as the basis for this thesis.

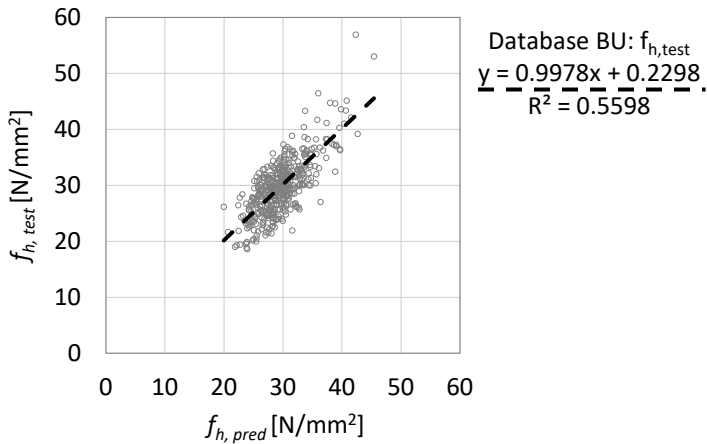


Figure 42. Comparison of test results with predicted values according to Model 2 developed by Blass & Uibel (2007)

5.1.2 Results of databases TO, TMS and 50|50

Embedment strength mean values, 5%-quantiles and CV of all unique databases – TO, TMS and 50 |50 referenced to 12% moisture content are summarised in Table 7, Table 8 and Table 9 respectively.

Table 7. Embedment strength results of database TO

α	Dowel \varnothing [mm]	Specimen thickness [mm]	$\zeta = \frac{\sum t_{0,i}}{\sum t_{90,j}}$	Number of layers	f_h [N/mm ²]		CV [%]
					mean, $u=12\%$	0.05, $u=12\%$	
0°	10	45	~1.25	3	31.6	25.2	12.2
	12	45			31.8	24.7	13.8
	20	100			24.3	21.3	7.8
45°	20	100	1.5	5	23.1	20.4	8.3
90°	10	45	~1.25	3	30.8	25.2	13.9
	12	45			30.7	26.5	9.8
	20	100			23.1	21.1	5.6

Table 8. Embedment strength results of database TMS (only cross-laminated timber)

α	Dowel \emptyset [mm]	Specimen thickness [mm]	$\zeta = \frac{\sum t_{0,i}}{\sum t_{90,j}}$	Number of layers	f_h [N/mm ²]		CV [%]
					mean, $u=12\%$	0.05, $u=12\%$	
0°	20	100	1.5	3	24.1	22.3	6.4
				5	23.9	22.2	6.4
				9	25.4	23.7	4.8

Table 9. Embedment strength results of database 50|50

α	Dowel \emptyset [mm]	Specimen thickness [mm]	$\zeta = \frac{\sum t_{0,i}}{\sum t_{90,j}}$	Number of layers	f_h [N/mm ²]		CV [%]
					mean, $u=12\%$	0.05, $u=12\%$	
0°	20	80	1.0	3	20.7	18.4	8.7
90°					19.1	17.6	6.2

These results were compared with the Model 2 provided by Blass & Uibel (2007) – see Eq. (7). The mean value is overestimated up to 30 % in the case of database 50|50, and up to 20% in the case of the others. It is also visible in Figure 43, where the majority of the data points stay below the correlation line. Therefore, several influence parameters were analysed separately to find possible causes.

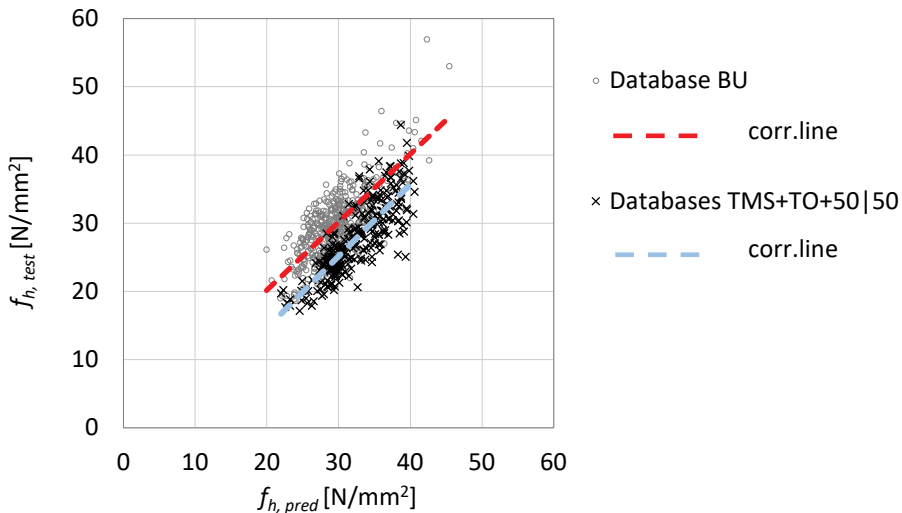


Figure 43. Comparison of test results of databases TMS, TO and 50|50 and Model 2 by Blass & Uibel (2007)

5.1.3 Influence of the moisture content

As previously stated, models proposed by Blass & Uibel (2007) were developed without moisture-corrected values. Figure 44 (left and middle) presents the moisture content distribution by specimen configuration and dowel diameter. The actual, declared moisture content of specimens differed from the 12% reference value, especially for thinner samples. Figure 44 (right) presents the deviation of the correlation line once the corresponding procedure has been performed. Most affected are the higher embedment strength values of thinner specimens and small dowel diameters. Overall, the total mean value of embedment strength decreased by 3.7% due to the correction.

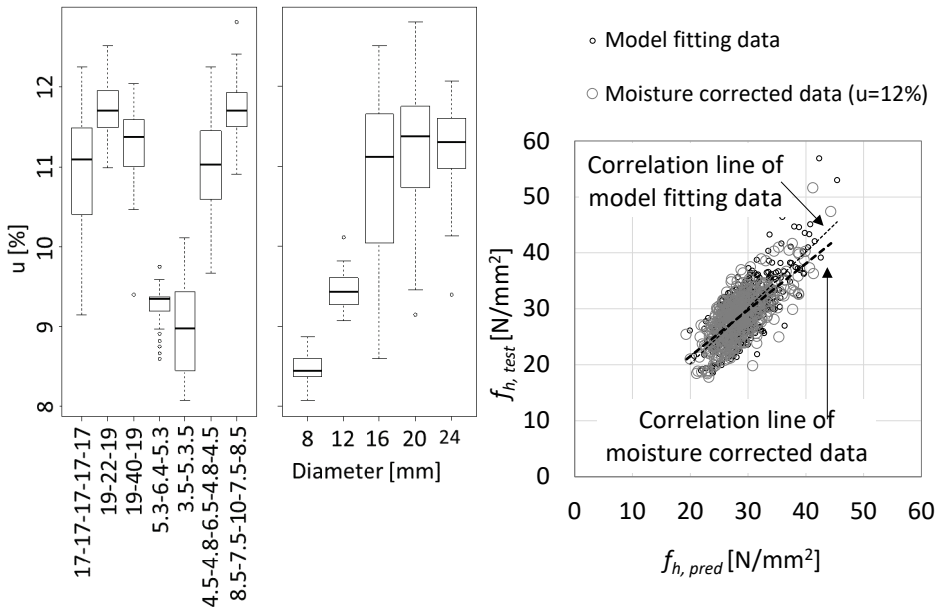


Figure 44. Left and middle: distribution of moisture content by specimen configuration and by dowel diameter; right: Model 2 with moisture corrected embedment values

5.1.4 Influence of the density

Density, as one independent variable in Model 2, is powered by 1.16, unlike Eq. (4) for solid wood, where the relation is linear. The same applies to moisture corrected data, as can be seen in Figure 45. When considering all the databases, the exponent is 1.46. Since database BU covers a wide range of densities, diameters, and configurations, in further comparisons, the influence of the density is excluded by dividing the embedment strength by $\rho^{1.16}$.

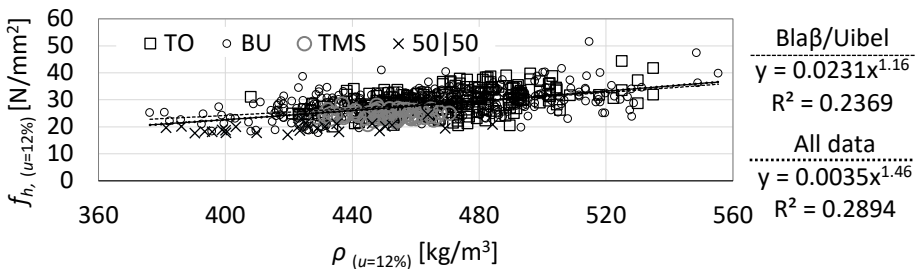


Figure 45. Embedment strength vs density of database BU and all databases

5.1.5 Influence of the diameter

The diameter was the second variable in regression analysis, developing the design model of Blass & Uibel (2007). Therefore, results by diameter groups fit very well with the regression line – see Figure 48. Dowels with smaller diameters – eight and twelve millimetres – have more substantial deviation, but this is caused by the moisture correction emphasised before.

However, in analysing the original Model 2 without moisture correction in Figure 42, it must be noted that results of the samples with a smaller diameter are dominantly above the regression line, i.e. underestimated. The ratio of embedment strength to the diameter, according to Eq. (7), is linear, similar to the solid wood – see Eq. (4). Figure 46 presents a normalised embedment strength dependence on diameter. Since the database BU covers a wide range of densities, diameters, and configurations, only these values were considered. There is an exponential increase of embedment strength at smaller dowel diameters, which leads to a conclusion that the model should consider this, similarly proposed for hardwood by Hübner (2013).

For further comparison of different layup configurations, the influence of the diameter was excluded by referencing it to the diameter of 20 mm, i.e., dividing the embedment strength by $(d/20)^{-0.286}$. Figure 47 compares all databases by diameter, and it is evident that most values from other databases are not in line with the BU database. Loading angle was not considered in this comparison.

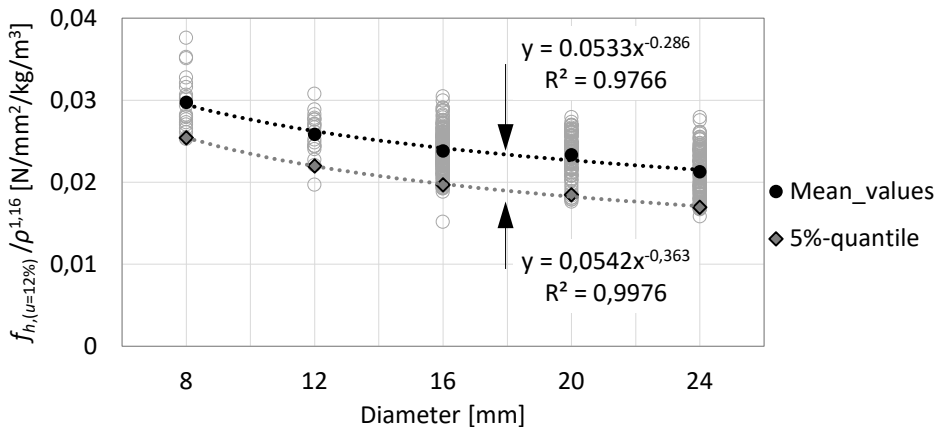


Figure 46. Normalised embedment strength vs dowel diameter based on BU database

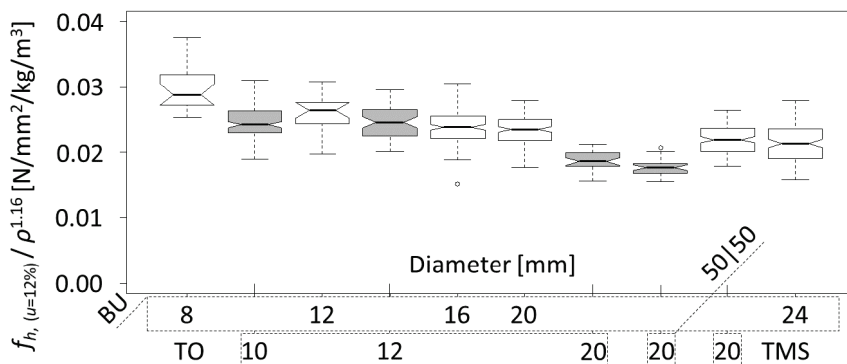


Figure 47. Comparison of the results by diameter groups of all databases

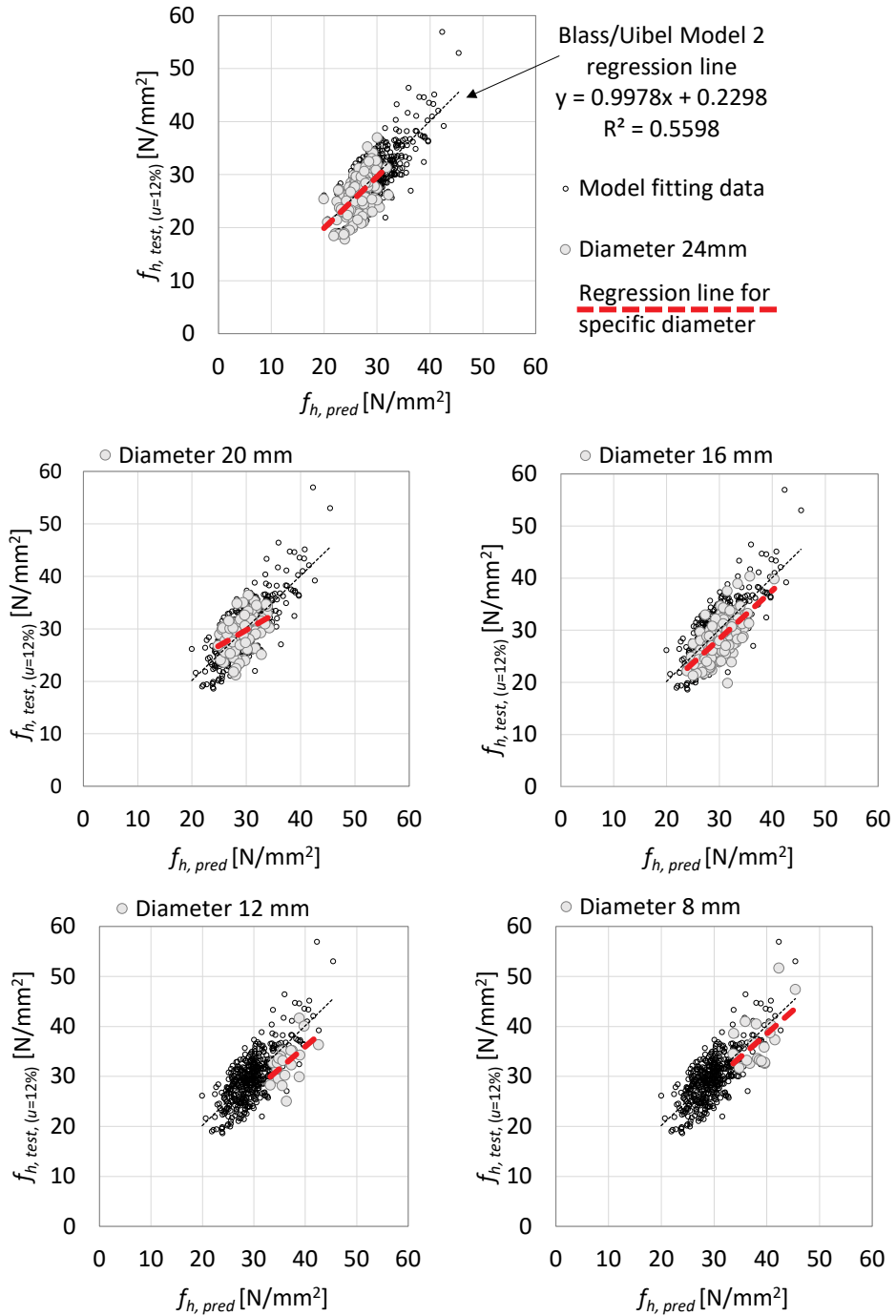


Figure 48. Distribution of the results by dowel diameter (moisture corrected data)

5.1.6 Influence of the loading angle

In Eq. (7), the influence of the loading angle is expressed analytically by the Hankinson formula $- 1.1 \cdot \sin^2\alpha + \cos^2\alpha$. Figure 49 compares the normalised embedment strength values referenced to the dowel diameter of 20 mm of databases BU and TO, since both include the loading angles 0, 45 and 90 degrees. It turns out that the reduction of the embedment strength remains in the range of 10%, but the lowest value has a loading angle of 45 degrees. The difference between mean values of loading angles of 0 and 90 degrees is 6%. A similar phenomenon has been identified by (Nakashima et al., 2012). When considering the result in the multi-regression analysis, the slightly better correlation coefficient of Eq. (7) can be achieved.

The manner of embedment failure can explain this appearance. Figure 50 presents the load-displacement curves of specimens loaded at an angle of 45 and 90 degrees. Their nature is somewhat different. Although in both cases, a clearly visible plateau shaped out, at 90 degrees, the graph continues to grow after reaching the plastic state, which is due to the densification of crossed layers, also called as hardening effect. A cut-out and front view of the 90-degree sample is shown in Figure 51, left and middle, the corresponding failure art of the 45-degree specimen is on the right. At 45 degrees, the dowel is not able to compress the wood fibres in either layer entirely and seemingly cuts into the test piece. Furthermore, in crossed layers of 90-degree specimens, additional tensile forces will occur when they have locked between longitudinal layers. This phenomenon, the rope effect, as well as the densification of the crossed layers, is also described in (Schweigler et al., 2016) in the context of LVL.

The influence of the densification is also expressed in Table 10. The increase of the embedment strength of 0- and 90-degree samples at higher deformation levels is up to 5.7%. 45-degree specimens do not follow the same pattern - the value decreases by 2.7%.

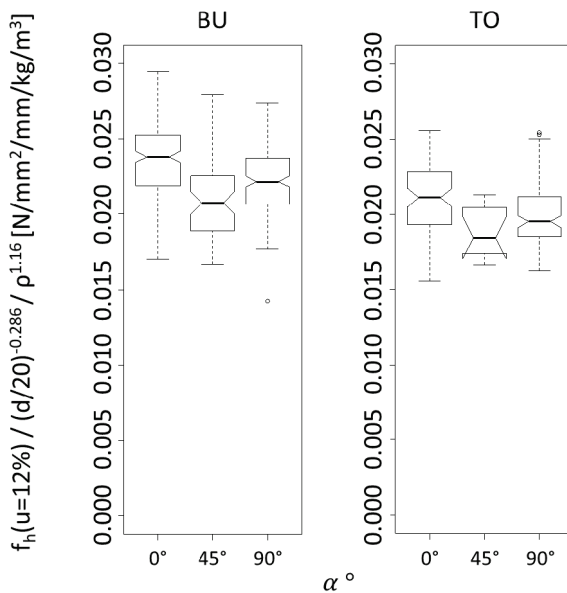


Figure 49. Comparison of the results by loading angle of databases BU and TO

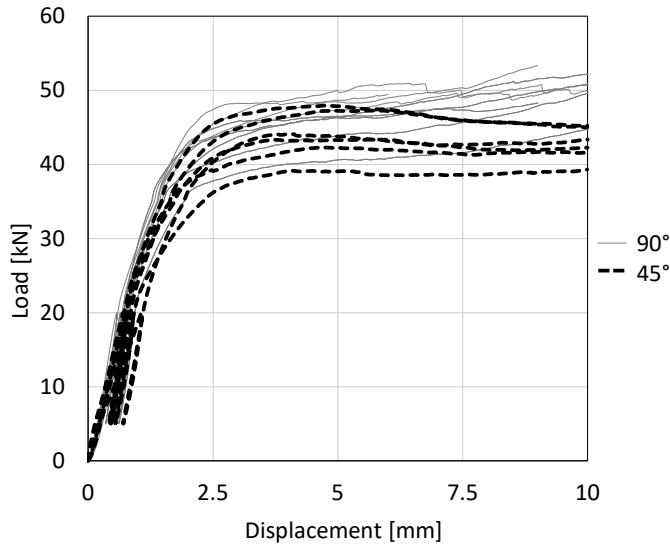


Figure 50. Typical embedment test curves loaded at an angle 45 and 90 degrees

Table 10. Embedment strength at different deformation levels in TO database

α	$f_{h,mean,5mm}$ [N/mm ²]	$f_{h,mean,7mm}$ [N/mm ²]	$f_{h,mean,9mm}$ [N/mm ²]
0°	31.4	32.1 (+2.1%)	33.0 (+5.1%)
45°	23.3	22.6 (-2.7%)	22.6 (-2.7%)
90°	30.7	31.2 (+1.7%)	32.5 (+5.7%)



Figure 51. Left and middle: densification in crossed layers; right: embedment by sample loaded at an angle of 45 degree

5.1.7 Influence of the layer thickness and layup

The first indication of the effect of the layer thickness and layup to embedment strength revealed from the parameter study with a database TMS (Tuhkanen et al., 2018). The results of the embedment test are presented in Table 11 and Figure 52 (right) as a diagram. In the table, 3-layer samples as reference are highlighted in grey and Δ expresses the difference from this value. Figure 52 (left) compares the results of 3-, 5- and 9-layer glulam and cross-laminated timber specimens by the meaning of box-plot.

Table 11. Mean values, 5%-quantiles and CV for embedment strength referenced to 12% MC. Δ expresses the difference from 3-layer specimen

n	$f_{h,mean}$ [N/mm ²]			$f_{h,05}$ [N/mm ²]			CV [%]			
	GLT	Δ	CLT	Δ	GLT	Δ	CLT	GLT	CLT	
3	29.1		24.1		27.3		22.3	5.1	6.4	
5	28.5	-2.1%	23.9	-0.8%	26.3	-3.6%	22.2	-0.4%	5.0	6.4
9	29.4	+1.0%	25.4	+5.4%	27.0	-1.1%	23.7	+6.3%	4.9	4.8

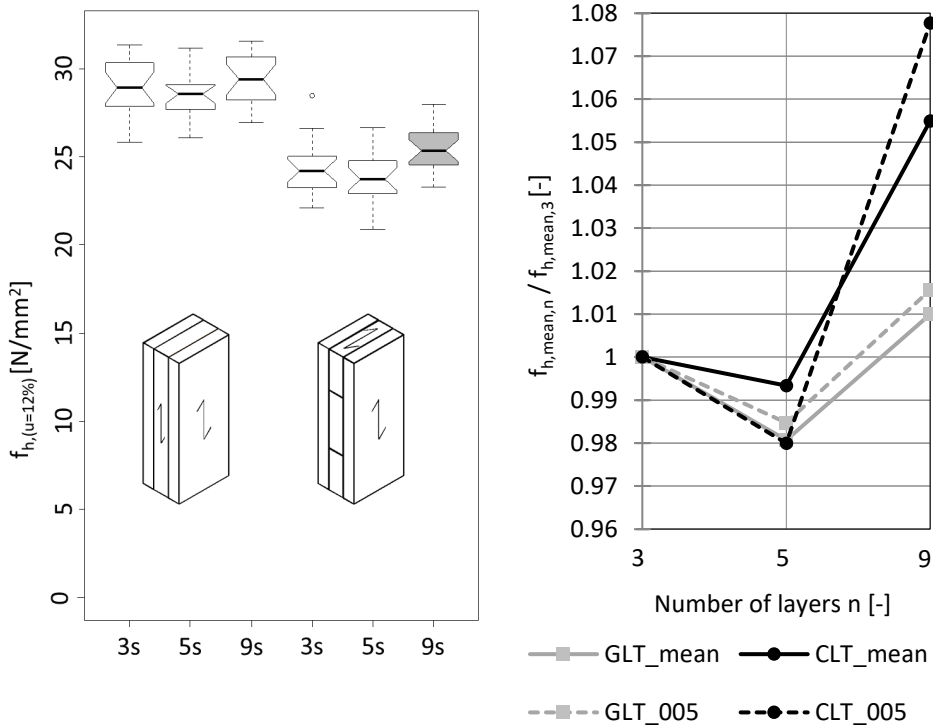


Figure 52. Comparison of the embedment strength of identical samples with different number and thickness of layers. Left: boxplot; right: mean values and 5%-quantile related to 3-layer specimen

The differences between the mean values of the glulam groups are small, going up to 3.1%. In contrast, the cross-laminated timber tends to show a clear trend toward higher values for embedment strength by thinner layers. Mean values between 5 and 9-layer samples reach 6.7%; even the difference between the mean density values is up to 1.5%. The analysis was performed to test the statistical significance of the results. When comparing the results of the 3- and 5-layer specimens with 9-layer specimens, the difference is significant, with $p = 0.0513$ and $p = 0.0059$, respectively (Anova/ Tukey's HSD). The glulam results do not show a similar tendency; therefore, the size effect and the higher number of adhesive layers can be excluded as a possible cause of this difference in cross-laminated timber group.

One possible explanation is the locking effect which can be recognised in Figure 53. Adjacent surfaces prevent splitting of the individual layers and are more effective in thinner layers. Crossed layers will try to recover the initial shape after loading, and it is strongly pronounced in thicker layers. It is important to note that the bowed shape is not caused by plastic or elastic bending of the dowels. The partly split areas in the longitudinal outer layers and the internal layer of 3-layer specimen permits determine the locking range. The maximum measured crack depths were 10-15 mm, which means that the effective locking area is up to 15 mm.

The additional increase of the embedment strength comes from the previously described rope-effect. Figure 54 presents the shear failure in crossed layers due to the tensile forces. More internal crossed layers will increase the area that works in shear, while thin layers will reduce the horizontal crack propagation under the dowel, which would otherwise reduce the shear area.

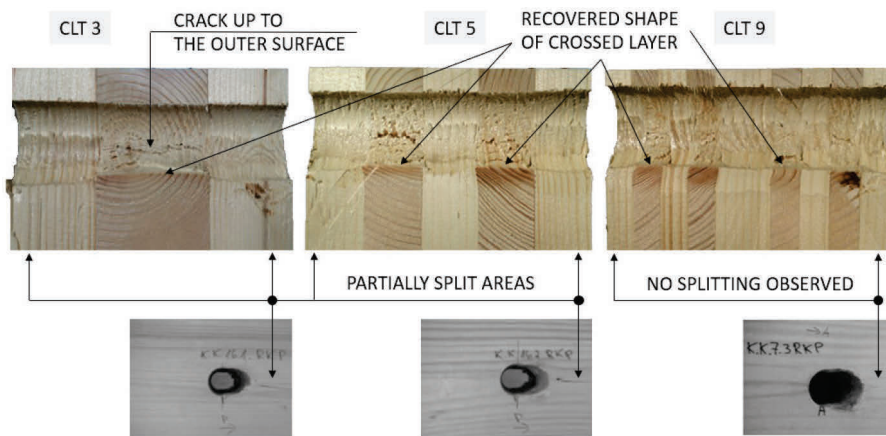


Figure 53. Locking effect between adjacent layers



Figure 54. Shear failure in crossed layer due to the rope effect

Figure 55 compares the specimen groups by configuration in database BU, referenced to the diameter of 20 mm. All loading angles are included in these groups; therefore, no definitive conclusions can be drawn. However, the configuration 19-40-19 has significantly lower values, which probably reflects the lowest build-up ratio $\zeta = 0.95$. The highest values can be found in the groups with five layers, except the configuration 4.5-4.8-6.5-4.8-4.5. When comparing groups by the number of layers, three-layer specimens have a 7% lower mean value compared to five-layer samples in total.

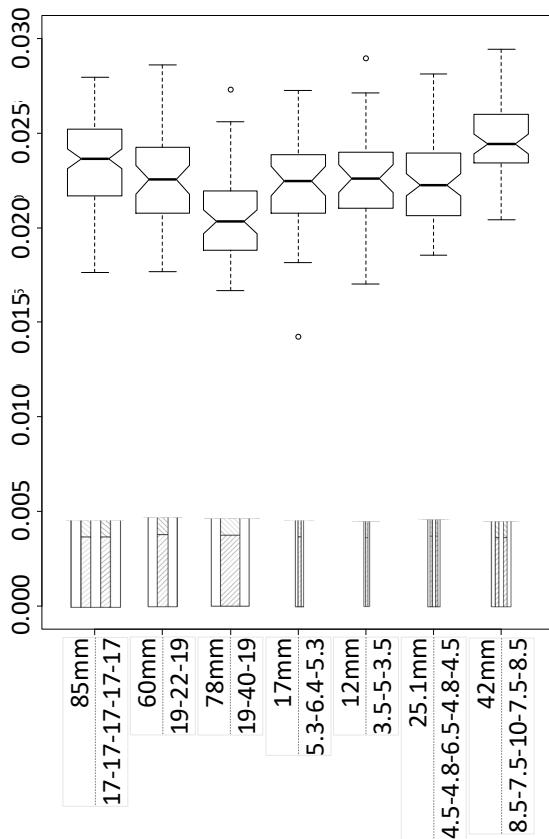


Figure 55. Comparison of the groups by configuration in database BU

In Figure 56, the same groups are split in two according to the loading angles 0 and 90 degrees. The ratio of the mean embedment strength perpendicular to the grain to embedment strength parallel to the grain is shown above the graphic. In all cases, the value is higher in the predominant layer direction. What is out of the ordinary is sample configuration 19-40-19, which should be almost equal when loaded at 0 and 90 degrees (highlighted in the drawing). Contrary to expectations, though, the mean value in the transverse directions differs 13%. Furthermore, at 0 degrees, the embedment strength is far lower than at 90 degrees in most of the other configurations, despite the higher percentage of layers in the loading direction. One possible explanation could be that when the internal layer is in the loading direction, splitting is prevented on both sides – compare Figure 53 (left)). In outer layers, densification and a rope effect still exist.

Contrary to that fact, a particular test campaign with database 50|50 did not confirm this phenomenon. The embedment strength values in both directions were in principle equal. It must be emphasised that the specimens were produced from one small plate, and no special monitoring of knots or other defects was done during manufacturing. This issue needs further investigation.

Concerning Model 2, Figure 57 presents the distribution of the results by configuration. The most significant deviations from the correlation line occur in the group 19-40-19 and 3.5-5-3.5, the latter again, reflects the moisture correction discussed previously.

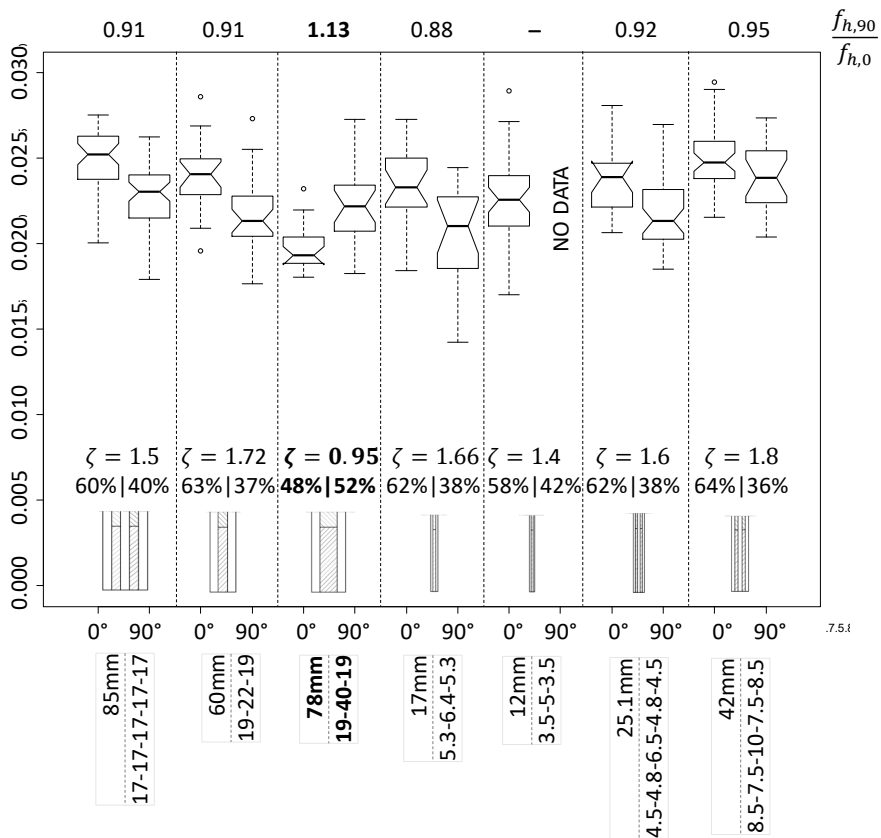


Figure 56. Comparison of the groups by configuration and loading angle in database BU

5.1.8 Remarks on influencing factors

In previous chapters, several factors influencing embedment strength in cross-laminated timber were analysed and discussed. Since the broadest selection of parameters was present in the BU database, mostly this data was used. Parameter studies TMS and 50|50 covered a very narrow range of configurations and only one dowel diameter, which was also the purpose. It is difficult to express the factor that will influence the result most, as there were many combinations of variables. However, what can be highlighted is the low moisture content of part of the specimen groups and the fact that samples with thin layers were used prevalingly to develop the model. It was not clearly expressed in comparison among three and five-layer configurations, but the effect of the thickness of the layers was indicated by both the parameter study TMS, and the sample with 40mm-thick layer in BU database. Other factors such as the surface of the dowel and exceeded limits of specimen thickness (dowel slenderness) in databases TMS, TO and 50|50 was not measured or considered.

Since the database TO is the second largest and covers three different angles and three dowel diameters, an additional comparison of normalised values was made. That means all results were moisture and density corrected and referenced to the diameter of 20 mm. By all angles, 0, 45 and 90 degrees, values of database BU were ~11% higher than database TO. This is much lower than compared to developed Model 2, where the

difference was 17%, 25% and 12% accordingly. This will also confirm that the model will overestimate the results in the practical range.

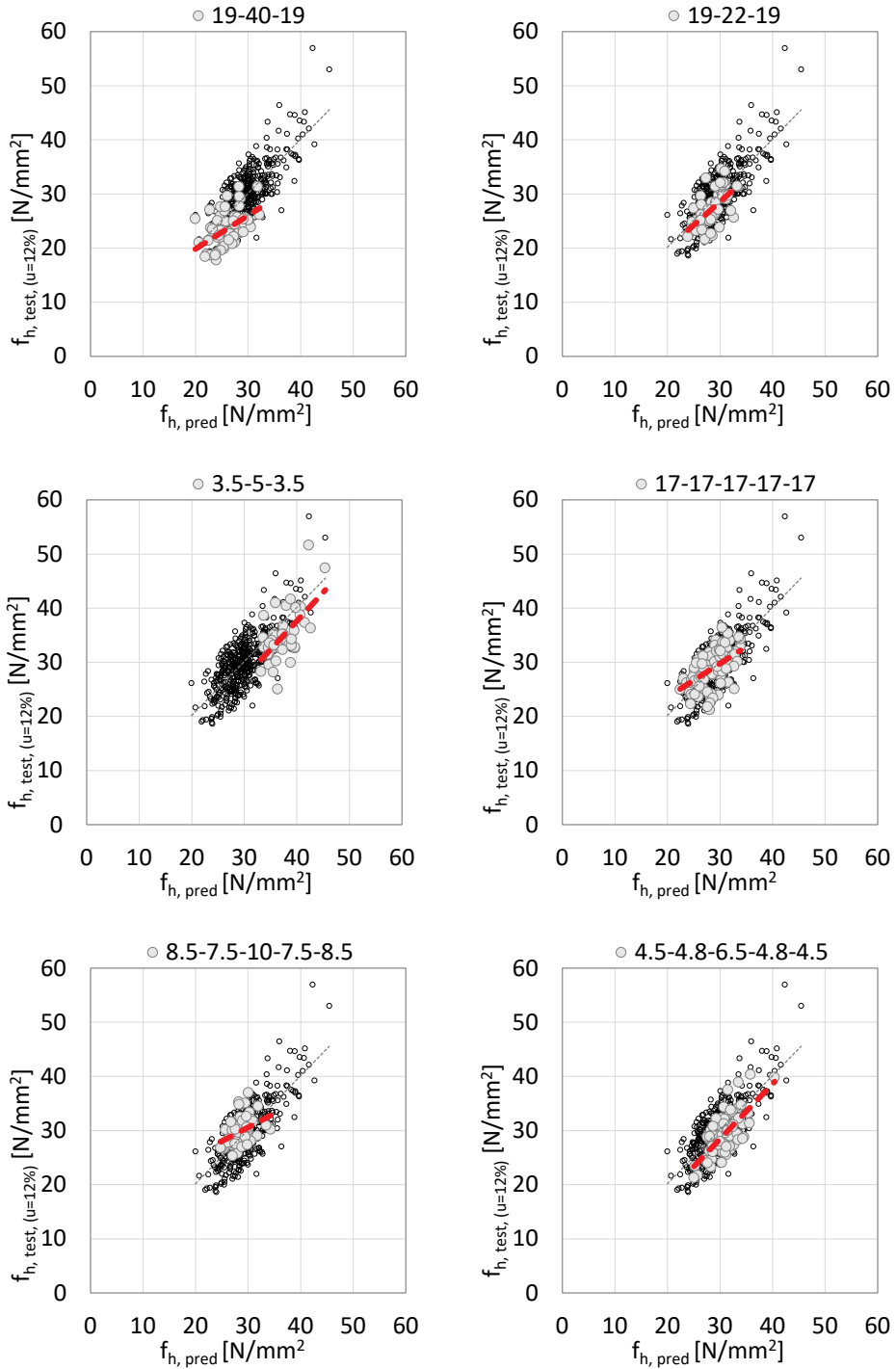


Figure 57. Distribution of the results by dowel diameter

5.1.9 Embedment strength model analysis and proposal

Figure 58 presents the result of multiple regression analysis, where all databases were included. First, the format of the equation was kept the same as Eq. (7) resulted in Eq. (45):

$$f_{h,pred} = \frac{0.016(1 - 0.015d)\rho^{1.28}}{1.1\sin^2\alpha + \cos^2\alpha} \quad (45)$$

where $f_{h,pred}$ [N/mm²] - predicted embedment strength; d [mm] - diameter of dowel-type fastener; ρ [kg/m³] - density of wood; α [°] - loading angle to the outer layers.

The correlation coefficient R decreased to 0.69 compared to the original 0.75. The slope and the ordinate intersection point of the correlation line changed without a significant shift.

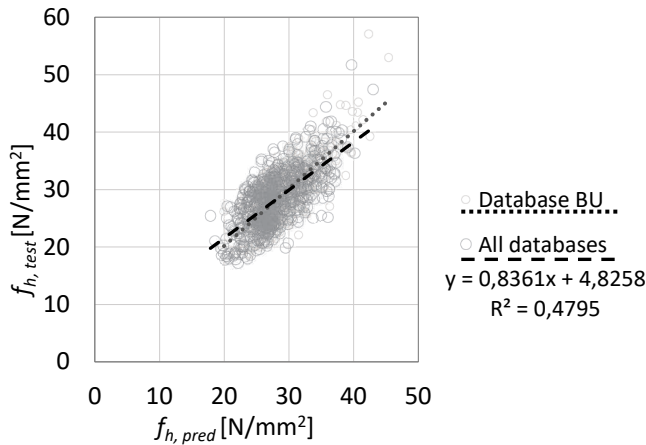


Figure 58. Comparison of the test data with the prediction model with an old format, all data included.

The data correlated slightly better when a new equation format was used. Here, the embedment strength dependence on the diameter is exponential:

$$f_{h,pred} = \frac{0.02 \cdot \rho^{1.29} \cdot d^{-0.23}}{1.1\sin^2\alpha + \cos^2\alpha} \quad (46)$$

This model, in turn, can be improved if the influence of the loading angle is considered according to Figure 49, and the following equation expresses the model:

$$f_{h,pred} = \frac{0.014 \cdot \rho^{1.34} \cdot d^{-0.22}}{\cos^2(2\alpha) + 1.075 \cdot \sin^2(2\alpha) + 0.05 \left(\frac{\alpha}{90^\circ}\right)} \quad (47)$$

Both models are presented in Figure 59. In both cases, the model still overestimates the embedment strength in the samples, where the layer thickness is in practical range. Therefore, multiple linear regression analysis with relevant specimen groups has proceeded:

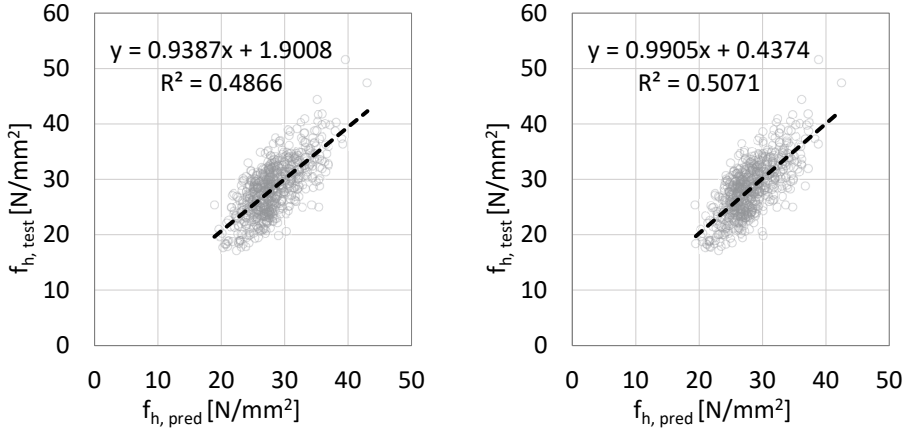


Figure 59. Left: comparison of all test results with the prediction model Eq. (46); right: the same model considering the real influence of the loading angle

- TO: complete database (layer thickness 20 mm)
- TMS: three- and five-layer samples (layer thicknesses 20, 30 and 40 mm)
- 50|50: complete database (layer thickness 20 and 40 mm)
- BU: sample groups 19-40-19 and 19-22-19

This selection contains 367 tests, dowel diameters of 10, 12, 20 and 24 mm are presented. The mean density value, 5%-quantiles and CV of the selected group are shown in Table 12. CV of embedment strength of the group is 18.8%.

Table 12 Density values of selected specimens ($u = 12\%$)

Number of tests	$\rho_{mean} \left[\frac{kg}{m^3} \right]$	$\rho_{05} \left[\frac{kg}{m^3} \right]$	CV[%]
367	457	405	6.7

The result of multiple linear regression analysis for the embedment strength mean value is expressed by the following:

$$f_{h,pred} = \frac{0.08 \cdot \rho^{1.09} \cdot d^{-0.32}}{\cos^2(2\alpha) + 1.075 \cdot \sin^2(2\alpha) + 0.05 \left(\frac{\alpha}{90^\circ} \right)} \quad (48)$$

Figure 60 (left) compares the test results with predicted values; a good correlation of $r = 0.79$ can be found.

The corresponding model for characteristic value can be expressed by the following:

$$f_{h,k} = \frac{0.057 \cdot \rho_k^{1.12} \cdot d^{-0.32}}{\cos^2(2\alpha) + 1.075 \cdot \sin^2(2\alpha) + 0.05 \left(\frac{\alpha}{90^\circ} \right)} \quad (49)$$

where $f_{h,k}$ [N/mm²] - characteristic embedment strength; d [mm] - diameter of dowel-type fastener; ρ_k [kg/m³] - characteristic density; α [°] - loading angle to the outer layers.

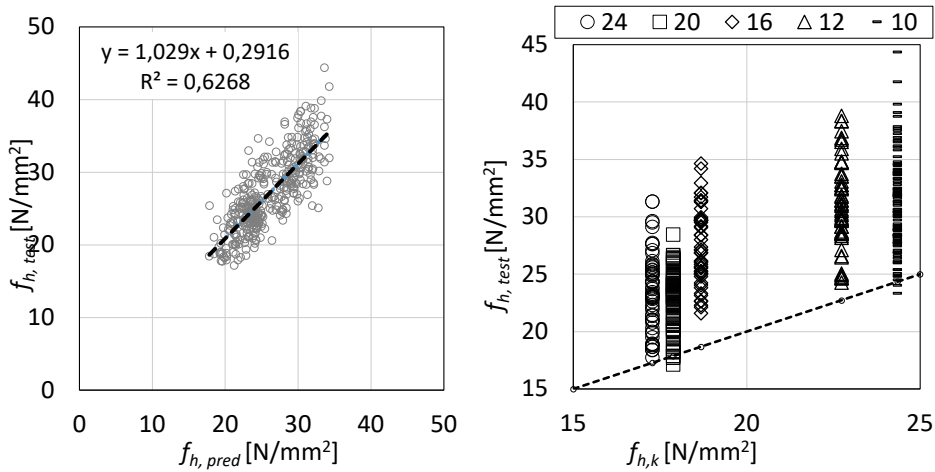


Figure 60. Left: comparison of the test results of specimens with a layer thickness of 19 to 40 mm with a new prediction model Eq. (48); right: comparison of test results of dowel groups by diameter and predicted characteristic values. The dashed line presents the characteristic value

5.2 Connection test results

5.2.1 Yield moment of the dowel

The dowels were bent up to 45 degrees, type SBD up to 30 degrees. It must be mentioned that only one SBD dowel was tested. Due to the high steel strength, the machine worked near the limit, and no more tests were made for safety reasons. Despite this, the measured value was used in theoretical calculations to validate the test results. All results, including moment values at 15 degrees as required based on (EN 409, 2009), are shown in Table 13. Tensile strength f_u values based on four tests for both types were 1243 MPa [CV 4.7%] for SBD and 574 MPa [CV 3.3%] for WS.

When using tested tensile strength in Eq. (2), values 25% and 30% lower emerge in comparison with the measured yield moment for type WS and SBD accordingly. When using Eq. (3) and assuming $f_y = 0,94 \cdot f_u$, differences are -8% and -18% respectively. A significant discrepancy compared to the DoP appears in the case of dowel type SBD, where 58% lower value compared to the test is declared in the document (Rothblaas, 2017).

Although visible cracks appeared on the tensile side of the bent SBD dowel (see Figure 61), there was sufficient plastic deformation without braking for bending angles up to 40° for both dowel types, which permits the assumption of the use of the plastic bending capacity, including strain hardening of the dowel.

Table 13. Yield moment of tested dowels

Dowel type	Number of tests	$M_{45^\circ, mean}$ [Nm]	$M_{45^\circ, 05}$ [Nm]	CV (%)	$M_{15^\circ, mean}$ [Nm]	$M_{15^\circ, 05}$ [Nm]
SFS-7x153	10	35.4	34.7	1.26	33,5	32,8
SBD-7.5x95	1	102 (stop at 30°)	-	-	100	-

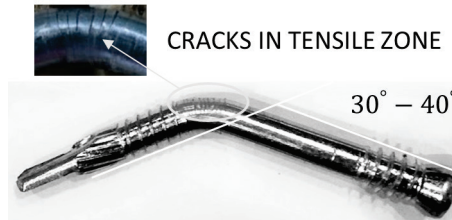


Figure 61. Cracks in the tensile zone of bent SBD dowel

5.2.2 The load-carrying capacity of the dowel and the rope effect

Connection test results are summarised in Table 14. As a reminder, the values of some groups are based on one or two experiments only (cf. Table 1). Due to the asymmetry of the short dowel placement and the possible impact of the drill tip, the load-carrying capacity per dowel (two shear planes) is presented. Since the values in the table are absolute, normalisation by density was performed before further comparison of the relevant groups.

Table 14. Load-carrying capacity per dowel based on connection tests

α	Dowel type	$F_{v,R,mean}$ [kN]	$F_{v,R,05}$ [kN]	CV [%]
0°	SBD-7.5x95	14.0	13.0	4.2
	SBD-7.5x195	14.8	-	-
	WS-7x153	10.6	-	-
45°	SBD-7.5x95	13.0	-	-
	SBD-7.5x195	13.4	-	-
	WS-7x95	9.9	-	-
90°	WS-7x233	9.6	9.3	6.7
	SBD-7.5x95	14.0	12.7	6.6
	SBD-7.5x195	14.9	-	-
	WS-7x153	12.5	-	-

It was assumed that the rope effect occurs during the test due to the threads on both ends of the dowel. Visual observations confirm that the threaded parts of short dowels activated against pull-out: tests using long dowels needed additional screws on either side of the steel plate to prevent splitting the whole specimen (see Figure 62). Samples with short dowels (threaded parts were inside the timber) did not need any additional measures – all of them failed in the embedding and yielding of the dowel, while no other failure types (specimen splitting, row shear, block shear) occurred. The cutouts of the failed connections are presented in Figure 63 and Figure 64. In the case of type SBD, failure mode (g), according to Eq. (1) was decisive. Still, due to the smaller diameter and lower steel strength, type WS was near to the mode (h), confirming that the dowel was slightly bent on both side of the steel plate, and the embedded area next to the outer surface was shorter than on the long SBD dowels.

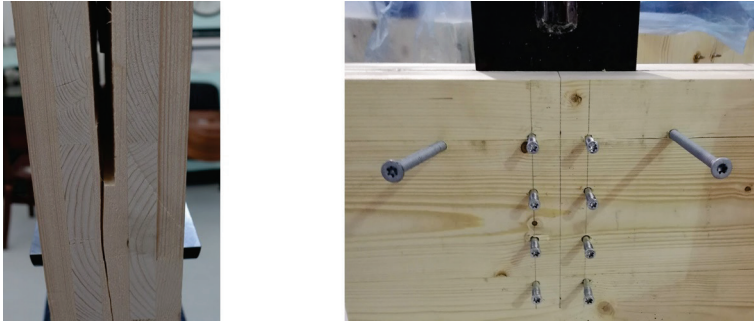


Figure 62. Left: splitting of the whole connection; right: reinforcement to avoid splitting



Figure 63. Left: embedded area of long SBD; right: the same for long WS



Figure 64. Left: dowel failures in connection; right: embedded area under the drill tip SBD

In order to compare the expected difference of the load-carrying capacity of the long and short dowel (both calculated without rope effect) and the real difference from test results, the following calculation was made. Specimens were divided into three groups, where both dowels (long and short) were represented:

- Loading angle 0° - SBD-7.5x95 versus SBD-7.5x195
- Loading angle 90° - SBD-7.5x95 versus SBD-7.5x195
- Loading angle 45° - WS-7x93 versus WS-7x233

For every group, the mean density was found. This value was taken as a reference to normalise the embedment strength, according to Eq. (50):

$$\bar{f}_h = f_h \cdot \left(\frac{\rho_{mean}}{\rho} \right)^{1.16} \quad (50)$$

, where \bar{f}_h [N/mm²] - normalised embedment strength, f_h [N/mm²] - embedment strength test value, ρ_{mean} [kg/m³] - mean density of the connection group, ρ [kg/m³] - density of the embedment specimen.

Then, the density normalised embedment strength was referenced to the diameter of the dowel of the corresponding connection group (7 or 7.5 mm) dividing the embedment strength by $(d/d_{ref})^{-0.286}$.

The estimated load-carrying capacity of the dowel was calculated according to Eq. (1) using normalised mean embedment strength and yield moment obtained from the bending test. The extent of the length of the dowel (t_1) in the timber was 46.5 mm for shear plane on the dowels head side. For the shear plane on the side of the drill tip, corresponding values were 31.5 mm for type SBD and 27 mm for type WS – see Figure 65.

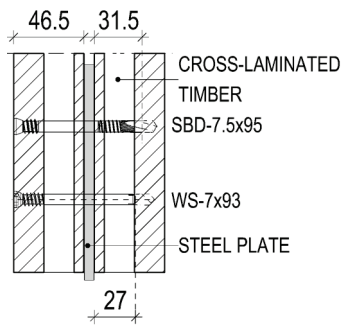


Figure 65. t_1 values for dowel type SBD and WS

According to Eq. (1), failure mode (g) was decisive for every shear plane. However, the shear plane on the side of the drill tip of short SBD dowel was close to failure mode (f), which is also recognised in Figure 64 (right). The same figure indicates that the drill tip as a whole does not contribute to the bearing capacity and the stress under the dowel was concentrated in the two inner layers. This might be the reason for the premature brittle failure (before the 15 mm limit) of the connections with short dowels, as can be seen in Figure 66.

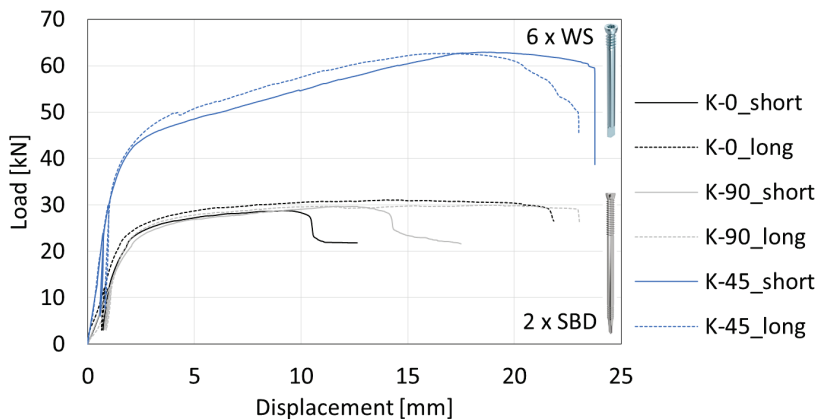


Figure 66. Typical load-displacement diagram of selected connection groups

Numerical comparison of the test results did not confirm the influence of the rope effect on the load-carrying capacity for SBD dowels. According to Eq. (1), the expected difference in the load-carrying capacity between long and short dowels due to the drill tip would be up to 3.7%. Figure 67 (left and middle) compares the load-carrying capacity referenced to the mean density, and it turns out the difference is much higher, up to 9%. In the case of the rope effect, it should be smaller. Still, despite the premature failure of the shear plane on the side of the drill tip, the connection continuously carried the load, confirming the activation on the threaded part of the dowel.

Due to the smaller diameter and lower steel strength, both shear planes (especially the one on the head side) of short WS dowel were closer to failure mode (h), which is independent of the penetration length t_1 . Therefore, the load-displacement diagram of long and short WS dowel look more similar – see Figure 66. The expected difference in load-carrying capacity between them according to Eq. (1) was 11.8%, but test results did not confirm that – see Figure 67 (right). This outcome makes it possible to conclude that due to sufficient plastic behaviour, the rope effect was activated, which increased the load-carrying capacity of the short dowel.

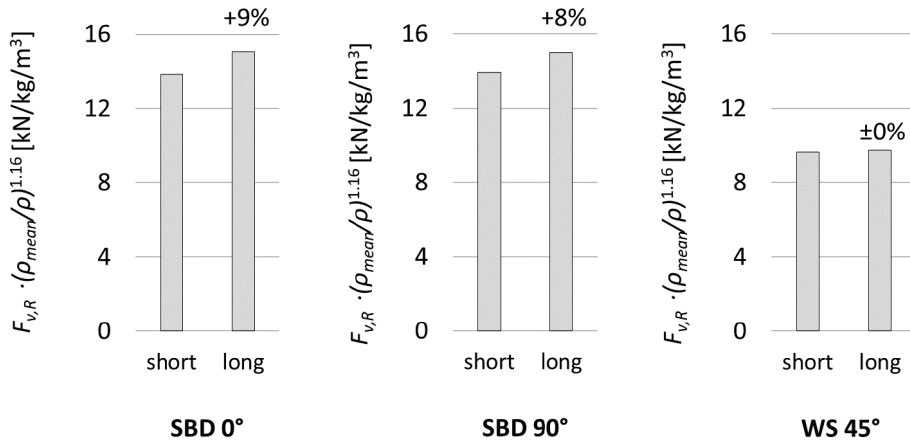


Figure 67. Comparison of the normalised load-carrying capacity by dowel length

5.2.3 Comparison with EYM and the application of new embedment strength model

The load-carrying capacity per one dowel was calculated according to Eq. (1) using corresponding mean embedment strength of each sample. Since the embedment tests were done with dowel diameters of 10, 12 and 20 mm, values were referenced to the dowel diameter used in the connections (7 and 7.5 mm). A good agreement between the test ($F_{v,R,test}$) and predicted value ($F_{v,R,pred}$) was found – see Figure 68.

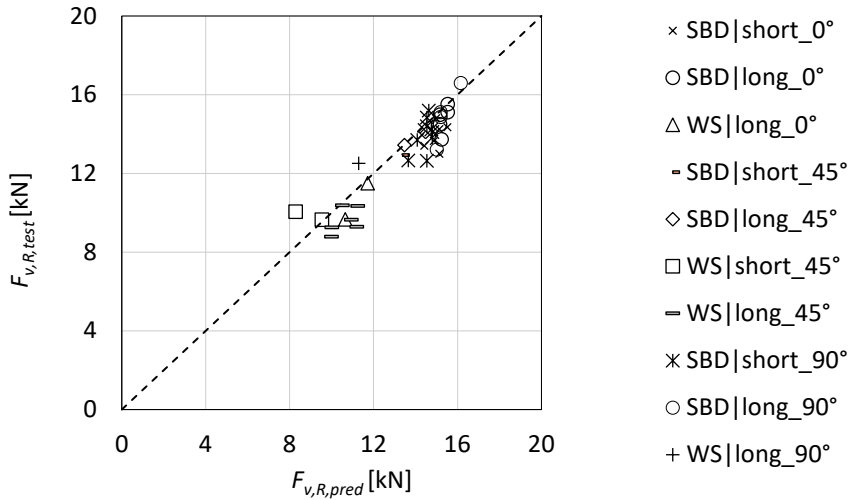


Figure 68. Comparison of test results and predicted load-carrying capacity of one dowel (calculation based on real, normalised embedment values)

Figure 69 compares the test results and predicted load-carrying capacity per dowel, which were calculated using the embedment strength model proposed by Blass & Uibel (2007) (see Eq. (7)) and a new model according to Eq. (48). A significantly better correlation was achieved using the second one. When applying Blass & Uibel Model 2, the mean value of all samples was overestimated 14%, while the corresponding value for the new, improved model was only 4.5%. A possible reason for this overestimation is that short SBD dowels did not exploit their full potential due to the premature failure of the shear plane on the side of the drill tip.

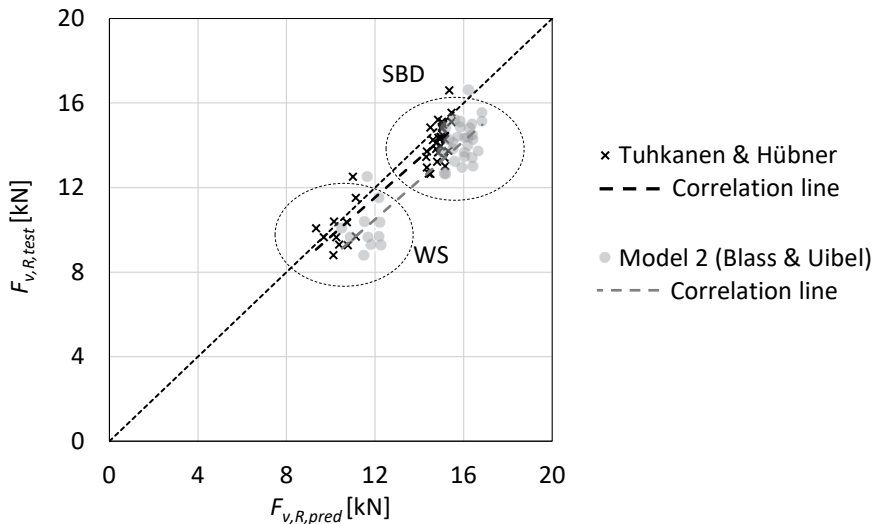


Figure 69. Comparison of test results and predicted load-carrying capacity of one dowel (calculation based on different embedment strength models)

5.3 Racking strength and stiffness of the wall

5.3.1 Test result

Racking strength and stiffness value of the tested shear wall is given in Table 15. Figure 70 presents measured sliding, uplift and global top displacement. Deformations in the compressed edge were measured and based thereon, the approximate rotation point of the wall was derived (see Figure 71, left). The measure from this point to the compressed edge of the wall was also taken as the length of the compression zone.

Figure 71 (right) presents contributions of the different deformation mechanisms to the global top displacement at maximum load. It must be noted that the outer layers of the panel were horizontal, leading to lower bending stiffness in the plane. However, the contribution of rocking has the highest value and sliding negligible. It can also be seen in Figure 72, where the load path follows the direction of the panel corner uplift. The first dowel broke at around 65kN (by hearing a noise). After opening the connection, altogether seven dowels near the edge had failed. It is probable that failure was caused by a combination of dowel bending, shear and tension (caused by the thread).

5.3.2 Comparison of the result with selected design models

Estimated racking strength according to the model proposed by Reynolds et al. (2017) was calculated using the mean load-carrying capacity of the dowel from Table 14. The tensile strength of the connection unit (two dowels) furthest from the point of rotation was taken as $T = 2 \cdot 14 = 28kN$. When considering the compression zone length from Figure 71 (left), the calculated strength of the wall is 52.6kN, which is 70% of the tested value. The result corresponds to the level where the wall behaves linearly – see Figure 70.

Table 15. Racking strength F_{rg} and stiffness R according to EN 594 (CEN, 2011)

Wall type	F_{max} [kN]	$v_{F_{rg}}$ [mm]	R [kN/mm]
Setup L-I	74.4 (failed in connection)	60.0	2.2

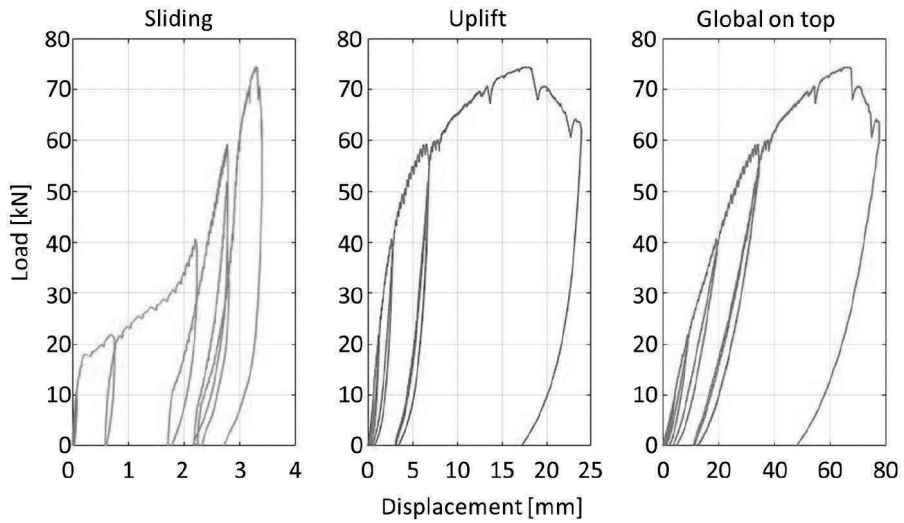


Figure 70. Measured displacements in Setup L-I

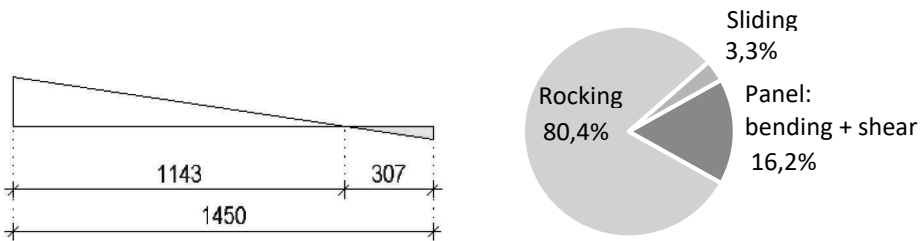


Figure 71. Left: rotation point of the shear wall; right: contributions of the different deformation mechanisms to the global top displacement at maximum load



Figure 72. Contributions of rocking to the top displacement in Setup L-I

The second model proposed by Flatscher (2017) required as input the function which describes the load-displacement relationship of the connection unit in two directions. Figure 73 presents the test curves for a two-dowel connection in the

direction of uplift and shear. Corresponding loading angles respect to the outer layers were 90 and 0 degrees. Approximation curve for one direction based on the method suggested by (Flatscher, 2017) is presented on the same figure (left). Coefficients $C_1 - C_6$ required for the first method were calculated in MATLAB (The MathWorks Inc., 2019) – see Appendix. Corresponding input parameters are listed in Table 16.

Table 16. Input parameters to calculate coefficients $C_1 - C_6$

Parameter	F_{max} [kN]	v_{max} [mm]	K_{ini} [kN/mm]	F_A [kN]	v_B [mm]	F_B [kN/mm]
	29.7	11.6	2.6	27.3	16.5	-5.7

A slightly better fit can be achieved using fifth-degree polynomials which are expressed by the following:

$$F(v)_{rocking} = 0,0004v^5 - 0,0226v^4 + 0,4341v^3 - 3,8911v^2 + 16,7568v - 0,8288 \quad (51)$$

$$F(v)_{shear} = 0,0002v^5 - 0,0127v^4 + 0,2881v^3 - 2,9727v^2 + 14,1618v - 0,0290 \quad (52)$$

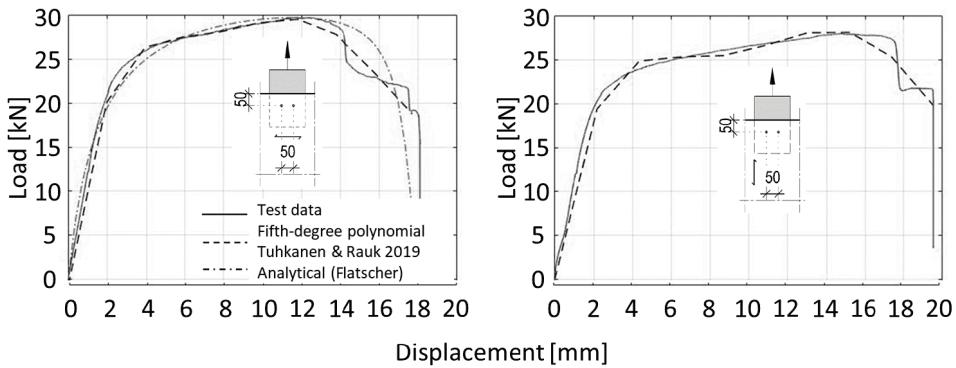


Figure 73. Approximation curves for load-displacement diagrams of the connection with two dowels loaded perpendicular and parallel to the outer layers

It must be noted that consideration of the post maximum softening of the connection is fictive. It is unreasonable, or even impossible to describe such a drop in the load-displacement curve. Furthermore, it is not allowed, since it indicates brittle failure. However, in this case, brittle failure was assumed to be in one of two shear planes of the dowel (on the drill tip side). Part of the connection still carried the load, and the post maximum was considered.

When calculating the maximum racking strength for Setup L-I, agreement with the test result can be found: the predicted value is 82.5kN, which is 11% higher than the test result. As noted previously, brittle failure in one shear plane and breaking of the dowel (steel failure) might be the reason for that. However, using slender dowels might be more

reasonable to propagate failure mode (h) and thereby activate the post maximum capacity of the connection.

Table 17 summarises the comparison of two selected models. Racking strength calculation based on both models was done in detail with the help of MATLAB (The MathWorks Inc., 2019) in (Rauk, 2019) [in Estonian].

Table 17. Comparison of the tested racking strength with selected design models

Wall type	F_{max} [kN]	$F_{rg,REYNOLDS}$ [kN]	$F_{rg,FLATSCHER}$ [kN]
Setup L-I	74.4	52.6 (-30%)	82.5 (+11%)

In practice, it is more appropriate to use only one approximation curve for both directions as long as they are very similar. This fact could be highlighted as an advantage for slotted-in steel plate connection with dowels – the load-displacement behaviour in both directions is predictable and does not differ significant. It would also be a prerequisite for optimised and systematised design. Upon knowing the performance of individual connection unit and determining the deformation limit of the building, shear wall system components carrying the corresponding wind load can be selected. Here, the simplification in the calculation was not expressed with this rather complicated model, but with the result, which could be a table of CLT shear wall products, for example.

6 CONCLUSION

In this thesis, first, the importance of connections in timber structures is emphasised, and then the focus is set on the connection requirements in prefabricated modular buildings. The bottlenecks and drawbacks of the modular construction and design are addressed and discussed more deeply, especially issues related to ensuring horizontal stiffness of the building and continuity in the vertical direction. An independent cross-laminated timber shear wall system as a possible solution is introduced, the purpose of which was to separate calculations for vertical and horizontal loads and thereby simplify the design process.

In the second part, slotted-in steel plate connection is introduced and discussed for two reasons: first, to emphasize the ability to maximise the potential of cross-laminated timber shear wall; and secondly, to highlight the connection's requirements in modules manufacturing and erection. Therefore, self-perforating dowels are introduced. The layered structure of cross-laminated timber and specific geometrical properties of self-perforating dowels determine the main research questions.

The third part introduces the methods, laboratory experiments and embedment strength databases used to achieve the set goals of the thesis.

The final section presents the results, discussion and proposals made based on them. The main results are briefly summarised here again.

Embedment strength in cross-laminated timber

- The available model for embedment strength proposed by Blass & Uibel (2007) will overestimate the values for cross-laminated timber with layer thicknesses in a practical range (from 20 to 40 mm).
- The influence of the layer thickness of cross-laminated timber to the embedment strength was found in the parameter study.
- The exponential relation between dowel diameter and embedment strength was found.
- Hankinson's formula does not describe the influence of the loading angle (respect to the outer layers) to embedment strength correct. A new formula was proposed.
- A new embedment strength model for cross-laminated timber with layer thicknesses from 20 to 40 mm and layup factor $\zeta = 0.95 \dots 1.72$ was proposed.

Slotted-in steel plate connection with self-perforating dowels

- For self-perforating dowels, the equation for yield moment of the dowel $M_{y,R}$ in EN 1995-1-1 (CEN, 2009a) underestimates the values obtained from experiments.
- A significant difference was found in DoP for SBD dowel where declared yield moment of the fastener was 58% lower than test value.
- Threaded parts of the self-perforating dowels activated during the test against pull-out. However, no increase in load-carrying capacity was found for SBD dowels since premature failure on the side of the drill tip occurred first.
- Due to sufficient plastic behaviour and activation of the rope effect, an increase of 11.8% of the load-carrying capacity of dowel type WS was found.
- Good agreement between test results and EYM was found.
- A new embedment strength model proposed in this thesis was validated with connection tests, and good agreement was found.

Line-connected cross-laminated timber shear wall

- The studied connection was applied to the full-scale shear wall and loaded up to the failure. Comparison of the test result with two models with a different character showed good agreement.
- Use of displacement-based method proposed by Flatscher (2017) permits to utilise the connection maximally.
- The benefits of slotted-in steel plate connection with dowels were highlighted when the model proposed by (Flatscher, 2017) was applied: load-displacement behaviour of the connection in both directions (uplift and shear) is very similar and well predictable.

Cross-laminated timber is an essential supplement in the modular building value chain. Due to automated production, this product fits perfectly into the paradigm of modular construction. High in-plane stiffness allows the use of cross-laminated timber in shear wall systems, especially.

Slotted-in steel plate connection with self-perforating dowels meets the criteria required for shear walls, particularly. Centred load transfer to the foundation and optimal and well predictable load-displacement behaviour are the main benefits to highlight. Uniform load transfer combined with proper design model allows the maximisation of the connection's potential and creates preconditions for simplified design. Semi-automated installation of the dowels adds value in terms of modular construction. The ability to dismantle the building components serves a sustainable way of thinking.

References

- ASTM International. (2018). *ASTM D5764-97a: Standard test method for evaluating dowel-bearing strength of wood and wood-based products*. ASTM International.
- Bernasconi, A. (2016a). Concept and design of the CLT-structure of the four residential towers with 9 storeys in the city of Milan. *WCTE 2016 - World Conference on Timber Engineering*.
- Bernasconi, A. (2016b). Four residential towers as CLT timber construction in the city of Milan. *WCTE 2016 - World Conference on Timber Engineering*.
- Blaß, H. J., Bienhaus, A., & Krämer, V. (2001). Effective bending capacity of dowel-type fasteners. *Proceedings of the International RILEM Symposium Joints in Timber Structures*, 22, 71–88.
- Blass, H. J., & Sandhaas, C. (2017). *Timber Engineering: Principles for design*. In *IFAC Proceedings Volumes*. KIT Scientific Publishing.
<https://doi.org/https://doi.org/10.5445/KSP/1000069616>
- Blass, H. J., & Uibel, T. (2007). Tragfähigkeit von stiftförmigen Verbindungsmitteln in Brettsperholz. In *Karlsruher Berichte zum Ingenieurholzbau*, 8.
- Brandner, R. (2012). *Stochastic System Actions and Effects in Engineered Timber Products and Structures* (Volume 2). Verlag der Technischen Universität Graz.
- Brandner, R., Flatscher, G., Ringhofer, A., Schickhofer, G., & Thiel, A. (2016). Cross laminated timber (CLT): overview and development. *European Journal of Wood and Wood Products*, 74(3), 331–351. <https://doi.org/10.1007/s00107-015-0999-5>
- Cabrero, J. M., & Yurrita, M. (2018). Performance assessment of existing models to predict brittle failure modes of steel-to-timber connections loaded parallel-to-grain with dowel-type fasteners. *Engineering Structures*, 171(March), 895–910. <https://doi.org/10.1016/j.engstruct.2018.03.037>
- Casagrande, D., Rossi, S., Sartori, T., & Tomasi, R. (2016). Proposal of an analytical procedure and a simplified numerical model for elastic response of single-storey timber shear-walls. *Construction and Building Materials*, 102, 1101–1112. <https://doi.org/10.1016/j.conbuildmat.2014.12.114>
- Ceccotti, A., Sandhaas, C., Okabe, M., Yasumura, M., Minowa, C., & Kawai, N. (2013). SOFIE project - 3D shaking table test on a seven-storey full-scale cross-laminated timber building. *Earthquake Engineering and Structural Dynamics*, 42(13), 2003–2021. <https://doi.org/10.1002/eqe.2309>
- CEN. (1999). *EN 26891:1999 Timber structures-Joints made with mechanical fasteners-General principles for the determination of strength and deformation characteristics*. CEN.
- CEN. (2002). *EN 12512: Timber structures - Test methods - Cyclic testing of joints made with mechanical fasteners*. CEN.
- CEN. (2007). EN383: Timber Structures - Test methods - Determination of embedment strength and foundation values for dowel type fasteners. In CEN. CEN.
- CEN. (2009a). *EN 1995-1-1:2009. Eurocode 5 Design of timber structures. Part 1-1 : General – Common rules and rules for buildings*. CEN.
- CEN. (2009b). *EN ISO 6892-1: Metallic materials - Tensile testing - Part 1: Method of test at room temperature* (Issue 1117). CEN.
- CEN. (2011). *EN 594: Timber structures - Test methods - Racking strength and stiffness of timber frame wall panels*. CEN.

- CEN. (2016). EN 384. Structural timber - Determination of characteristic values of mechanical properties and density. CEN.
- Chen, Z., Chui, Y. H., Ni, C., Doudak, G., & Mohammad, M. (2014). Load distribution in timber structures consisting of multiple lateral load resisting elements with different stiffnesses. *Journal of Performance of Constructed Facilities*, 28(6), 1–7. [https://doi.org/10.1061/\(ASCE\)CF.1943-5509.0000587](https://doi.org/10.1061/(ASCE)CF.1943-5509.0000587)
- Colling, F. (2017). *Aussteifung von Gebäuden in Holztafelbauart* (2.Auflage). Ingenieurbüro Holzbau.
- D'Arenzo, G., Rinaldin, G., Fossetti, M., & Fragiaco, M. (2019). An innovative shear-tension angle bracket for Cross-Laminated Timber structures: Experimental tests and numerical modelling. *Engineering Structures*, 197(October 2018), 109434. <https://doi.org/10.1016/j.engstruct.2019.109434>
- Daerga, P. A., Girhammar, U. A., & Källsner, B. (2012). Slotted-in steel-plate connections for panel wall elements - Experimental and analytical study. *WCTE 2012 - World Conference on Timber Engineering*.
- DIN. (1994). *DIN-Taschenbuch 34, Holzbau Normen*. Beuth Verlag GmbH.
- Dong, W., Wang, Z., Zhou, J., Zhang, H., Yao, Y., Zheng, W., Gong, M., & Shi, X. (2020). Embedment strength of smooth dowel-type fasteners in cross-laminated timber. *Construction and Building Materials*, 233, 117243. <https://doi.org/10.1016/j.conbuildmat.2019.117243>
- Dorn, M., de Borst, K., & Eberhardsteiner, J. (2013). Experiments on dowel-type timber connections. *Engineering Structures*, 47, 67–80. <https://doi.org/10.1016/j.engstruct.2012.09.010>
- Ehlbeck, J., & Werner, H. (1992). Softwood and hardwood embedding strength for dowel-type fasteners. *CIB-W18 Timber Structures, Paper 25-7*.
- EN 1383. (2016). *Timber structures - Test methods - Pull through resistance of timber fasteners*. CEN.
- EN 409. (2009). *Timber structures - Test methods - Determination of the yield moment of dowel type fasteners*. CEN.
- Enerpac. (2019). *Enerpac*. <https://www.enerpac.com/>
- Erchinger, C. (2009). *Zum Verhalten von mehrschichtigen Stahl-Holz-Stabdübelverbindungen im Brandfall [Doctoral Thesis]*. ETH Zürich. <http://e-collection.library.ethz.ch/view/eth:2352>
- Flatscher, G. (2017). *Evaluation and approximation of timber connection properties for displacement-based analysis of CLT wall systems [DoctoralThesis]*. Graz University of Technology.
- Franke, S., Franke, B., & Tuhkanen, E. (2018). Test methods for determination of design parameters of fasteners. In P. (eds. . Sandhaas, C., Munch-Andersen, J., Dietsch (Ed.), *Design of Connections in Timber Structures: A state-of-the-art report by COST Action FP1402 / WG3* (pp. 33–59). Shaker Verlag.
- Franke, S., & Magnière, N. (2014). Discussion of testing and evaluation methods for the embedment behaviour of connections. *International Network on Timber Engineering Research (INTER)*, September, Paper 47-7-1.
- Gavric, I., Fragiaco, M., & Ceccotti, A. (2015). Cyclic behavior of typical screwed connections for cross-laminated (CLT) structures. *European Journal of Wood and Wood Products*, 73(2), 179–191. <https://doi.org/10.1007/s00107-014-0877-6>

- Gavric, I., & Popovski, M. (2014). Design models for CLT shearwalls and assemblies based on connection properties. *Proceedings of Meeting 47, INTER-International Network on Timber Engineering Research, January*, 269–280. <https://doi.org/10.13140/RG.2.1.3845.0728>
- Gehri, E. (1982). *Fachwerkträger aus Buche und Fichte mit Stahlknotenplatten in eingeschlitzten Hölzern. Internal Report 82-1.*
- Gehri, E. (1993). *Grundlagen der Verbindungstechnik (SAH-Kurs)*. ETH Zürich, (in German).
- Gehri, E. (2000). *Leistungsfähige Verbindungen - Kriterien und Konzepte (SAH-Kurs)* (pp. 13–25).
- Girhammar, U. A., & Källsner, B. (2016). Horizontal Stabilisation of Sheathed Timber Frame Structures Using Plastic Design Methods – Introducing a Handbook Part 2: Design of Joints and Anchoring Devices. *Procedia Engineering*, 161, 628–635. <https://doi.org/10.1016/j.proeng.2016.08.716>
- Hankinson, R. L. (1921). Investigation of crushing strength of spruce at varying angles of grain. In *Air Service In-form Circular: Vol. III* (Issue 259).
- Hashemi, A., Zarnani, P., Masoudnia, R., & Quenneville, P. (2017). Seismic resistant rocking coupled walls with innovative Resilient Slip Friction (RSF) joints. *Journal of Constructional Steel Research*, 129, 215–226. <https://doi.org/10.1016/j.jcsr.2016.11.016>
- HMB. (2019). *HBM*. <https://www.hbm.com>
- Hristovski, V., Dujic, B., Stojmanovska, M., & Mircevska, V. (2013). Full-scale shaking-table tests of XLam panel systems and numerical verification: Specimen 1. *Journal of Structural Engineering (United States)*, 139(11), 2010–2018. [https://doi.org/10.1061/\(ASCE\)ST.1943-541X.0000754](https://doi.org/10.1061/(ASCE)ST.1943-541X.0000754)
- Hristovski, V., Mircevska, V., Dujic, B., & Garevski, M. (2018). Comparative dynamic investigation of cross-laminated wooden panel systems: Shaking-table tests and analysis. *Advances in Structural Engineering*, 21(10), 1421–1436. <https://doi.org/10.1177/1369433217749766>
- Hübner, U. (2013). *Mechanische Kenngrößen von Buchen-, Eschen- und Robinienholz für lastabtragende Bauteile [DoctoralThesis]*. In *Institut für Holzbau und Holztechnologie*. Technische Universität Graz.
- Huß, W., Kaufmann, M., & Merz, K. (2018). Holzbau - Raummodule. In *Holzbau - Raummodule*. DETAIL. <https://doi.org/10.11129/9783955534370>
- International Energy Agency and the United Nations Environment Programme. (2018). *2018 Global Status Report: Global Alliance for Buildings and Construction*. <https://doi.org/https://doi.org/10.1038/s41370-017-0014-9>
- ISO. (2009). *ISO 10984-2:2009: Timber structures - Dowel-type fasteners - Part 2: Determination of embedding strength*. International Organization for Standardization.
- ISO. (2013). *ISO 898-1:2013 Mechanical properties of fasteners made of carbon steel and alloy steel - Part 1: Bolts, screws and studs with specified property classes - Coarse thread and fine pitch thread*.
- Jockwer, R., & Dietsch, P. (2018). Review of design approaches and test results on brittle failure modes of connections loaded at an angle to the grain. *Engineering Structures*, 171(June), 362–372. <https://doi.org/10.1016/j.engstruct.2018.05.061>
- Johansen, K. W. (1949). Theory of Timber Connections. *IABSE: International Association of Bridge and Structural Engineering*, 9, 249–262.

- Källsner, B., & Girhammar, U. A. (2009). Plastic models for analysis of fully anchored light-frame timber shear walls. *Engineering Structures*, 31(9), 2171–2181. <https://doi.org/10.1016/j.engstruct.2009.03.023>
- Kanazawa, K., Kitamori, A., Yamanishi, T., Nakashima, S., Araki, Y., & Isoda, H. (2018). A case study on in-plane shear performance of composite structure with CLT infilled in steel frames. *World Conference on Timber Engineering*.
- Kaufmann, H., Krötsch, S., & Winter, S. (2018). Manual of Multistorey Timber Construction. In *Manual of Multistorey Timber Construction*. DETAIL. <https://doi.org/10.11129/9783955533953>
- Kennedy, S., Salenikovich, A., Munoz, W., & Mohammad, M. (2014). Design equations for dowel embedment strength and withdrawal resistance for threaded fasteners in CLT. *WCTE 2014 - World Conference on Timber Engineering*.
- Kitamori, A., Nakashima, S., & Isoda, H. (2014). Development of CLT shear frame using metal plate insert connections. *WCTE 2014 - World Conference on Timber Engineering*.
- Köhler, J. (2020). *Regression Analysis Principles* (personally sent by the author).
- Koponen, S. (1991). *Embedding characteristics of wood in the grain direction*. Rep.25 - ISBN 951-22-0848-2.
- Latour, M., & Rizzano, G. (2015). Cyclic behavior and modeling of a dissipative connector for cross-laminated timber panel buildings. *Journal of Earthquake Engineering*, 19(1), 137–171. <https://doi.org/10.1080/13632469.2014.948645>
- Lukacs, I., Björnfot, A., & Tomasi, R. (2019). Strength and stiffness of cross-laminated timber (CLT) shear walls: State-of-the-art of analytical approaches. *Engineering Structures*, 178, 136–147. <https://doi.org/10.1016/j.engstruct.2018.05.126>
- Meyer, A. (1957). Die Tragfähigkeit von Nagelverbindungen bei statischer Belastung. *Holz Als Roh- Und Werkstoff*, 15(2), 96–109. <https://doi.org/10.1007/BF02609174>
- Mischler, A. (1998). *Bedeutung der Duktilität für das Tragverhalten von Stahl-Holz-Bolzenverbindungen [Doctoral Thesis]*.
- Mischler, A. (2001). Multiple Shear Steel-to-Timber Connections with Self-Drilling Dowels. In S. Aicher & H. W. Reinhardt (Eds.), *International RILEM Symposium on Joints in Timber Structures* (Vol. PRO22, pp. 143–152). RILEM Publications S.A.R.L.
- Morandi, F., De Cesaris, S., Garai, M., & Barbaresi, L. (2018). Measurement of flanking transmission for the characterisation and classification of cross laminated timber junctions. *Applied Acoustics*, 141, 213–222. <https://doi.org/10.1016/j.apacoust.2018.07.009>
- Nakashima, S., Kitamori, A., Araki, Y., & Isoda, H. (2016). Effect of array on tensile load carrying capacity CLT drift pinned joint. *WCTE 2016 - World Conference on Timber Engineering*.
- Nakashima, S., Kitamori, A., Komatsu, K., Que, Z., & Isoda, H. (2014). Development and evaluation of CLT shear wall using drift pinned joint. *WCTE 2014 - World Conference on Timber Engineering*.
- Nakashima, S., Kitamori, A., Mori, T., & Komatsu, K. (2012). Evaluation of tensile performance of drift pinned joint with steel plate on cross laminated timber. *WCTE 2012 - World Conference on Timber Engineering*.
- Nakashima, S., Kitamori, A., Mori, T., & Komatsu, K. (2014). Propose Alternative Design Criteria for Dowel Type Joint with CLT. In *Materials and Joints in Timber Structures* (Vol. 9, pp. 739–748). https://doi.org/10.1007/978-94-007-7811-5_66

- Ottenhaus, L.-M., Li, M., & Smith, T. (2018). Structural performance of large-scale dowelled CLT connections under monotonic and cyclic loading. *Engineering Structures*, *176*, 41–48. <https://doi.org/10.1016/j.engstruct.2018.09.002>
- Ottenhaus, L.-M., Li, M., Smith, T., & Quenneville, P. (2016). Ductility and overstrength of dowelled LVL and CLT connections under cyclic loading. *WCTE 2016 - World Conference on Timber Engineering*.
- Pirnbacher, G., Traetta, G., & Schickhofer, G. (2006). Anwendung der Johansen-Theorie für gekreuzt geschichtete Strukturen. In T. Moosbrugger, G. Schickhofer, H. Unterwieser, & H. Krenn (Eds.), *5. Grazer Holzbau-Fachtagung, Tagungsband Brettsperholz: Ein Blick auf Forschung und Entwicklung*.
- Polastri, A., Giongo, I., Angeli, A., & Brandner, R. (2018). Mechanical characterization of a pre-fabricated connection system for cross laminated timber structures in seismic regions. *Engineering Structures*, *167*(September 2017), 705–715. <https://doi.org/10.1016/j.engstruct.2017.12.022>
- Polastri, A., Giongo, I., & Piazza, M. (2017). An innovative connection system for cross-laminated timber structures. *Structural Engineering International: Journal of the International Association for Bridge and Structural Engineering (IABSE)*, *27*(4), 502–511. <https://doi.org/10.2749/222137917X14881937844649>
- Pope, D. J., & Hilson, B. O. (1995). Embedment testing for bolts: a comparison of the European and American procedures. *Journal of the Institute of Wood Science*, *14*(6), 568–571.
- Porteous, J., & Kermani, A. (2007). Structural Timber Design to Eurocode 5. In *Structural Timber Design to Eurocode 5* (2nd ed.). Wiley-Blackwell. <https://doi.org/10.1002/9780470697818>
- Pozza, L., Saetta, A., Savoia, M., & Talledo, D. (2018). Angle bracket connections for CLT structures: Experimental characterization and numerical modelling. *Construction and Building Materials*, *191*, 95–113. <https://doi.org/10.1016/j.conbuildmat.2018.09.112>
- Purbond. (2018). <http://www.henkel-adhesives.com>.
- Project AURP, (2019). https://www.etis.ee/Portal/Projects/Display/9f7b7424-614a-4a2f-9003-b403a92cff61?tabId=tab_GeneralData
- Rammer, D. R., & Winistorfer, S. G. (2001). Effect of moisture content on dowel-bearing strength. *Wood and Fiber Science*, *33*(1), 126–139.
- Rauk, L. (2019). *Experimental investigation of cross laminated timber shear walls (Master Thesis)*. Tallinn University of Technology. In Estonian.
- Reynolds, T., Foster, R., Bregulla, J., Chang, W. S., Harris, R., & Ramage, M. (2017). Lateral-Load Resistance of Cross-Laminated Timber Shear Walls. *Journal of Structural Engineering (United States)*, *143*(12), 06017006. [https://doi.org/10.1061/\(ASCE\)ST.1943-541X.0001912](https://doi.org/10.1061/(ASCE)ST.1943-541X.0001912)
- RIL205-1. (2017). *Puurakenteiden suunnitteluohje Eurokoodi*. RIL.
- Ringhofer, A., Brandner, R., & Blaß, H. J. (2018). Cross laminated timber (CLT): Design approaches for dowel-type fasteners and connections. *Engineering Structures*, *171*, 849–861. <https://doi.org/10.1016/j.engstruct.2018.05.032>
- Ringhofer, A., Brandner, R., & Schickhofer, G. (2015). Withdrawal resistance of self-tapping screws in unidirectional and orthogonal layered timber products. *Materials and Structures/Materiaux et Constructions*, *48*(5), 1435–1447. <https://doi.org/10.1617/s11527-013-0244-9>

- Ringhofer, A., & Schickhofer, G. (2014). Multi-storey residential buildings in CLT - Interdisciplinary principles of design and construction. *WCTE 2014 - World Conference on Timber Engineering, Proceedings*.
- Rossi, S., Crocetti, R., Honfi, D., & Hansson, E. F. (2016). Load-bearing capacity of ductile multiple shear steel-to-timber connections. *WCTE 2016 - World Conference on Timber Engineering, March 2017*.
- Rothoblaas. (2017). *SBD - Declaration of Performance*. Karlsruher Institut für Technologie (KIT) - Versuchsanstalt für Stahl, Holz und Steine (No. 0769).
- Rothoblaas. (2019). *Rotho Blaas*. <https://www.rothoblaas.com>
- Rug, W., & Mönck, W. (2015). *Holzbau. Bemessung und Konstruktion* (16th ed.). Beuth Verlag GmbH.
- Sandhaas, C. (2012). *Mechanical Behaviour of Timber Joints With Slotted-in Steel Plates [Doctoral Thesis]*. Technische Universitet Delft.
- Sandhaas, C., Van De Kuilen, J. W., Blass, H. J., & Ravenshorst, G. (2010). Embedment tests parallel-to-grain and ductility in tropical hardwood species. *11th World Conference on Timber Engineering 2010, WCTE 2010, 1*, 482–491.
- Sandhaas, C., & van de Kuilen, J. W. G. (2017). Strength and stiffness of timber joints with very high strength steel dowels. *Engineering Structures, 131*, 394–404. <https://doi.org/10.1016/j.engstruct.2016.10.046>
- Sawata, K., Kawamura, H., Takanashi, R., Ohashi, Y., & Sasaki, Y. (2016). Effects of arrangement of steel plates on strength of dowel-type cross laminated timber joints with two slotted-in steel plates subjected to lateral force. *WCTE 2016 - World Conference on Timber Engineering*.
- Sawata, K., Sasaki, T., & Kanetaka, S. (2006). Estimation of shear strength of dowel-type timber connections with multiple slotted-in steel plates by European yield theory. *Journal of Wood Science, 52*(6), 496–502. <https://doi.org/10.1007/s10086-006-0800-9>
- Schickhofer, G. (2009). *Holzbau. Nachweisführungen für Konstruktionen aus Holz (Scriptum)* (V1.3.1). Technische Universität Graz. (in German).
- Schickhofer, G., & Ganster, K. (2018). [M]odul und Raster – Das n*[M] der Standardisierung und Vorfertigung. *3. Klagenfurter Holzbau-Fachtagung*, 1–40.
- Schmid, M. (2002). *Anwendung der Bruchmechanik auf Verbindungen mit Holz [online]* [Karlsruher Institut für Technologie (KIT)]. <https://doi.org/10.5445/IR/7222002>
- Schreyer, A. C., Lam, F., & Prion, H. G. L. (2004). Comparison of Slender Dowel-Type Fasteners for Slotted-in Steel Plate Connections under Monotonic and Cyclic Loading. *World Conference on Timber Engineering, 1*–6.
- Schweigler, M., Bader, T. K., Hochreiner, G., Unger, G., & Eberhardsteiner, J. (2016). Load-to-grain angle dependence of the embedment behavior of dowel-type fasteners in laminated veneer lumber. *Construction and Building Materials, 126*, 1020–1033. <https://doi.org/10.1016/j.conbuildmat.2016.09.051>
- Scotta, R., Marchi, L., Trutalli, D., & Pozza, L. (2016). A dissipative connector for CLT buildings: Concept, design and testing. *Materials, 9*(3), 1–17. <https://doi.org/10.3390/ma9030139>
- Serrano, E., Enquist, B., & Vessby, J. (2010). Vertical relative displacements in a medium-rise CLT-building. *Structures and Architecture - Proceedings of the 1st International Conference on Structures and Architecture, ICSA 2010, 2008*(April 2008), 398–405. <https://doi.org/10.1201/b10428-52>

- Serrano, E., Enquist, B., & Vessby, J. (2014). Long term in-situ measurements of displacement, temperature and relative humidity in a multi-storey residential CLT building. *WCTE 2014 - World Conference on Timber Engineering*.
- SFS-Intec. (2013). *WS - Declaration of performance*. Technische Universität Graz, Lignum Test Center.
- SFS-Intec. (2019). *SFS-Intec*. <https://www.sfsintec.biz/>
- Sharafi, P., Mortazavi, M., Samali, B., & Ronagh, H. (2018). Interlocking system for enhancing the integrity of multi-storey modular buildings. *Automation in Construction*, 85(September 2017), 263–272. <https://doi.org/10.1016/j.autcon.2017.10.023>
- Sjödín, J., Serrano, E., & Enquist, B. (2008). An experimental and numerical study of the effect of friction in single dowel joints. *Holz Als Roh - Und Werkstoff*, 66(5), 363–372. <https://doi.org/10.1007/s00107-008-0267-z>
- Spörk, A. (2007). *Lochleibungsfestigkeit von Nadelhölzern-Einflussfaktoren und Modellvergleiche*. TU Graz.
- The MathWorks Inc. (2019). *MATLAB*. <https://www.mathworks.com/>
- Thelandersson, S., & Larsen, H. J. (Eds.). (2003). *Timber Engineering*. John Wiley & Sons. LTD.
- Tlustochowicz, G. (2011). *Stabilising System for Multi-Storey Beam and Post Timber Buildings [Doctoral Thesis]*. Luleå University of Technology.
- Tlustochowicz, G., Serrano, E., & Steiger, R. (2011). State-of-the-art review on timber connections with glued-in steel rods. *Materials and Structures/Materiaux et Constructions*, 44(5), 997–1020. <https://doi.org/10.1617/s11527-010-9682-9>
- Tomasi, R., & Smith, I. (2015). Experimental characterization of monotonic and cyclic loading responses of CLT Panel-To-Foundation Angle Bracket Connections. *Journal of Materials in Civil Engineering*, 27(6), 04014189. [https://doi.org/10.1061/\(ASCE\)MT.1943-5533.0001144](https://doi.org/10.1061/(ASCE)MT.1943-5533.0001144)
- Traetta, G., & Schickhofer, G. (2007). Einflussfaktoren auf die Lochleibungsfestigkeit von Fichte und Kiefer für Stabdübelverbindungen. 6. *Grazer Holzbau-Fachtagung 6. GraHFT'07 Verbindungstechnik Im Ingenieurholzbau*.
- Trutalli, D., Marchi, L., Scotta, R., & Pozza, L. (2019). Capacity design of traditional and innovative ductile connections for earthquake-resistant CLT structures. *Bulletin of Earthquake Engineering*, 17(4), 2115–2136. <https://doi.org/10.1007/s10518-018-00536-6>
- Tuhkanen, E., Mölder, J., & Schickhofer, G. (2018). Influence of number of layers on embedment strength of dowel-type connections for glulam and cross-laminated timber. *Engineering Structures*, 176, 361–368. <https://doi.org/10.1016/j.engstruct.2018.09.005>
- Tuhkanen, E., & Ojamaa, M. (2019). Early experimental investigations on slotted-in steel plate connections with self-perforating dowels in CLT. *Wood Material Science and Engineering*. <https://doi.org/10.1080/17480272.2019.1626482>
- Tuhkanen, E., & Rauk, L. (2019). Potential of cross-laminated timber for independent shear wall systems. *Wood Material Science & Engineering*, 14(5), 355–365. <https://doi.org/10.1080/17480272.2019.1638450>
- Vessby, J., & Olsson, A. (2006). Stabilizing strategies for multi-story timber frame structures. *9th World Conference on Timber Engineering 2006, WCTE 2006*, 3, 2314–2321.

- Whale, L. R. J., Smith, I., & Hilson, B. O. (1987). Characteristic properties of nailed and bolted joints under short-term lateral load. Part 4. The influence of testing mode and fastener diameter upon embedment test data. *Journal of the Institute of Wood Science*, *11*(5), 156–161.
- Zarnani, P., & Quenneville, P. (2015). New design approach for controlling brittle failure modes of small-dowel-type connections in Cross-laminated Timber (CLT). *Construction and Building Materials*, *100*, 172–182.
<https://doi.org/10.1016/j.conbuildmat.2015.09.049>
- Zemic Europe B.V. (2019). *Zemic*. <https://www.zemiceurope.com/en>

Acknowledgements

It has been a long journey to write this final section at last. It may even be too long, but everything comes at a time or a little later as the saying goes. I must admit a lot of loneliness on this adventure, but this is something to consider before starting PhD studies. Yes, I still call it an adventure because curiosity and the heart's voice were what I followed, and loneliness must not be misunderstood here. That's what this section is about.

Time passes, and the main supervisors become co-supervisors and vice versa. I have three of them, each of whom had an important role to play. I want to express my gratitude to Professor Emeritus Karl Öiger, thanks to whom I set out on this journey in the first place. Professor Alar Just opened the door to the European research community for me and has been indispensable in improving the work as a whole. It cannot be overlooked that he also became a good friend during this time. Necessary support by Professor Targo Kalamees at the homestretch was absolutely invaluable.

I want to thank my colleagues at the Structural Engineering Research Group, especially Associated Professor Ivar Talvik and Katrin Nele Mäger for valuable advice at the latest stage of the work. Thanks to Priit Luhakooder for healthy competition in completing my dissertation, which I won this time. Thanks to the Department of Civil Engineering and Architecture for keeping me on the doctoral student list for an abnormally long time.

I want to express my most sincere gratitude to Professor Gerhard Schickhofer from Graz University of Technology, who invited me in 2014 to the Institute of Timber Engineering and Wood Technology for two months. The time I spent in Graz became a turning point in my studies. Here, I would like to take this opportunity to thank colleagues from that time, especially Georg Flatscher, Andreas Ringhofer, Alexandra Thiel, Thomas Bogensperger, Manfred Augustin, Katarina Bratulic, Eva Kavelar, Hildegard Weissnar and Mateo Izzi. At the very same time, COST Action FP1402 started, and I cannot fail to mention its impact on my growth as a scientist.

For some people, they may seem to enter your life by accident. Whether I believe in coincidences or not, they have come at the right time anyway, and I would like to thank them here. My students Joosep Mölder, Lauri Rauk and Martin Ojamaa did a tremendous job giving input to my work. Professors Hans Joachim Blass from Karlsruhe Institute of Technology and Thomas Uibel from Aachen University of Applied Sciences kindly shared their data, on which this work is partially based.

Peeter Linnas has been (almost always) very patient with my wishes in the lab; Hendrik Naar kindly shared his lab equipment. Erik Peeker's vast experience came in the right place at the right time. Mikko Viljakainen and Tero Lahtela from Unit Module Finland and Tarmo Tamm from Arcwood found me at the right moment, and we combined our common interests. Support from Rothoblaas and SFS-Intec complemented this rare coincidence. Peeter Peedomaa from Arcwood, who has always been worried about the future of timber engineering, deserves special thanks.

To make up for my shortcomings in the world of statistics and scripts, Jaanus Hallik, Jochen Köhler, Ulrich Hübner and Andrei Kervališvili appeared as if ordered. Valuable input, including indirect, from Michael Schweigler, also deserves mention here.

Being a doctoral student on my own, without permanent public financing, any funding was more than welcome, which included funding from the Karl Öiger Foundation, the DoRa Internationalisation Programme, a temporary scholarship from 'Doctoral Schools'

and a scholarship from Targo Kalamees for the last tests. Thanks to Urmas Jüriorg and Cad-süsteemide OÜ for tolerating my part-time work at the company.

The most important pillars of my accomplishments are my family and friends. My fishing group Eero, Raido and Rimo, and friend and colleague Tõnis deserve special thanks for keeping me in touch with the things that really matter in life. Thanks to my mother Marika and sister Kaja, for whom I am always expected or to whom I do not have to justify my absences. My warmest thanks go to my partner Reet, who never doubted or asked for reasons, and was understanding of the sacrifices that had to be made to achieve this result.

There were also people who are no longer among us, but who helped me along the way. Let this work be dedicated to them and uploaded to the cloud.

Abstract

Slotted-in steel plate connections with dowels in cross-laminated timber shear walls

The use of prefabricated room modules in multi-storey buildings has several significant advantages over conventional construction methods. Modularity at the level of both the room element components and the finished modules allows optimisation of the material, production process, transportation and assembly, which results in a shorter construction time. A critical bottleneck in the design is the calculation of horizontal stiffness of structures and ensuring the integrity of the entire building.

One possible strategy to provide a building's lateral strength and stiffness is to use independent cross-laminated timber walls between the modules, which allows vertical and horizontal loads to the structure to be dealt with separately, simplifying the design process. Given the high in-plane strength and stiffness of cross-laminated timber, the most critical point for such a solution is the wall connecting to the foundation. In addition to the strength and stiffness criteria, the connection must fit the automated manufacturing process and be feasible during assembly.

This doctoral thesis investigates the slotted-in steel plate connection with dowels in cross-laminated timber shear wall at the connection level as well in the entire wall. One of the most important input parameters for the calculation of the load-carrying capacity of the connection, embedment strength, has been studied based on the number and thickness of the layers of cross-laminated timber. In addition to numerous laboratory tests, available embedment strength data found in the literature have been used in the analysis. As a result, the influence of layer thickness on the embedment strength was determined. A new empirical calculation model for embedment strength was proposed, which considers the thickness of the layers of cross-laminated timber panels used in practice.

The primary purpose of the connection tests was to validate a new embedment strength model. As a result, a good correlation between the model and the actual experimental results was found. Since the semi-automatically installed self-perforating dowels were used in the connection, the effect of the drill tip and threads on the dowel's shank was studied. Activation of the rope effect was observed, but due to the high strength of the dowel and small penetration depth, no increase in the load-carrying capacity of the connection was found. In the case of dowels with a smaller diameter and lower steel strength, there was no premature brittle fracture, and the rope effect resulted in an 11.8% higher load-bearing capacity than smooth dowels.

The purpose of the line-connected full-scale shear wall test was to validate the results of the connection tests and highlight the importance of the design model. A full-length connection was chosen to provide uniform load transfer to the sub-structure, prevent brittle failure and maximise the potential of the wall and connection. The test results were compared with two different design models, one of which took into account the plastic behaviour of the connection as well as the post-maximum softening. An equation was derived to describe the full load-displacement diagram of the connection when loaded in a vertical and horizontal direction to apply the selected model. The non-linear model predicts more accurately the real load-carrying capacity of the wall and thereby exploiting the potential of the wall and joint. It was also concluded that the behaviour of a slotted-in steel plate connection with dowels in a cross-laminated timber wall is easily predictable when loaded in any direction, which simplifies the design process.

Lühikokkuvõte

Sisefreesitud terasplaadiga naagelliited ristkihtliimpuidust jäikusseintes

Tehases toodetud puidust ruumelementide kasutamine korruselamute ehituses omab võrreldes konventsionaalsete ehitusviisidega mitmeid olulisi eeliseid. Modulaarsus nii ruumelemendi komponentide kui ka valmis moodulite tasemel võimaldab optimeerida materjali, tootmisprotsessi, transporti ning montaaži, mistõttu saavutatakse kokkuvõttes lühem ehitusaeg. Hoone kavandamise ja ehitusprotsessi oluliseks kitsaskohaks on konstruktsioonide horisontaalsuunalise jäikuse arvutus ning hoone kui moodulite kogumi terviklikkuse tagamine.

Üks võimalik strateegia hoone horisontaalsuunaliseks jäigastamiseks on eraldiseivate ristkihtliimpuidust seinte kasutamine moodulite vahel. See võimaldab käsitleda hoonele mõjuvaid vertikaal- ja horisontaalsuunalisi koormuseid teineteisest lahus ning lihtsustada seeläbi projekteerimisprotsessi. Arvestades ristkihtliimpuidu suurt tugevust ja jäikust tasapinnalisel koormamisel, on sellise lahenduse kõige kriitilisemaks kohaks seina kinnitus vundamenti. Seejuures on oluline silmas pidada ka kasutatava liite sobivust modulaarehituse automatiseeritud töövoogu ning teostatavust moodulite monteerimisel.

Käesolev doktoritöö uurib sisefreesitud terasplaadiga naagelliiteid ristkihtliimpuidust jäikusseintes nii liite kui ka seina kui terviku tasemel. Liite kandevõime arvutamise üht olulisimat sisendparameetrit, muljumistugevust, on käsitletud lähtudes ristkihtliimpuidu kihtide arvust ja paksusest. Lisaks paljudele laborikatsetele kasutati analüüsis kirjanduses saadaolevaid muljumistugevuse andmeid. Tulemusena leiti kihi paksuse mõju muljumistugevusele ning pakuti välja uus empiiriline arvutusmudel, mis arvestab praktikas kasutatavate ristkihtpuidust paneelide kihtide paksusega.

Liitekatsete esmane eesmärk oli valideerida uut muljumistugevuse arvutusmudelit. Tulemusena leiti hea korrelatsioon mudeli ja tegelike katsetulemuste vahel. Kuna liites kasutati tehase tingimustes poolautomaatselt paigaldatavaid puurnaagleid, siis uuriti naagli puurotsa ja keermete mõju liite kandevõimele. Täheledati köieefekti aktiveerumist, kuid naagli suure voolupiirile vastava momendi ja väikese süvistusügavuse koosmõjul tekkiva rabeda purunemise tõttu ei väljendud see liite kandevõime kasvus. Väiksema diameetriga ning madalama terase tugevusega puurnaaglite korral enneaegset rabedat purunemist ei esinenud ning köieefekti kaudu saavutati 11.8% suurem kandevõime võrreldes siledate naaglitega.

Täismõodus, alumisest servast kinnitatud jäikusseina katsetamise eesmärgiks oli valideerida liitekatsete tulemusi ning näidata arvutusmudeli valiku tähtsust projekteerimisprotsessis. Ühtlane, kogu seina pikkune liide valiti põhjusel, et võimaldada koormuse ühtlasemat ülekannet aluskonstruktsioonile, vältida rabedat purunemist ning selle kaudu maksimeerida seina ja liite potentsiaali. Katsetulemusi võrreldi kahe erineva arvutusmudeliga, millest üks arvestas liite plastset käitumist ning piirkoormuse järgset pehmenemist. Arvutusmudeli rakendamiseks tuletati võrrandid, mis kirjeldavad liite kogu jõu-deformatsiooni diagrammi koormamisel vertikaal- ja horisontaalsuunas. Mittelineaarse arvutusmudeli kasutamine võimaldas täpsemalt prognoosida seina tegelikku kandevõimet ning kasutada ära liite kogu potentsiaal. Lisaks sellele järeldati, et sisefreesitud terasplaadiga naagelliite käitumine ristkihtliimpuidust seinas erinevas suunas koormamisel on hästi prognoositav, mis omakorda lihtsustab projekteerimisprotsessi.

Appendix

Boundary conditions to determine the coefficients $C_1 - C_6$ and simplified coefficients.

$$\frac{dF}{dv}(v = 0) = K_{ini}$$

$$\frac{dF}{dv}(v = v_{max}) = K_{max} = 0$$

$$F(v = v_{max}) = F_{max}$$

$$F(v = v_A) = F_A$$

$$F(v = v_B) = F_B$$

$$\frac{dF}{dv}(v = v_B) = K_B$$

$$C1 = (F_{max} * (v_B - v_{max}) * v_{max} * (16 * F_{max}^2 * (v_B - v_{max})^3 + 8 * F_{max} * K_{ini} * v_B^2 * (4 * v_B - v_{max}) * v_{max} + 25 * K_B * K_{ini} * v_B^2 * (4 * v_B^3 - 4 * v_B^2 * v_{max} - v_B * v_{max}^2 + v_{max}^3)) - FA * (25 * K_B * K_{ini} * v_B^2 * (v_B - v_{max})^2 * v_{max} * (4 * v_B^2 - v_{max}^2) + 4 * F_{max}^2 * v_{max} * (9 * v_B^4 - 24 * v_B^3 * v_{max} + 27 * v_B^2 * v_{max}^2 - 16 * v_B * v_{max}^3 + 4 * v_{max}^4) + F_{max} * v_B^2 * (25 * K_B * v_B * (v_B - v_{max})^2 * (2 * v_B - v_{max}) + 2 * K_{ini} * v_{max}^2 * (16 * v_B^2 - 21 * v_B * v_{max} + 4 * v_{max}^2)))) / (K_{ini} * v_B^2 * v_{max}^2 * (-F_{max} * (v_B - v_{max}) * (4 * F_{max} * (3 * v_B - v_{max}) * v_{max} + 25 * K_B * v_B * (2 * v_B^2 - 3 * v_B * v_{max} + v_{max}^2)) + FA * (25 * K_B * v_B * (v_B - v_{max})^2 * (2 * v_B - v_{max}) + F_{max} * v_{max} * (11 * v_B^2 - 16 * v_B * v_{max} + 4 * v_{max}^2))))$$

$$C2 = (-2 * F_{max} * (v_B - v_{max}) * (16 * F_{max}^2 * (v_B - v_{max})^3 + 8 * F_{max} * K_{ini} * v_B^2 * v_{max} * (2 * v_B^2 - 3 * v_B * v_{max} + v_{max}^2)) + FA * (50 * K_B * K_{ini} * v_B^2 * (v_B - v_{max})^2 * (2 * v_B - v_{max}) * v_{max} + 8 * F_{max}^2 * (5 * v_B^4 - 16 * v_B^3 * v_{max} + 22 * v_B^2 * v_{max}^2 - 15 * v_B * v_{max}^3 + 4 * v_{max}^4) + F_{max} * v_B^2 * (25 * K_B * (v_B - v_{max})^2 * (2 * v_B - v_{max}) - K_{ini} * v_{max} * (16 * v_B^2 + 16 * v_B * v_{max} + v_{max}^2)))) / (K_{ini} * v_B^2 * v_{max}^2 * (-F_{max} * (v_B - v_{max}) * (4 * F_{max} * (3 * v_B - v_{max}) * v_{max} + 25 * K_B * v_B * (2 * v_B^2 - 3 * v_B * v_{max} + v_{max}^2)) + FA * (25 * K_B * v_B * (v_B - v_{max})^2 * (2 * v_B - v_{max}) + F_{max} * v_{max} * (11 * v_B^2 - 16 * v_B * v_{max} + 4 * v_{max}^2))))$$

$$C3 = 1 / K_{ini}$$

$$C4 = (F_{max} * (25 * K_B * K_{ini} * v_B^2 * (v_B - v_{max})^2 * (2 * v_B - v_{max}) * v_{max} - 8 * F_{max}^2 * (2 * v_B^3 * v_{max} - 3 * v_B * v_{max}^3 + v_{max}^4) + F_{max} * v_B * (-25 * K_B * (v_B - v_{max})^2 * (4 * v_B^2 - v_{max}^2) + K_{ini} * v_{max}^2 * (16 * v_B^2 - 20 * v_B * v_{max} + 5 * v_{max}^2))) + FA * (-25 * K_B * K_{ini} * v_B^2 * (v_B - v_{max})^2 * (2 * v_B - v_{max}) * v_{max} + 4 * F_{max}^2 * (3 * v_B^3 * v_{max} - 6 * v_B * v_{max}^3 + 2 * v_{max}^4) + 5 * F_{max} * v_B * (v_B - v_{max}) * (K_{ini} * v_{max}^2 * (-3 * v_B + v_{max}) + 5 * K_B * (4 * v_B^3 - 4 * v_B^2 * v_{max} - v_B * v_{max}^2 + v_{max}^3)))) / (F_{max} * K_{ini} * v_B * v_{max} * (FA * (-25 * K_B * v_B * (v_B - v_{max})^2 * (2 * v_B - v_{max}) + F_{max} * v_{max} * (-11 * v_B^2 + 16 * v_B * v_{max} - 4 * v_{max}^2)) + F_{max} * (v_B - v_{max}) * (4 * F_{max} * (3 * v_B - v_{max}) * v_{max} + 25 * K_B * v_B * (2 * v_B^2 - 3 * v_B * v_{max} + v_{max}^2))))$$

$$C5 = (-25 * FA * K_B * K_{ini} * v_B^2 * (v_B - v_{max})^2 * v_{max} * (4 * v_B^2 - v_{max}^2) + 4 * F_{max}^3 * v_{max} * (5 * v_B^4 - 28 * v_B^3 * v_{max} + 39 * v_B^2 * v_{max}^2 - 20 * v_B * v_{max}^3 + 4 * v_{max}^4) + 5 * F_{max} * v_B^2 * (v_B - v_{max}) * v_{max} * (5 * K_B * K_{ini} * (4 * v_B^3 - 4 * v_B^2 * v_{max} - v_B * v_{max}^2 + v_{max}^3) + 2 * FA * (K_{ini} * v_{max} * (-4 * v_B + v_{max}) + 5 * K_B * (2 * v_B^2 - 3 * v_B * v_{max} + v_{max}^2))) + F_{max}^2 * (-25 * K_B * v_B^2 * (v_B - v_{max})^2 * (2 * v_B^2 + 3 * v_B * v_{max} - 2 * v_{max}^2) + v_{max} * (2 * K_{ini} * v_B^2 * v_{max} * (20 * v_B^2 - 24 * v_B * v_{max} + 5 * v_{max}^2) + FA * (-45 * v_B^4 + 144 * v_B^3 * v_{max} - 168 * v_B^2 * v_{max}^2 + 80 * v_B * v_{max}^3 - 16 * v_{max}^4)))) / (F_{max} * K_{ini} * v_B^2 * v_{max}^2 * (-F_{max} * (v_B - v_{max}) * (4 * F_{max} * (3 * v_B - v_{max}) * v_{max} + 25 * K_B * v_B * (2 * v_B^2 - 3 * v_B * v_{max} + v_{max}^2)) + FA * (25 * K_B * v_B * (v_B - v_{max})^2 * (2 * v_B - v_{max}) + F_{max} * v_{max} * (11 * v_B^2 - 16 * v_B * v_{max} + 4 * v_{max}^2))))$$

$$C6 = (-2 * FA * (10 * F_{max} * K_{ini} * v_B^3 * (v_B - v_{max}) * v_{max} + 25 * K_B * K_{ini} * v_B^2 * (v_B - v_{max})^2 * (2 * v_B - v_{max}) * v_{max} + F_{max}^2 * (5 * v_B^2 - 8 * v_B * v_{max} + 4 * v_{max}^2) + F_{max} * (50 * K_B * K_{ini} * v_B^2 * (v_B - v_{max})^2 * (2 * v_B - v_{max}) * v_{max} + 8 * F_{max}^2 * (5 * v_B^4 - 20 * v_B^3 * v_{max} + 28 * v_B^2 * v_{max}^2 - 17 * v_B * v_{max}^3 + 4 * v_{max}^4) + F_{max} * v_B^2 * (-25 * K_B * (v_B - v_{max})^2 * (2 * v_B - v_{max}) + K_{ini} * v_{max} * (20 * v_B^2 - 20 * v_B * v_{max} + v_{max}^2)))) / (F_{max} * K_{ini} * v_B^2 * v_{max}^2 * (FA * (-25 * K_B * v_B * (v_B - v_{max})^2 * (2 * v_B - v_{max}) + F_{max} * v_{max} * (-11 * v_B^2 + 16 * v_B * v_{max} - 4 * v_{max}^2)) + F_{max} * (v_B - v_{max}) * (4 * F_{max} * (3 * v_B - v_{max}) * v_{max} + 25 * K_B * v_B * (2 * v_B^2 - 3 * v_B * v_{max} + v_{max}^2))))$$

Curriculum vitae

Personal data

Name: Eero Tuhkanen
Date of birth: 24.11.1979
Place of birth: Viljandi
Citizenship: Estonia

Contact data

E-mail: eero.tuhkanen@taltech.ee

Education

2008 – ... Tallinn University of Technology, PhD
2004 – 2007 Tallinn University of Technology, MSc
1998 – 2003 Tallinn University of Technology, diploma
1995 – 1998 Carl Robert Jakobson Gymnasium, secondary education

Language competence

Estonian Native
English Fluent
German Fluent

Professional employment

2016 – ... Tallinna Tehnikaülikool, lecturer
2011 – 2016 Tallinna Tehnikaülikool, assistant
2011 – ... Cad-süsteemide OÜ, software consultant
2001 – 2011 TA-Konsult OÜ, structural designer

Elulookirjeldus

Isikuandmed

Nimi: Eero Tuhkanen
Sünniaeg: 24.11.1979
Sünnikoht: Viljandi
Kodakondsus: Eesti

Kontaktandmed

E-post: eero.tuhkanen@taltech.ee

Hariduskäik

2008 – ... Tallinna Tehnikaülikool, PhD
2004 – 2007 Tallinna Tehnikaülikool, MSc
1998 – 2003 Tallinna Tehnikaülikool, diplomiope
1995 – 1998 Carl Robert Jakobsoni nimeline gümnaasium, keskharidus

Keelteoskus

Eesti keel Emakeel
Inglise keel Kesktase
Saksa keel Kesktase

Teenistuskäik

2016 – ... Tallinna Tehnikaülikool, lektor
2011 – 2016 Tallinna Tehnikaülikool, assistent
2011 – ... Cad-süsteemide OÜ, tarkvara konsultant
2001 – 2011 TA-Konsult OÜ, konstruktor

ISSN 2585-6901 (PDF)
ISBN 978-9949-83-687-1 (PDF)